University of Strathclyde

Institute of Photonics

Laser Action in Solution-Processed Gain Media

by

Yujie Chen

A thesis presented in fulfilment of the requirements for the degree of Doctor of Philosophy in Physics at the University of Strathclyde in Glasgow (UK)

2012

Frontispiece

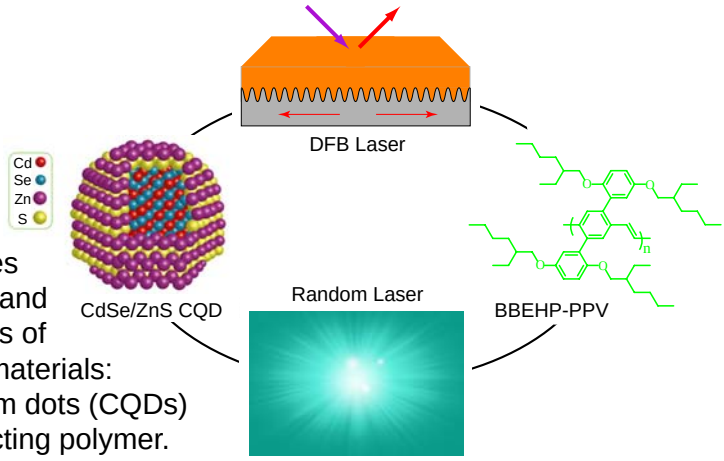

Two types of laser structures (distributed-feedback laser and random laser) and two kinds of solution-processable gain materials: CdSe/ZnS colloidal quantum dots (CQDs) and an organic semiconducting polymer.

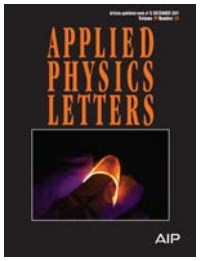

Flexible DFB CQD laser

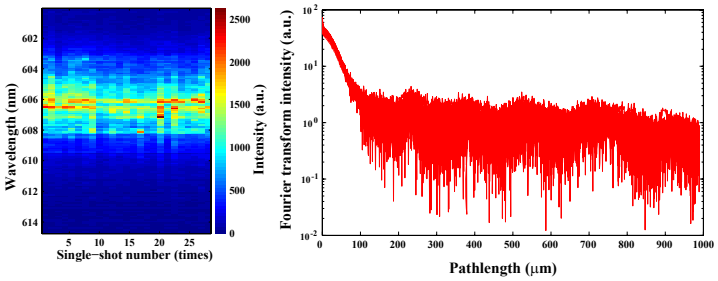

CQD random laser

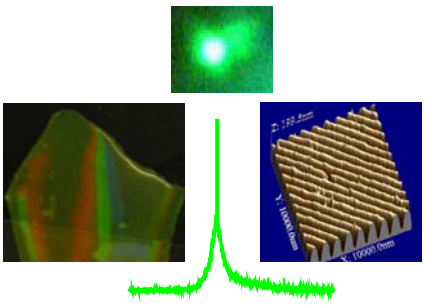

Flexible DFB organic composite laser

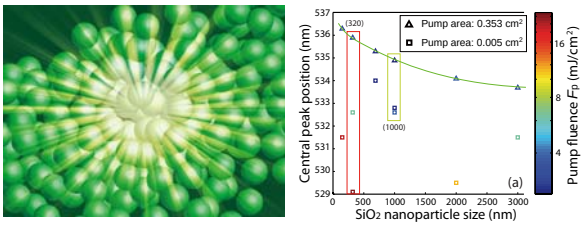

organic random laser

Copyright Statement

Signed: Date:

Acknowledgments

My PhD study was financially funded by the Scottish Universities Physics Alliance (SUPA). This work was supported by UK EPSRC under the 'HYPIX' project.

The completion of my PhD thesis could not have been done without the advice and help of a large number of people. I first would like to thank my supervisor, Prof. Martin D. Dawson, who gave me a free research environment with great support and encouraged my somewhat 'random' ideas with valuable advice to pursue my research interests during my PhD study in the Institute of Photonics (IoP) at the University of Strathclyde in Glasgow, UK. Thanks should also go to Dr. Erdan Gu, who is the one made me aware of the SUPA Prize Studentship leading me to join IoP and has provided all kinds of help.

I am greatly indebted to Dr. Nicolas Laurand for taking his valuable time and offering great suggestions in this work. I also thank Johannes Herrnsdorf and Benoit Guilhabert for benefitting from fruitful discussion with them.

I would also like to express my gratitude to the following friends and colleagues, without whom my PhD studies could have had a lot more difficulties than I have encountered: Dr. Ian M. Watson, Lynda McLaughlin, Tim Holt, Sharon Kelly, Lisa Flanagan, Dr. Jennifer Hastie, Dr. Alan Kemp, Dr Stephane Calvez, Simon Andrews, Zheng Gong, Min Wu, Jonathan McKendry, Ewan Mulhern, Loyd McKnight, Enyuan Xie, Shuailong Zhang, and Pengfei Tian from *IoP*, Alex L. Kanibolotsky, Allan R Mackintosh and Prof. Peter J. Skabara from the *Department of Pure and Applied Chemistry*, Yue Wang, Dr. Graham A. Turnbull and Prof. Ifor D. W. Samuel from *University of St Andrews*, and Dr. Zhizhong Chen, Yuebin Tao, Ningyang Liu and Lei Wang from *Peking University*.

Finally, I am dedicating this thesis to my family in great appreciation of their tremendous support for all these years. In particular, I am thankful for having Yanfeng Zhang, who is my lovely wife and inspirational research collaborator, enjoying life together for these four memorable years in Glasgow.

And my gratitude also goes to lots of others that helped ...

Abstract

In this thesis, we study laser action in solution-processed gain media, in which 'conventional' (distributed-feedback, DFB) and 'random' (multiple scattering) lasing are covered, using colloidal quantum dots (CQDs) and organic semiconductors.

For CQD-based laser action, we demonstrated a flexible DFB CQD laser. A submicron-scale passive bendable grating structure was fabricated, followed by drop-coating a CdSe/ZnS CQDs layer to form the active region. Such a DFB CQD laser has a threshold of 4 mJ/cm^2 and operates in transverse electric polarized multiple-modes. The lasing emission can also be changed in a 610-640 nm spectral window simply by using different sizes of CQDs.

We also report CQD random lasing in CdSe/ZnS CQDs deposited into rough micron-scale grooves fabricated on the surface of a glass substrate. The lasing threshold is about 25 mJ/cm^2 and stability of the lasing mode positions are analysed from the recorded single-shot spectra and the corresponding power Fourier transform spectra.

For polymer-based laser action, a free-standing organic composite membrane DFB laser was demonstrated. In this case, we incorporated an organic semiconductor polymer (BBEHP-PPV) as the gain element in a polymer matrix to form an active organic composite, the optical gain and loss characteristics of which are measured. An active grating structure was fabricated, which successfully supported lasing emission centred at 521 nm with a threshold of 1.1 mJ/cm^2.

Random laser action in a semiconducting polymer has also been investigated. We found that it is possible to modify the lasing emission wavelength of a photonic glass-based disordered organic gain system over a 7-nm waveband. The emission wavelength is shifted by changing the size of the spheres in the nano-scale range, thereby altering the transport mean free path, and/or by varying the pump spot size and pump fluence.

Contents

List of Figures

List of Tables

Part I

General Introduction

Chapter 1

Introduction to Laser Action

In this chapter, the motivation of this thesis is first elaborated. Our standpoint of studying laser action in solution-processed gain media is presented. In order to provide basic background information for understanding the main work in the following chapters, the fundamentals of laser action, in systems of particularly types of distributed feedback lasers and random lasers, are briefly discussed with their key concepts. Two types of solution-processable gain materials, including colloidal quantum dots and organic semiconducting polymers are introduced with their basic properties. In particular CdSe/ZnS core-shell nanostructures and a green light-emitting PPV derivative (BBEHP-PPV) are discussed in our case. Finally an outline is given as an overview of the thesis.

1.1 Motivation

The acronym **LASER** stands for '*light amplification by stimulated emission of radiation*'. Since it was invented in 1960 [1], the laser has revolutionized the world that we live in. Lasers [2–6], such as gas lasers, inorganic solid-state semiconductor lasers, fibre lasers and liquid dye molecule lasers, have been demonstrated and put into practical applications in many areas. However, new developments are continually emerging. Recent topics including flexible lasers, random lasers and plasmonic lasers (lasing spaser) are continuing to push the boundaries of this field.

It was our intention to harness the great advantages, such as low-cost, ease and flexibility of processing (particularly compared to the processing of traditional solid-state material), and wide range of wavelength tunability of solution-processable gain materials to fabricate novel lasers, which could open up new applications in hybrid optoelectronic devices. In particular, large area display with flexible (bendable and/or stretchable) substrate is one demanding area to go in terms of applying solution-processed gain laser devices. Other than that, optical switching, data communication and chemical sensing are the important fields in which such solution-processed gain lasers can be used. At the current stage, colloidal quantum dots or semiconducting polymers are two kinds of promising solution-processable gain materials, since they can cover across the visible spectrum and easily to be modified. They also can have high photoluminescence quantum yield and are capable of transport carriers thus possible to be electrically pumped in the future. Thus this thesis provides a summary of new results on laser action in solution-processed gain media (CdSe/ZnS colloidal quantum dots as well as a green light-emitting semiconducting polymer).

1.2 Fundamentals of Laser Action

After almost 52 years of rapid and continuing development of all kinds of lasers, one thing that has not changed is the essence of making a laser. What basic a laser needs in principle are three ingredients [7, 8]: energy injection (pumping), a gain medium and optical feedback (a resonator). For energy injection, currently it is easier to use optical pumping for solution-processed lasers that we will present in this thesis. For the gain medium, because of their potential low-cost and ease of fabrication, solution-processable gain materials like colloidal quantum dots and organic semiconducting polymers are very promising candidates for making a laser. In terms of feedback, laser structures that are suitable for solution-

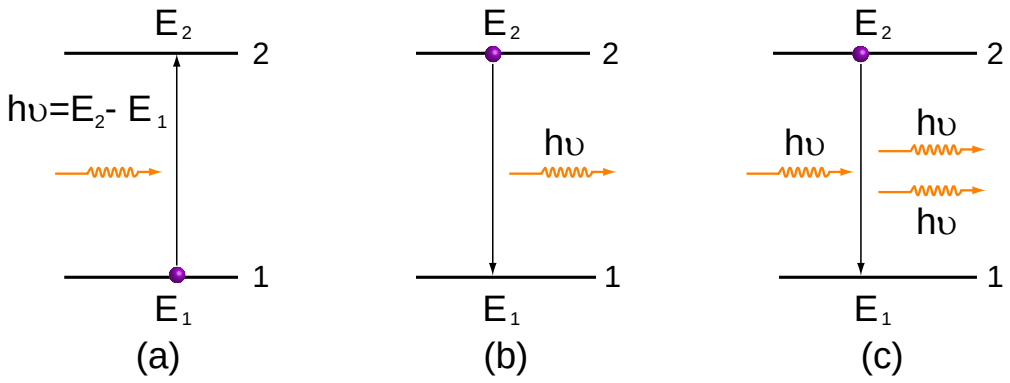

Figure 1.1: Schematic diagrams of three processes: (a) absorption, (b) spontaneous and (c) stimulated emission.

processed gain media can be, for example, a distributed feedback (DFB) grating using Bragg scattering in a periodic grating structure (see Subsection 1.3.1) and a random laser harnessing multiple scattering with 'naturally occurring' resonators in a disordered system (see Subsection 1.3.2).

1.2.1 The Laser Concept

Absorption, Spontaneous and Stimulated Emission

Fundamental processes regarding light interacting with matter that are key to laser action include phenomena of absorption [Fig 1.1(a)], spontaneous [Fig 1.1(b)] and stimulated [Fig 1.1(c)] emission. In order to understand these processes, let us first picture an electron in a molecule with two energy levels E_1 and E_2 ($E_1 < E_2$), respectively. Assuming E_1 is the ground state level and E_2 is the excited state level, the energy difference can then be expressed as a photon with energy of $h\nu = (E_2 - E_1)$, in which ν is the frequency of the photon. In its natural thermodynamic equilibrium, the electron in the molecule will tend to stay in its lowest energy state (ground level). When there is a light wave incident with photon energy ($h\nu$) that can match the difference between the molecule's two energy levels ($E_2 - E_1$), the *absorption* process can occur and the electron can be up the excited state.

When the electron in the molecule is in an unstable state, it tends to release the excess energy after a period of time (i.e. decay lifetime). One way of going back to its stable state is that the excited electron itself decays to its ground state and releases the extra energy as a photon. This is called *spontaneous emission*.

The probability of such transition is determined by:

$$\left(\frac{dN_2}{dt}\right)_{sp} = -AN_2 \tag{1.1}$$

where A is so-called Einstein A coefficient. In particular, if the transition is radiative decay, then the spontaneous emission lifetime can be obtained via $\tau_{sp} = 1/A$. In the semiclassical case (the electromagnetic field is treated through Maxwell's equations while the molecule or the atom itself is treated according to quantum mechanics), through calculating the electric dipole moment of the molecule (or atom) of interest, A can be expressed as:

$$A = \frac{16\pi^3\nu_0^3 n|\mu|^2}{3h\epsilon_0 c_0^3} \tag{1.2}$$

where ν_0 is the transition frequency, ϵ_0 is the vacuum permittivity, c_0 is the light velocity in the vacuum, h is the Planck constant, μ is the amplitude of the electric dipole moment, n is the refractive index of the medium around the dipole. It is noticed that when $|\mu| = 0$, $A = 0$, which means that the transition cannot be occurred, corresponding to the so-called 'forbidden transition'. To obtain the 'allowed transition', one must have $A \neq 0$ and hence $|\mu| \neq 0$.

It is also noted that the energy may dissipate via other ways such as heat (vibration, the so-called phonon) and/or charge states instead of radiating as light, phenomena which are referred to as nonradiative processes. This is usually very fast: in the time scale of less than a picosecond. Hence in an absorption process, the electron in the molecule absorbs one photon to produce a transition from a lower level to a upper level (transition $1 \rightarrow 2$) [Fig 1.1(a)]; while in the spontaneous emission process, it emits one photon to generate a transition from an upper level to a lower level (transition $2 \rightarrow 1$) [Fig 1.1(b)].

When it comes to the case that the electron in the molecule is in the excited state and there happens to be an electromagnetic wave of frequency ν, i.e. the photon energy matches the energy gap between E_1 and E_2 levels, incident onto it, the transition $2 \rightarrow 1$ can be triggered to occur creating a new photon with same frequency joining the incident wave. This is called *stimulated emission*. In such a process, it is noted that the rate $(\mathrm{d}N_2/\mathrm{d}t)_{st}$ at which transition $2 \rightarrow 1$ occurs should be proportional to the population N_2 of the upper level (E_2), written as:

$$\left(\frac{dN_2}{dt}\right)_{st} = -W_{21}N_2 \tag{1.3}$$

where W_{21} is the stimulated emission rate.

When reaching the thermodynamic equilibrium, for an established electromagnetic energy density with a spectral distribution ρ_ν, the number of transition $2 \to 1$ should be equal to that of $1 \to 2$. We thus have:

$$W_{21} = B_{21}\rho_{\nu 0} \tag{1.4}$$

$$W_{12} = B_{12}\rho_{\nu 0} \tag{1.5}$$

where B_{21} and B_{12} are the Einstein B coefficients. If the two levels are non-degenerate, we then have the following relations regarding the Einstein coefficients:

$$B_{12} = B_{21} = B \tag{1.6}$$

$$\frac{A}{B} = \frac{8\pi h\nu_0^3 n^3}{c^3} \tag{1.7}$$

Considering a plane wave with photon flux F (number of photons per unit area and time), we have:

$$W_{21} = \sigma_{21}F \tag{1.8}$$

where σ_{21} is the stimulated emission *cross section* (also called *gain cross section*). Similarly, the absorption process can be characterized by an *absorption cross section* σ_{12}.

The physical interpretation of the transition (i.e. stimulated emission or absorption) cross section is corresponding to the probability of the occurrence of the transition. For example, the larger the stimulated emission cross section, the bigger chance to have stimulated emission. For the absorption process, when the photon enters the area within the absorption cross section, it will be absorbed by the molecule (or the atom).

If the two levels are degenerate (e.g. g_1-fold for E_1 and g_2-fold for E_2), we then have $g_1W_{12} = g_2W_{21}$ and hence $g_1\sigma_{12} = g_2\sigma_{21}$.

Population Inversion and Pumping Configuration

According to Boltzmann statistics, the thermal equilibrium will tend to have $N_2 - (g_2N_1/g_1) < 0$ and if a nonequilibrium condition in which $N_2 > (g_2N_1/g_1)$ can be fulfilled, then we have *population inversion*, which is key to generating light amplification. It is realized that in general there exists a threshold condition to reach gain in order to generate laser action, in which the population inversion $N = N_2 - (g_2N_1/g_1)$ should reach a critical value N_c. In laser theory, for a simple

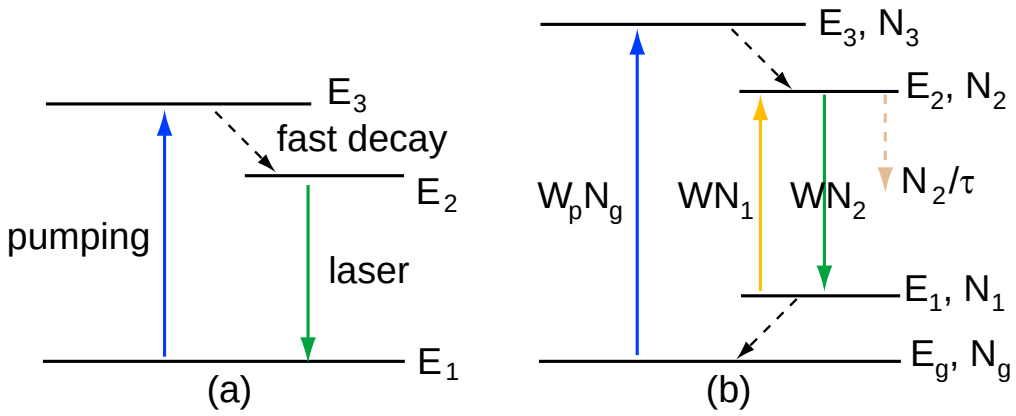

Figure 1.2: Schematic diagrams of (a) three-level and (b) four-level laser systems.

Fabry-Pérot (F-P) cavity laser having two end mirrors with reflectivities R_1 and R_2, respectively, the oscillation threshold can be expressed as [8]:

$$R_1 R_2 (1 - \Gamma_{\text{loss}})^2 \exp\{2\sigma_{21}[N_2 - (g_2 N_1/g_1)]L_{\text{active}}\} = 1 \tag{1.9}$$

where Γ_{loss} accounts for the cavity internal loss, and L_{active} is the length of the active region. Therefore the critical inversion (N_c) can be expressed as:

$$N_c = -[\ln(R_1 R_2) + 2\ln(1 - \Gamma_{\text{loss}})]/(2\sigma_{21} L_{\text{active}}) \tag{1.10}$$

Oscillation can build up from spontaneously emitted photons when the critical inversion is reached, leading to the amplification process which is the basis of a laser action.

However, in practical situation a classical two-level system is not able to work for laser action due to the inability to achieve population inversion. Therefore, historically, people looked at three- and four-level systems for laser action, schemes of which can be seen in Fig. 1.2. In the following discussion, let us take a four-level system [Fig. 1.2(b)] as an example. We assume that the molecule is excited through photo-pumping from its ground state (labelled as E_g) to an excited state E_3 and that it then rapidly decays nonradiatively to another state E_2. There is then a population inversion between levels 2 and 1, and the radiative decay from level 2 to level 1 can be via stimulated emission. The molecule should not be in level 1 too long and it usually goes back to the ground state via another rapid nonradiative decay.

For the transition $2 \rightarrow 1$, when the gain exceeds the loss (including absorption), the amplification process starts to build up. For simplicity, we assume that

the transitions $3 \to 2$ and $1 \to g$ are rapid (meaning $N_3 \cong N_1 \cong 0$). Based on these assumptions, the rate equation for the population of level 2 can then be written as:

$$\frac{\mathrm{d}N_2}{\mathrm{d}t} = R_p - WN_2 - \frac{N_2}{\tau} \tag{1.11}$$

where $R_p = (\mathrm{d}N_2/\mathrm{d}t)_p$ represents the pumping rate per unit volume, W is the transition rate, and τ the effective lifetime of the upper level taking into account the radiative and nonradiative decay. Bringing the lasing photon dynamics in a cavity (with τ_c being the cavity photon lifetime) into our further consideration, the rate equation for a laser is expressed as:

$$\frac{\mathrm{d}N}{\mathrm{d}t} = R_p - B\phi N - \frac{N}{\tau} \tag{1.12a}$$

$$\frac{\mathrm{d}\phi}{\mathrm{d}t} = \big(BV_a N - \frac{1}{\tau_c}\big)\phi \tag{1.12b}$$

where B represents the stimulated transition rate per photon per mode, $N \equiv N_2 - N_1 \cong N_2$, and V_a the volume of the mode in the active medium. The term $B\phi N$ in Eq. 1.12a is for a stimulated emission process, and the term N/τ represents spontaneous emission. The term BV_aN in Eq. 1.12b accounts for the growth rate of the photon population because of stimulated emission, and the term ϕ/τ_c is for the removal of photons due to cavity loss. Thus this set of equations is capable of describing the lasing behaviour and we should be capable of controlling laser action through the modification of, for example, cavity photon lifetime τ_c. This we will discuss in the case of random lasers later in Subsection 1.3.2 as well as via experimental demonstration in Chapter 5.

1.2.2 Amplified Spontaneous Emission (ASE)

Amplified spontaneous emission (ASE), historically also called *mirrorless laser action* as well, has been studied extensively in a number of papers by Allen and Peters [9–14], Casperson and Yariv [15], Gamo *et al.* [16], Casperson [17], Garrison *et al.* [18], and Pert [19], just to name a few. In the following, the phenomena of spectral narrowing and threshold characteristics are discussed briefly according to the basic theory of ASE. Such discussion sheds light on the understanding of light amplification, which is crucial to laser action.

Spectral Narrowing

For a Gaussian- or Lorentzian-line-shape emission spectrum, the ASE intensity in the low saturation regime has a well-known equation which has been derived

by researchers including Linford *et al.* [20]. Their equation was later modified by other researchers including Svelto *et al.* [21]. The simplified model elaborated in the following is based on the treatment made by Svelto *et al.* [8, 21].

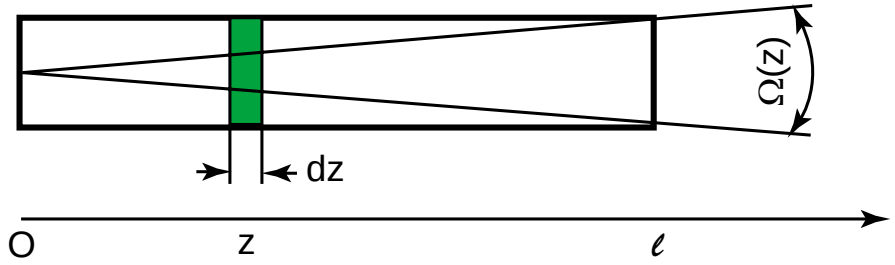

Figure 1.3: Geometry of the active region for the ASE calculation.

Assuming in a four-level active medium system where population inversion occurs, let N be the upper state population. The intensity variation of the ASE output (along the z coordinate of the active medium) can be expressed as:

$$\frac{\partial I_\nu}{\partial z} = \sigma N I_\nu + N A_\nu \frac{\Omega(z)}{4\pi} \tag{1.13}$$

where σ is the transition (stimulated emission) cross section at frequency ν, A_ν is the spectral rate of spontaneous emission, and $\Omega(z)$ is the solid angle of the emission (see Fig. 1.3). According to Svelto *et al.*'s calculation [21], after integrating both sides of Eq. 1.13, we have:

$$I_\nu(l,\nu) = \frac{\Omega}{4\pi}\phi I_s g_p \frac{h\nu[\exp(\sigma N l) - 1]}{\sigma} \tag{1.14}$$

where $\phi = \tau/\tau_r$ is the fluorescence quantum yield and $I_s = h\nu/(\sigma_p \tau)$ is the peak saturation intensity. The ASE output, when normalized to the peak value, can then be written as:

$$[I_\nu(l,\nu)/I_\nu(l,\nu_0)] = [\exp(\sigma N l) - 1]/[\exp(\sigma_p N l) - 1] \tag{1.15}$$

For different values of peak gain $G = \exp(\sigma N l)$, using Eq. 1.15, we plot the normalized ASE output spectra for a Lorentzian-line-shape emission, as shown in Fig. 1.4. It is noted that the dashed curve represents the spontaneous emission spectrum. The spectral narrowing of ASE can be clearly observed when the peak gain G increases, because the gain at the peak is much higher than that in the two wings. Such a phenomenon is common for ASE and laser action as will be seen in later chapters. For gain measurement, the gain coefficient $g = \sigma N$ can be

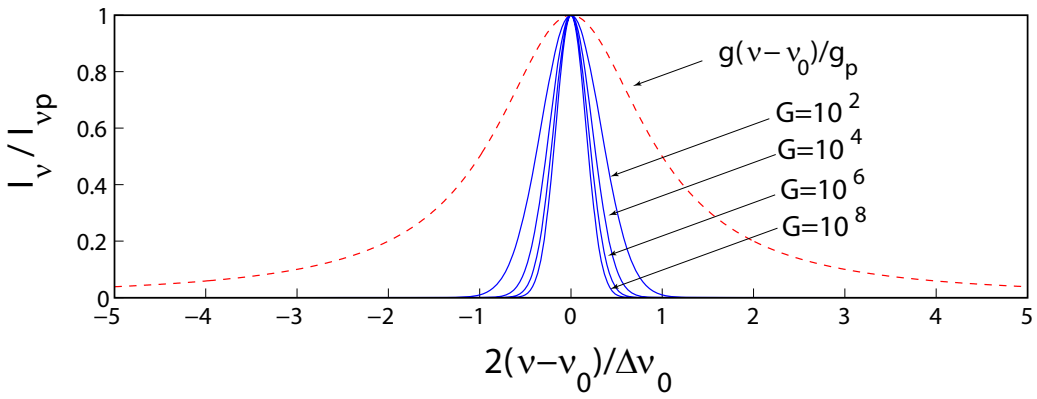

Figure 1.4: Normalized (Lorentzian-line-shape) ASE spectral emission at four different values of the peak, unsaturated, single-pass gain. ν_0 is the peak frequency and $\Delta\nu_0$ is the spontaneous emission linewidth.

measured via the variable-stripe-length (VSL) method, which was first introduced by K. L. Shaklee and R. F. Leheny [22]. For more details refer to Eq. 4.1 and Fig. 4.3(a) in Chapter 4.

Threshold Characteristics

According to the study done by Lee W. Casperson [17], the threshold characteristics of ASE in a homogeneous broadened gain system can be described by:

$$(1 - 2x_0)\ln(I_{nor}/x_0 + 1) + 2I_{nor} = Z_h \tag{1.16}$$

where I_{nor} is the normalized output intensity, x_0 the spontaneous emission parameter, and Z_h the normalized homogeneous length parameter. $Z_h = g_h l$ and g_h is the unsaturated homogeneous gain coefficient which depends on the pump parameter. Curves based on Eq. 1.16 are plotted in Fig. 1.5 showing the threshold behaviour of the ASE output. Such description of threshold characteristics is also suitable for most classical laser systems. However, if all photons generated from spontaneous emission couple into only one mode, then a thresholdless laser is possible, which was first reported by Martini and Jacobovitz [23]. It should be pointed out clearly here that in our case, as presented in later chapters, for laser action in gain media we studied, a threshold bahaviour is seen and considered as a clear sign of whether we reach the regime of light amplification/lasing or not.

It is worth mentioning that when measuring the threshold behaviour, one may see a gradual steepening of the output intensity, which corresponding to the so-called 'soft' threshold [8]. Such behaviour can be seen in our ASE and

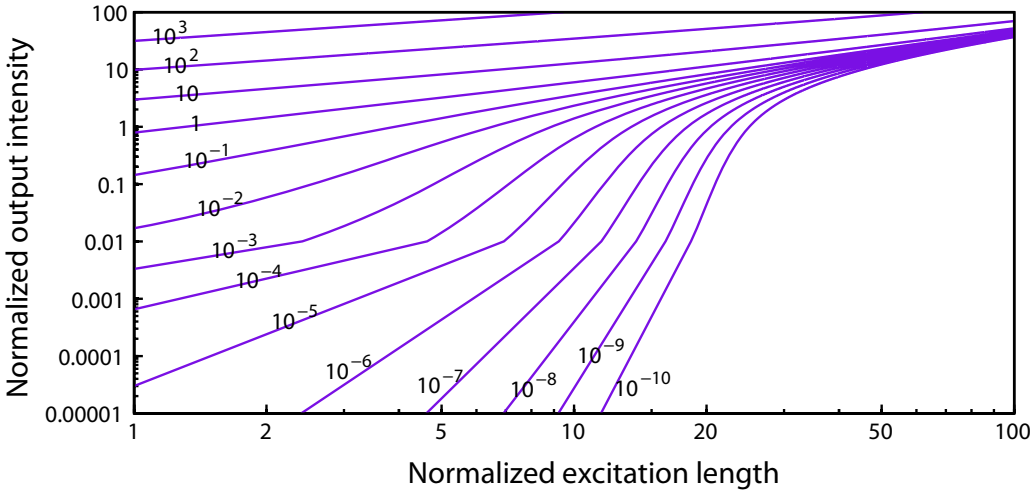

Figure 1.5: Normalized output intensity I_{nor} in a homogeneously broadened gain system as a function of the normalized length Z_h, for various values of x_0 (spontaneous emission parameter).

laser demonstrations reported in the following chapters. The origin of such phenomenon is due to the saturated gain (i.e. the output intensity is close to the saturated intensity) when close to threshold. If the gain medium is far away from saturated (i.e. the output intensity is far less than the saturated intensity), then one may see the output intensity with a well defined sharp threshold, the so-called 'hard' threshold.

However, it is also noted that spectral narrowing of emission may be attributed to other mechanisms like leaky-mode emission [24]; however, no threshold behaviour is expected to be observed in that case [25].

1.3 Basics of Two Types of Lasers

1.3.1 Distributed-Feedback (DFB) Laser

In a DFB laser, periodic grating structures provide feedback and the light to be amplified can travel back and forward through Bragg scattering. A laser beam can then be emitted out in defined directions.

Diffractive Resonators

Instead of using mirrors (e.g. a Fabry-Pérot cavity) or total internal reflection (e.g. whispering-gallery-mode cavity) for feedback, a DFB laser uses a diffractive

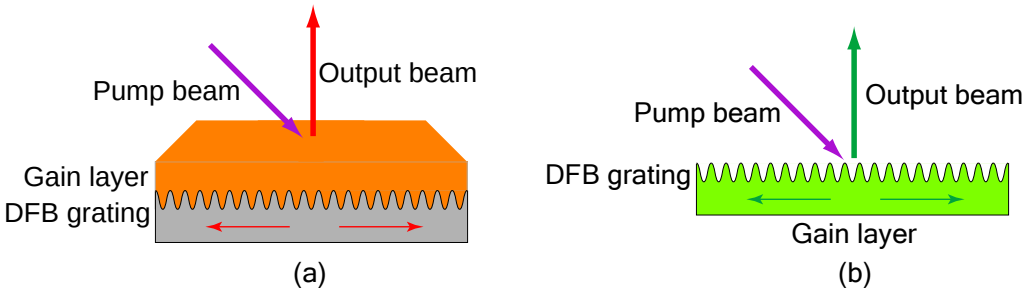

Figure 1.6: Diffractive resonators: (a) passive and (b) active grating strucutres.

resonator formed by periodic grating structures, of which the length scale is in the wavelength regime of interest. Such a design is generally easier to realize compared with the very high-standard requirement of good-quality end facets for feedback in a mirror-assisted laser configuration [26]. It can also be very compact and compatible with the processing techniques (like spin-coating method) and using solution-processable gain materials (like colloidal quantum dots and organic semiconducting polymers) that we mainly used in this work.

For laser demonstration so far, researchers have explored many different types of diffractive resonators, including one-dimensional (1D) corrugated structures [27], two- and three-dimensional (2D/3D) photonic crystal structures [28, 29], and circular grating structures [30]. In any particular grating structure, a set of wavelengths can be coupled from a travelling wave into another one travelling oppositely, if the Bragg condition is met:

$$m\lambda = 2n_{eff}\Lambda \tag{1.17}$$

where λ is the (vacuum) wavelength of the travelling wave, Λ the period of the grating structure, m the order of diffraction, and n_{eff} the effective refractive index.

In this work, we use a 1D grating (replicated from a standard commercial blank digital versatile disk, DVD) to demonstrate a DFB laser, a corrugated structure which can be made using either passive (see Chapter 2) or active (see Chapter 4) materials, as illustrated in Fig. 1.6.

Feedback Mechanism: Bragg Scattering

In terms of the feedback mechanism in a working DFB laser, H. Kogelnik and C. V. Shank first applied a model using coupled-wave theory to study the las-

ing modes of a DFB structure, the resonant frequencies with their threshold gains, and the spectral selectivity [31]. The simplified coupled-wave model considers two oppositely travelling electromagnetic waves in the grating structure, and each wave can receive light via Bragg scattering from the other one. This offers a feedback that can be distributed throughout a certain length of the periodic structure. When there is gain existing in the system and there is sufficient feedback, oscillation may then occur. Because the wavelength is sensitive to the Bragg effect, spectral selection can be achieved.

When expressing such a model in the language of mathematics, Kogelnik and Shank [31] assumed that electromagnetic waves traveling in the DFB structure can be described by complex amplitudes $\mathcal{R}(z)$ and $\mathcal{S}(z)$ with corresponding electric fields written as:

$$\mathcal{E}(z) = \mathcal{R}(z)\exp(-j\beta_0 z) + \mathcal{S}(z)\exp(j\beta_0 z) \tag{1.18}$$

where $\beta_0 = n_0\omega_0/c$ (when at the Bragg condition) with n_0 the average refractive index and ω_0 the Bragg frequency. The propagation behaviour (assumed to be in the z direction) of the travelling waves can be predicted by the scalar wave equation written as:

$$\frac{\partial^2}{\partial z^2}\mathcal{E}(z) + k^2\mathcal{E}(z) = 0 \tag{1.19}$$

where $k = 2\pi n/\lambda$.

If the gain is small over the distance of the wavelength scale and the perturbations of the gain $[\alpha(z) = \alpha_0 + \alpha_1\cos(2\beta_0 z)]$ and refractive index $[n(z) = n_0 + n_1\cos(2n_0 z)]$ are small too, then the longitudinal field distribution of modes (oscillation states) in the DFB structure can be derived as:

$$\mathcal{R}(z) = \sinh\gamma(z + L/2) \tag{1.20a}$$

$$\mathcal{S}(z) = \pm\sinh\gamma(z - L/2) \tag{1.20b}$$

where γ is the complex propagation constant and L is the length of the grating structure.

For mathematical simplicity, here the model considers only internal waves starting at the grating boundaries and collecting their initial energy from the oppositely travelling wave through Bragg scattering. For a given value of γ, the corresponding resonant (normalized) frequency $\delta[\equiv n(\omega-\omega_0)/c]$ and its threshold

gain constant α can be obtained via the solution of the coupled-wave equations:

$$\alpha - j\delta = \gamma \coth(\gamma L) = \pm j\kappa \cdot \cosh(\gamma L) \tag{1.21}$$

where κ is the coupling coefficient, defined by $\kappa = \pi n_1/\lambda_0 + j\alpha_1/2$, which is a crucial parameter of the coupled-wave model for a DFB laser. It represents the strength of the backward Bragg scattering, and indicates how much feedback can be supported by the grating structure [31]. The modes of the ideal DFB structure are thus degenerate and symmetric as given by Eq. 1.21. However, for real systems, some modes may be dominated due to the so-called 'symmetry breaking' induced by any perturbation in the grating structure and/or the gain layer. An example of which can be seen in Chapter 2.

In particular, for a TE-mode [meaning that the direction of the **E**-field is parallel to the grooves of the grating structure, i.e., the y-component shown in Fig. 1.7(a)], using the result of the perturbation analysis (pure index modulation) [32, 33], the coupling coefficient for a DFB laser can be expressed as:

$$\kappa_{\mathrm{TE}} = \frac{{k_0}^2}{2\beta N^2} \int_{\mathrm{corrugation}} \Delta[n^2(x,z)][\mathcal{E}_y(x)]^2 \mathrm{d}x \tag{1.22}$$

where $N^2 = \int_{-\infty}^{+\infty} [\mathcal{E}_y(x)]^2 \mathrm{d}x$, $k_0 = 2\pi/\lambda_0$, β is the TE-mode propagation constant, and $\mathcal{E}_y(x)$ the y-component of the unperturbed **E**-field, given a grating structure shown in Fig. 1.7(a), which should satisfy the wave equation (similar to Eq. 1.19). According to A. Yariv's calculation [33], after solving the wave equation the eigenvalues β of the confined TE modes can then be determined by the following equation:

$$\tan[h(t - \omega g \Lambda)] = h(q+p)/(h^2 - pq) \tag{1.23}$$

where

$$\begin{cases} q = \sqrt{\beta^2 - {n_1}^2 {k_0}^2} \\ h = \sqrt{{n_2}^2 {k_0}^2 - \beta^2} \\ p = \sqrt{\beta^2 - {n_3}^2 {k_0}^2} \end{cases} \tag{1.24}$$

For a rectangular grating [Fig. 1.7(a)], when one only considers the perturbation of the refractive index, the TE-mode coupling coefficient κ_{TE} can be

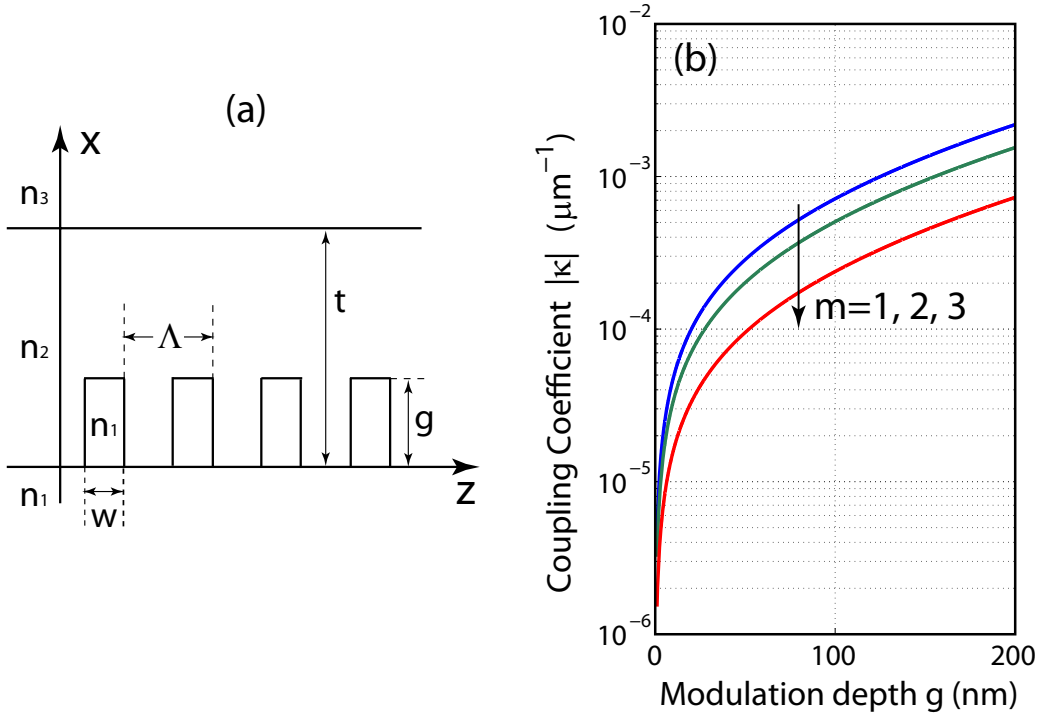

Figure 1.7: (a) A rectangular grating structure: t is the thickness of gain layer (in the y-plane) and g is the modulation depth. For a TE-mode, we only consider the y-component of the electric field of the propogating electromagnetic wave. (b) Coupling coefficient as a function of modulation depth (g) with various Bragg orders for the TE_0 mode. Here the plots use Eq. 1.25 with the same parameters as Ref. [32] provided: $n_1 = 3.4$, $n_2 = 3.6$, $n_3 = 3.59$, $t = 2$ μm, $\lambda_0 = 850$ nm, $w/\Lambda = 0.25$, showing the same curves as in Figure 3(a) in Ref. [32].

expressed as:

$$\kappa_{\mathrm{TE}} = \frac{{k_0}^2({n_1}^2 - {n_2}^2)}{4\pi\beta m N^2}\sin\left(\frac{\pi m\omega}{\Lambda}\right)\left\{g_2 + \frac{\sin(2g_2h)}{2h} + \frac{q}{h^2}[1-\cos(2g_2h)] + \frac{q^2}{h^2}\left[g_2 - \frac{\sin(2g_2h)}{2h}\right] + [1-\exp(-2qg_1)]/q\right\} \tag{1.25}$$

where

$$\begin{cases} g_1 = \omega g/\Lambda \\ g_2 = (1-\omega/\Lambda)g \end{cases} \tag{1.26}$$

By way of example, here we apply parameters given in Ref. [32] and use Eq. 1.25 to plot the TE-mode coupling coefficient in Fig. 1.7(b) as a function of modulation depth with various Bragg orders ($m = 1, 2, 3$), showing the same curve as W. Sterifer *et al.* did in Ref. [32]. They also studied the case for TM-mode (the transverse magnetic field is parallel to the direction of the grooves of

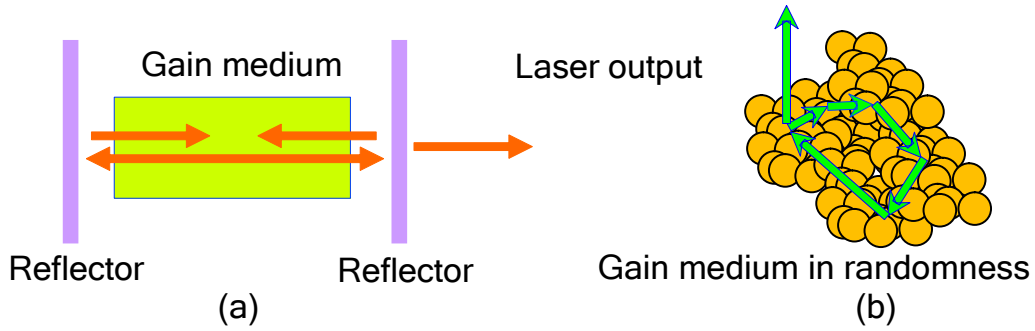

Figure 1.8: The concept of a random laser: diagram of a (a) conventional (e.g. F-P cavity) laser and (b) multiple-scattering-induced random laser.

the grating structure) coupling coefficient in another paper [34], showing that for most DFB lasers, the TE-mode κ_{TE} is larger than the TM-mode κ_{TM}. That explains our observation in TE-mode lasing emission from our DFB colloidal quantum dot laser (see Chapter 2).

1.3.2 The Random Laser

The Idea of the Random Laser

In recent years, *random lasers* have became an important topic within the scientific community. The pioneering investigation on random lasing was actually initiated by Letokhov in the 1960s [35, 36]. However, it did not catch too much attention at that time, partly because the laser community was mainly focused on more traditional lasers and their applications. Therefore there were very few papers studying random laser action during the time between the 1970s and 1990s [37]. However, it is noticeable that in the 1990s more and more researchers became interested in this topic, partly inspired and encouraged by a series of new experiments demonstrating random laser action done by, for example, Lawandy *et al.* [38] and Cao *et al.* [39]. Most importantly, researchers started to appreciate the rich and complex physics in a random laser, which may open up a completely new perspective on disorder in photonic materials and novel applications in a variety of promising areas [40, 41]. These include display, laser paint, a physical source for a random number generator, sensing systems, and medical diagnostics. For example, checking the random lasing emission from dye-doped human tissues enables researchers to distinguish cancerous human tissues from healthy tissues [42].

In order to introduce the basic concept of random laser action, Fig. 1.8 shows

a diagram of the comparison between a regular laser and a random laser. In a regular laser [taking a P-F cavity laser as an example, see Fig. 1.8(a)], the light emitted in the gain medium bounces back and forth between two mirrors (reflectors) that form a resonator. After several passes through the amplifying (gain) material in the resonator, the gain amplification can be large enough to produce laser light. In a random laser, no such 'obvious' resonator can be identified but multiple scattering between scattering centres in the disordered materials keeps the light trapped long enough for the amplification to become efficient, and for laser light to radiate in random directions.

Thus for a regular laser, we require two more components over and above energy injection (pumping). As mentioned before, one is a gain material offering light amplification; the other is an optical cavity providing feedback. For a random laser on the other hand, (borrowing what S. Wiersma put in a review article [41]) two rules apply. In rule number one, light is multiply scattered owing to randomness and amplified by stimulated emission. In rule number two, there exists a threshold, because of the multiple scattering, above which total gain exceeds total loss.

Feedback Mechanism: Multiple Scattering

Concerns regarding the lasing properties of random lasers have been raised by some laser researchers; however, considerable progress on investigating laser characteristics shared with traditional lasers has been made to address most of the issues. For example, the phenomena of lasing signatures, like threshold behaviour and spectral narrowing have been studied, for instance, by Letokhov [36], Lawandy *et al.* [38], John *et al.* [43], Balachandran *et al.* [44], Cao *et al.* [39], and Frolov *et al.* [45]. The dynamical response and relaxation oscillations in random laser action have also been looked at, for example, by Soukoulis *et al.* [46] and van der Molen *et al.* [47]. In studies of the coherent properties of random laser action, photon statistics have been investigated, for instance, by Ambartsumyan *et al.* [48], Zacharakis *et al.* [49], Cao *et al.* [50], Patra [51], and Florescu and John [52]. The understanding so far of the coherence in light emission from an amplifying scattering system indicates that Bose-Einstein (incoherent) and Poissonian (coherent) distributions of photon statistics coexists in a random laser, and for a system with strong scattering, the Poissonian distribution−corresponding to highly coherent properties typically for a standard laser [53]− can dominate above lasing threshold. Mechanisms accounting for random laser action have been under extensive study, particularly on lasing mode

properties (e.g. extended and/or localized modes) that are key to understanding the origin of random lasing [43, 54–69]. For example, recently a mapping technique has been developed in Vardeny's group [63, 70] to spatially resolve random laser emission spectra, the Fourier power transform of which can then refer back to the measured bright areas corresponding to the so-called 'naturally occurring resonators' (Fig. 1.9). Nevertheless, it is far from clear that there is complete understanding of the rich and complex physics in a random laser system and thus further investigations are still demanded in terms of time-dependent behaviour, dynamical processes, mode stability, quantum-noise effects in random laser action, etc. [71].

Although there are still several debated issues for the physical mechanism of random laser action, based on different experimental results and theoretical studies of random lasing (nonresonant/resonant feedback) [37, 41, 71, 75], it is now clear that random lasing starts from spontaneous emission, from which photons are amplified by stimulated emission through multiple scattering that confines the light in the gain regime long enough to achieve sufficient amplification. When the total gain exceeds the total loss, that is the net gain is above zero, then laser action can occur.

To determine the lasing mode mechanism in a random laser, the Ioffe-Regel criterion $k\ell_t \sim 1$ was used for defining the Anderson localization transition [76–78], where $k = 2\pi/\lambda$ is the wave vector and ℓ_t is the transport mean free path. The latter is defined as the average distance a wave travels before its direction of propagation is randomized [79]. When $k\ell_t < 1$ we are in the very strong scattering regime which is the case of absence of diffusion, leading to the confinement of localized modes in an $\sim \lambda$-scale; $k\ell_t \gg 1$ means the weak scattering regime where random laser action occurs from amplified extended modes through light diffusion.

In a diffusive random laser, which is what we studied in this work, the transport mean free path (ℓ_t) plays a vitally important role. Since modifying ℓ_t can control the diffusion coefficient $D(\lambda) \simeq v\ell_t$, where v is the effective speed of light in the disordered system [81]. This can then have an influence on the photon cavity decay time (τ_c) according to $\tau_c = L^2_{\text{thickness}}/8D(\lambda)$, where $L_{\text{thickness}}$ is the effective thickness of the disordered system [82]. Thus in such a random laser system, the lasing behaviour, through its rate equation (Eq. 1.12), can be modified via controlling ℓ_t (see Chapter 5 for more details). Meanwhile, ℓ_t can be measured via a coherent backscattering (CBS) experiment, which studies the interference effect of optical waves backscattered from a disordered dielectric medium (inset of Fig. 1.10) [83–85]. Parameter ℓ_t can then be extracted from the fitting of the

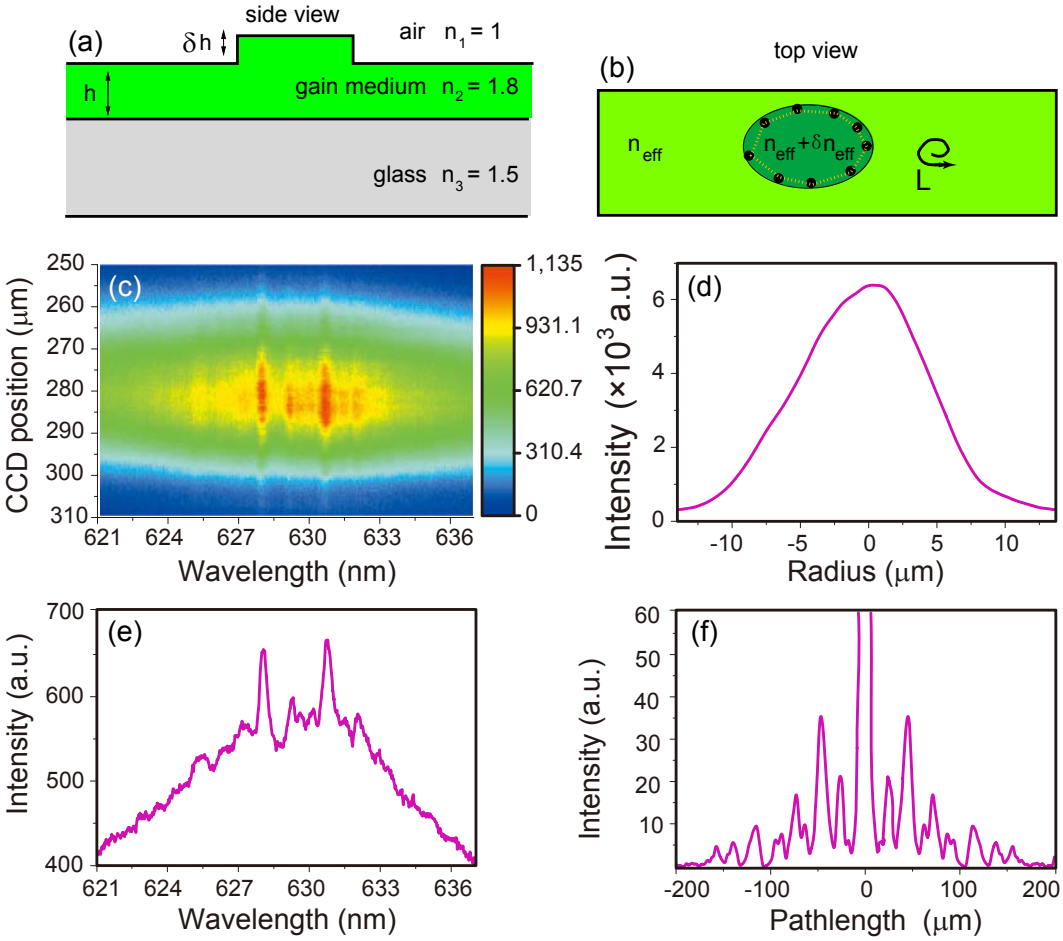

Figure 1.9: A 'naturally occurring' resonator: (a) schematic diagram of a gain medium (e.g. conjugated polymer thin film on a glass substrate) with thickness fluctuation; (b) schematic diagram of a whispering-gallery-mode type naturally occurring resonator induced by a thickness fluctuation δh, where L represents round trip resonator pathlength; (c) CCD image of spatially and spectrally resolved intensity distribution profile; (d) the intensity distribution curve at the wavelength of 630.8 nm extracted from image (c); (e) the corresponding lasing spectrum from the image (c); and (f) the power Fourier transform of (e). Note that from the extracted periodicity ($\Delta d = 22$ μm) in (f), one can obtain an effective resonator diameter $D \sim 25$ μm using the relation $D = 2 \cdot \Delta d/n$ [72, 73], which matches the intensity profile diameter ($D \sim 24$ μm) in (d). Adapted from Refs. [63, 74].

measured CBS cone curve (see Fig. 5.9 and Table 5.1 in Chapter 5) using the following two equations according to diffusion theory [80, 86, 87]:

$$\alpha(\theta) = \frac{3}{8\pi}\left\{1 + \frac{2z_0}{\ell_t} + \frac{1}{(1+k_\perp \ell_t)^2}\left[1 + \frac{1-\exp(-2k_\perp z_0)}{k_\perp \ell_t}\right]\right\} \tag{1.27}$$

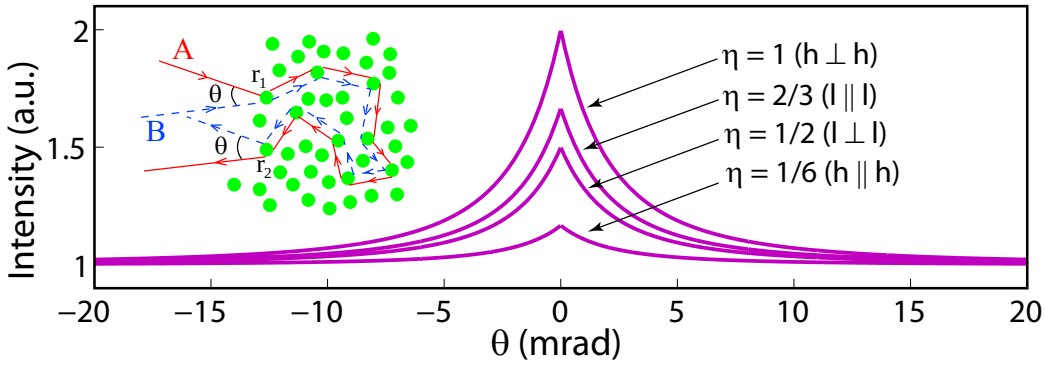

Figure 1.10: Coherent backscattering cone curves plotted based on the Eqs. 1.27 and 1.28 with different depopulation coefficients (η) for various polarization channels (l: linearly polarized; h: helicity of circularly polarized; $\perp$: perpendicular; $\parallel$: parallel, see Ref. [80]). Inset: in the multiple scattering scenario, two light beams propagate in a random medium, in which one is following the other's trace by time inversion and they can be interference constructively for the small angle regime.

where $\alpha(\theta)$ is the coherent albedo, $z_0 \simeq 2\ell_t/3$ and $k_\perp \simeq (2\pi/\lambda)|\theta|$ at small angles.

$$I_{\text{CBS}} = \frac{\alpha_d + \big[\alpha(\theta) - \alpha_d\big]\eta}{\alpha_d} \tag{1.28}$$

where α_d is the noncoherent albedo (the background intensity of the backscattering) and η is the depolarization coefficient. Figure 1.10 shows a series of CBS cone curves plotted according to these two equations using different values of η [80].

1.4 Solution-Processable Gain Materials

1.4.1 Colloidal Quantum Dots (CQDs)

Quantum Size Effect

Semiconductor nanocrystals, or colloidal quantum dots (CQDs), are quantum-confined nanocrystallines whose sizes are on the nanoscale (diameter below 10 nm, normally consisting of hundreds of thousands of atoms) [88, 89]. There exists a length scale given by the exciton Bohr radius (a_0) in bulk semiconductors. a_0 is determined by the strength of the electron-hole ($e-h$) Coulomb interaction. If the size of a CQD is comparable with or even smaller than a_0, the dimensions of the CQD will strongly affect the spatial extent of the $e-h$ pair state and thus

the electronic energies. This is the known quantum-size effect, resulting in the discrete structure of energy levels.

In such strongly confined CQDs (when the dimensions of the CQD are smaller than its corresponding a_0) the energy level separation can exceed several hundreds of meV [Fig. 1.11(a)] and colour tunability over 1 eV via quantum confinement can be simply obtained by varying the size of the nanocrystals [Fig. 1.11(b)]. The energy gap increases as the size of the dot decreases (from weak to strong quantum confinement). Consequently, emission ranging from the ultraviolet to the near-infrared is possible with the appropriate semiconductor system and quantum dots sizes.

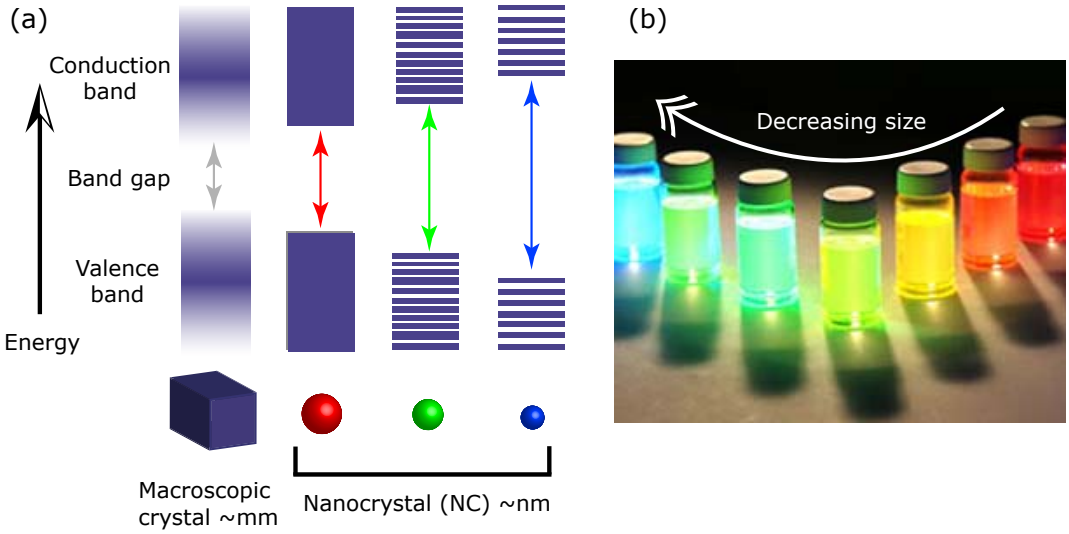

Figure 1.11: (a) CQDs band gap determined by the radius of the dot (adapted from Ref. [89]); and (b) colour CdSe-based CQDs (adapted from *Evident Technologies, Inc.*).

The most mature CQD material system for emission in the visible is based on II-VI cadmium selenide (CdSe). High-quality, monodispersed CdSe CQDs are typically fabricated by wet chemistry [Fig. 1.12(a)] through the decomposition of metal-organics and chalcogenides in a high temperature organic solvent [88, 90]. Significant improvement in the photoluminescence quantum yield efficiency can be obtained by adding a thin zinc sulphide (ZnS) shell around the CdSe core thereby passivating the surface and in turn reducing the probability of surface carrier trapping [91, 92]. Organic ligands [90] surrounding the CQDs [Fig. 1.12(b)] enable their dispersion in solvents or in a polymer matrix material, making drop-casting and spin-coating on a substrate possible. Such solution processing opens the door to simplified fabrication of photonic devices.

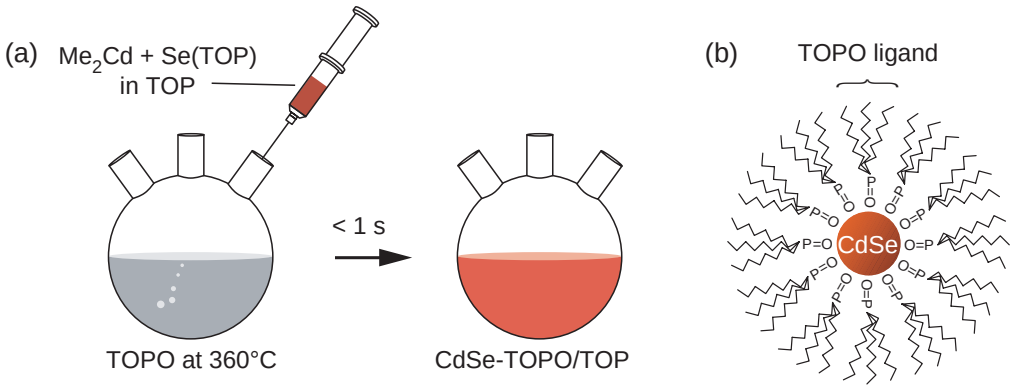

Figure 1.12: (a) A chemical (organometallic) technique used for the synthesis of monodispersed CdSe CQDs; and (b) CdSe CQD coated with passivating ligands in order to sustain their dispersion in solution. Adapted from Ref. [93].

CQDs as laser building blocks

There are many areas in which CQDs have promising applications [89], including photovoltaic devices, biosensing and imaging, light-emitting diodes (LEDs), photodetectors, display devices and lasers. Interest in the use of quantum dots for lasers stems from the three-dimensional quantum-confinement effects on the carriers that promise lower threshold, better temperature stability and narrower linewidth when compared to lasers that use gain regions with a lower level of confinement [89, 94]. Epitaxially-grown quantum dot lasers have been demonstrated and have shown some of this promise [95]. However, epitaxial quantum dots are relatively large (typical sizes above 10 nm) which leads to a weak confinement regime and thus the wavelength tunability can usually be achieved via choice of material. In addition, the epitaxial growth is rather complex compared to the simple chemical synthesis technique used in the growth of CQDs.

On the other hand, CQDs have strong quantum confinement as stated before, and are compatible with simple solution-processing. Owing to their characteristics including the compatibility with non-planar substrates, CQDs certainly have a role to play in the rapidly developing field of flexible or conformal photonics.

In a small CQD, the lowest radiative decay can be considered in a two-level system, in which two electrons (with one spin up and the other spin down) are in its ground state due to the rule of quantum mechanics. To reach the population inversion, one has to excite both these two electrons from ground state up to the excited state. This results in two $e-h$ pairs (i.e. biexciton).

As required for laser action, optical gain in CQDs was first demonstrated by

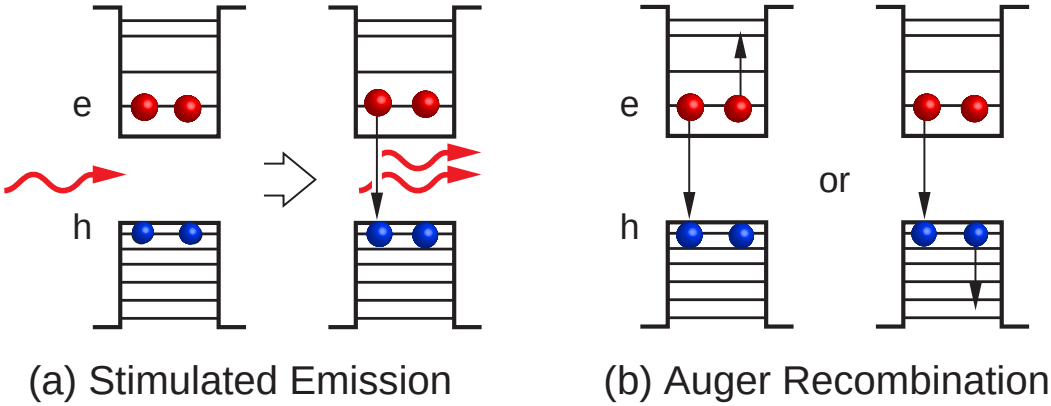

Figure 1.13: (a) In CQDs, the lowest optical transition can be simply considered as a two-level system having two electrons in the ground states. When both electrons are excited, CQDs can generate optical gain (i.e. population inversion). An incident photon triggers one electron to release another photon that is called *stimulated emission*. (b) The energy from $e-h$ recombination can also be transferred to either an electron or a hole, the process of which is called *nonradiative Auger recombination*. Adapted from Ref. [93].

V. Klimov and M. Bawendi *et al.* [96]. Using a two-level system with twofold spin-degenerate states to model the band-edge emission on CQDs, one finds that, for example in CdSe CQDs, population inversion occurs (i.e. having optical gain) when a carrier density of $N_{eh} = 1$ and completes (i.e. experiencing gain saturation) when $N_{eh} = 2$, where N_{eh} is the average number of electron-hole ($e-h$) pairs (excitons) per dot [93, 96]. This suggests that optical in CdSe CQDs relies on multiexciton states.

However, it was noted that Auger recombination in the CQDs (Fig. 1.13) can reduce the gain lifetime, via nonradiatively transferring the energy of an exciton (electron-hole pair) to a third charge carrier [99]. So far, engineering CQD material design [100] and/or using state-resolved (see e.g. subband structures and the corresponding absorption spectrum for CdSe CQDs shown in Fig. 1.14) optical pumping [101] can be used to boost gain performance. Studies show that core-shell nanosctructures can be either tailored to be in the so-called 'Type I' or 'Type II' regimes (Fig. 1.15). In particular, for Type II CQDs, Klimov *et al.* demonstrated that the Auger recombination can be eliminate when tailoring the core-shell nanostructure properly, and lasing can occur in the single-exciton regime (Fig. 1.16).

Also, shaping the spherical CQD structure into a rod-like nanocrystal (see two typical nanostructures in Fig. 1.17) has also been demonstrated to improve of

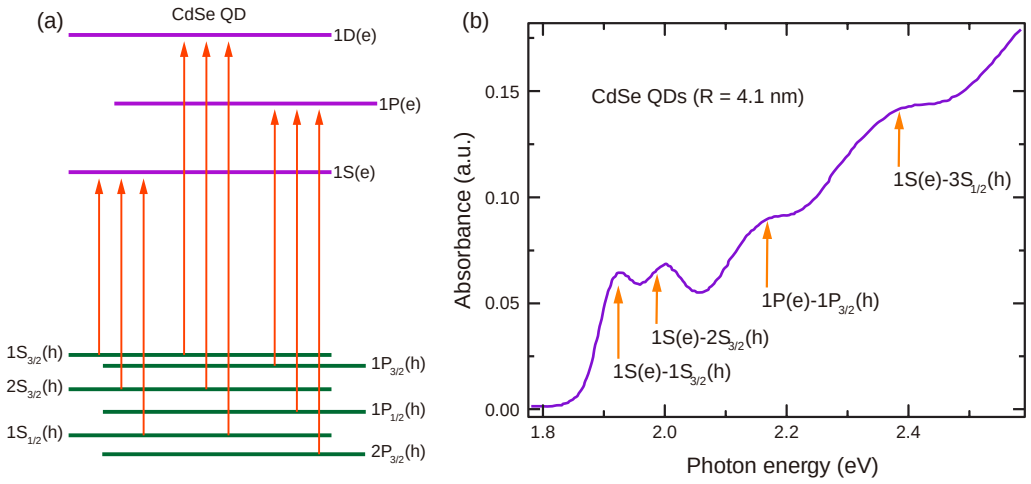

Figure 1.14: (a) Subband structures in a CdSe CQD, in which the arrows show the allowed interband optical transitions; and (b) linear absorption spectrum of 4.1-nm CdSe CQDs, in which arrows indicate transitions involving $1S/1P$ electron states. Adapted from Ref. [94].

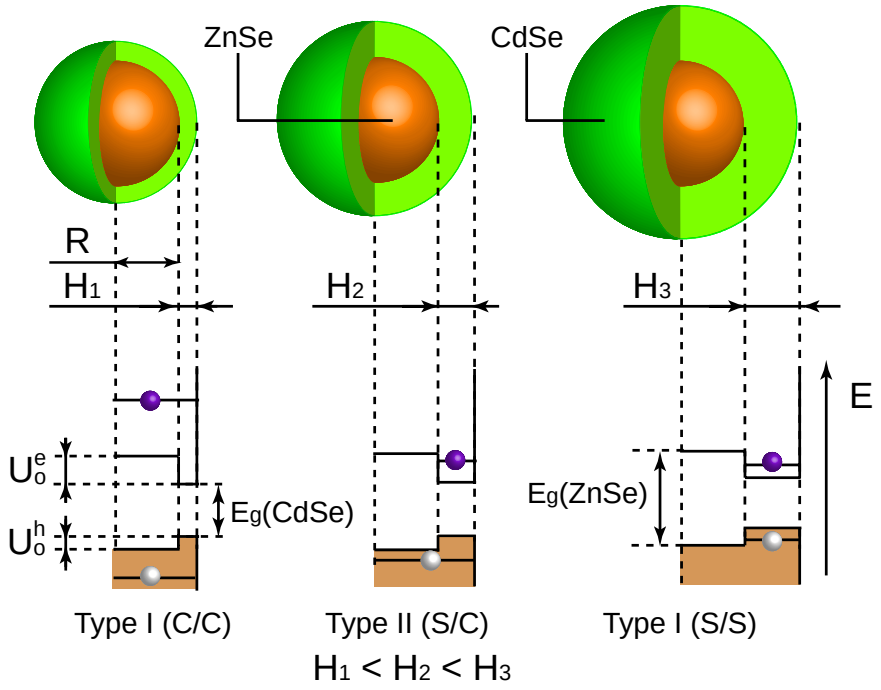

Figure 1.15: Core-shell nanosctructures can be tailored in regimes either called 'Type I' or 'Type II'. For Type I CQDs, both an electron and a hole are located in the same part of nanosctructure. For Type II CQDs, electrons and holes are separated and located in different parts of the core-shell nanosctructure. Adapted from Ref. [97].

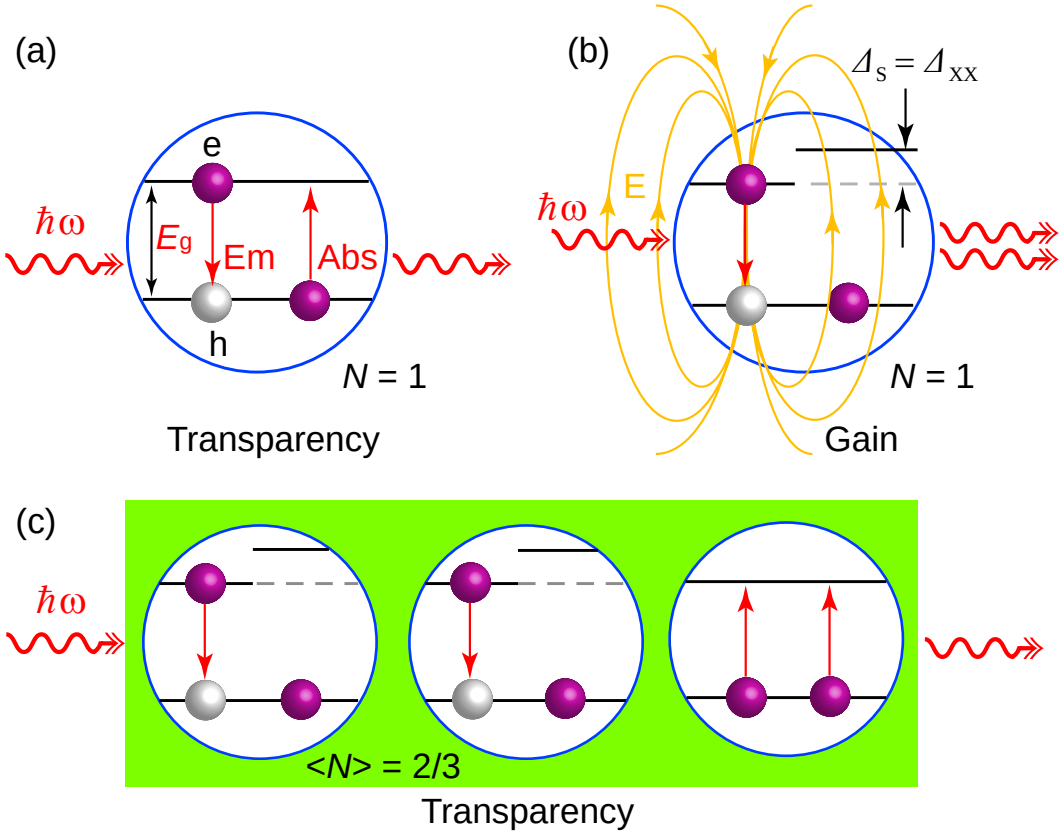

Figure 1.16: (a) Without the exciton-exciton (X−X) interaction, stimulated emission is washed out by self-absorption. (b) If taking into account the X−X interactions that spectrally displace the absorbing transition with respect to the emission band, the balance between stimulated emission and self-absorption can be broken. This can be attributed to the transition Stark shift ($\Delta_S = \Delta_{XX}$) induced by a local electric field (**E**) associated with a single-exciton state. Optical gain can occur in the single-exciton regime when the transition shift is greater than the ensemble spectral linewidth. (c) When Δ_S is large, stimulated emission in singly excited CQDs (assumed that their fraction in the CQD ensemble is n_x) competes only with self-absorption in unexcited CQDs [multiexcitons is neglected and their fraction is $(1-n_x)$]. The stimulated emission cross section of a singly excited CQD is one half of the absorption cross section of the lowest-energy CQD transition. Given that, one can finds that the condition $n_x/2 = (1 - n_x)$ is for the optical gain threshold. This suggests that the single-exciton gain onset corresponds to the situation in which 2/3 of the CQDs are excited with single excitons. Adapted from Ref. [98].

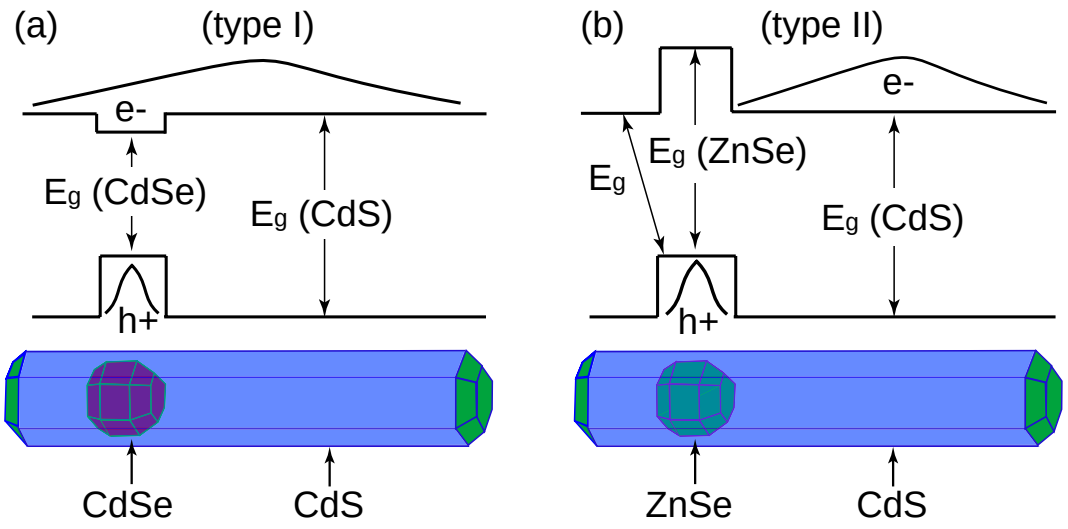

Figure 1.17: Schematic diagrams of two typical core-shell nanorod structures: (a) Type I CdSe/CdS and (b) Type II ZnSe/CdS, with their band structures and the electron and hole ground-state wave functions. Adapted from Ref. [102].

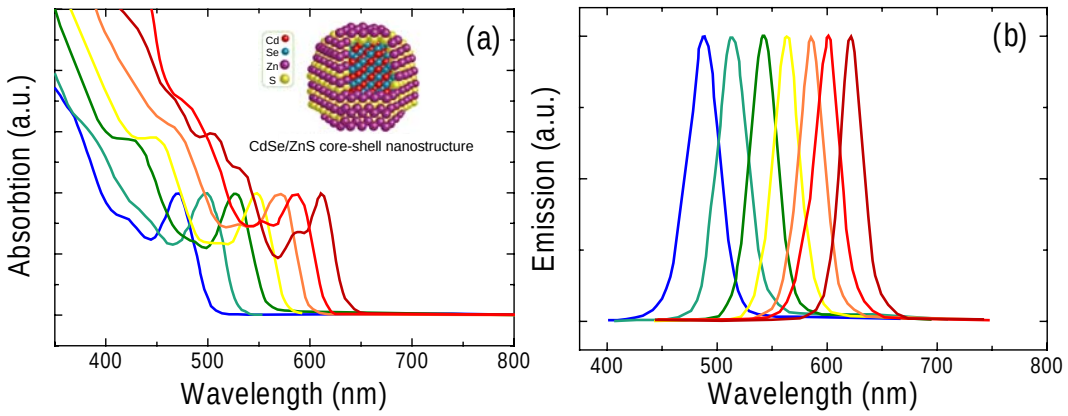

Figure 1.18: (a) Absorption and (b) emission of CdSe/ZnS core-shell nanostructure [inset in (a)] with core (CdSe) sizes in the range of 2-6 nm. Adapted from Data Sheet from *Evident Technologies, Inc.*

gain and lasing performance including suppress the Auger recombination leading the increasing of gain lifetime and thus reduced the lasing threshold. Nevertheless, the fabrication of spherical CQDs is more mature than rod-shaped nanocrystals and only spherical CQD products are commercially available at the moment. Thus this is part of the reason we chose CdSe/ZnS CQDs as our gain material for fabricating novel laser structures (see Chapters 2 and 3). The basic optical properties of these CQDs is summarized in Fig. 1.18.

1.4.2 Semiconducting (Conjugated) Polymers

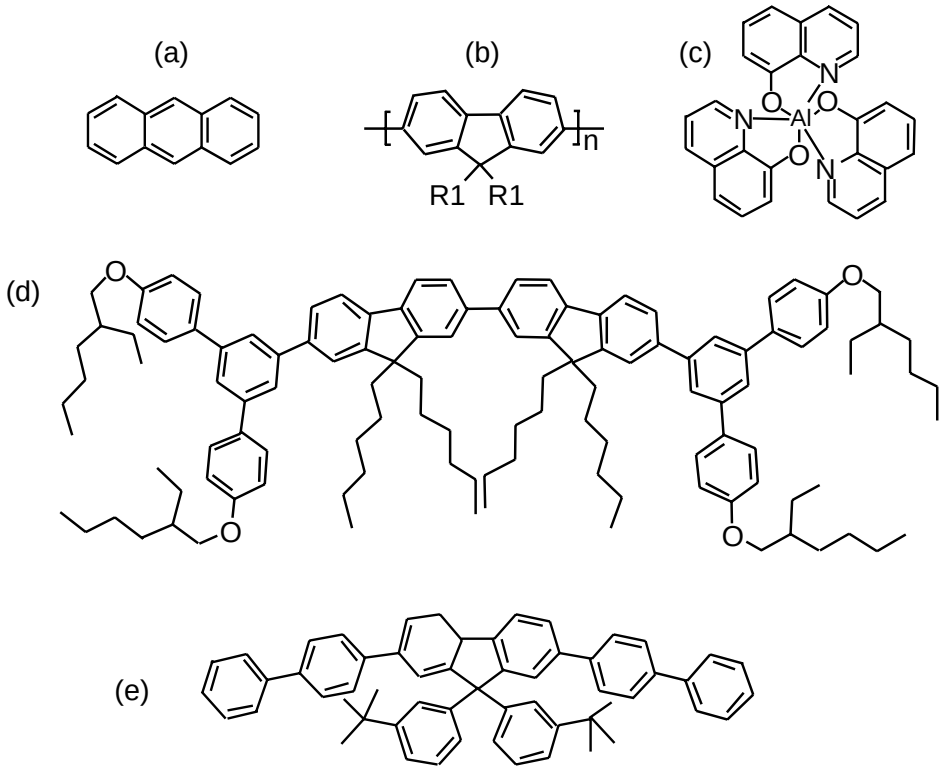

Figure 1.19: (a) anthracene, (b) aluminum tris(quinolate), (c) generic polyfluorene derivative, (d) bisfluorene cored dendrimer, and (e) spirolinked oligomer. Adapted from Ref. [26].

In general, based on the chemical structural features (see Fig. 1.19), there are four types of organic semiconductors (i.e. conjugated molecules) that are capable of lasing [26], including small molecules [e.g. aluminum tris(quinolate)], conjugated polymers [e.g. poly(*p*-phenylene vinylene) (PPV) and polyfluorene], conjugated dendrimers [that typically have a core chromophore with conjugated branches], and spiro-compounds (that usually formed by two coupled oligomers via a spiro-linkage). Regarding the processibility of organic semiconductors, it is noted that, normally, small molecules can only be produced via vacuum deposition, while conjugated polymers may be processed from solution via using precursor routes or attaching soluble sidechains to the polymer backbone. Adding side chains onto the monomer units of PPV can also generate various derivatives with modified energy gaps covering the visible spectrum.

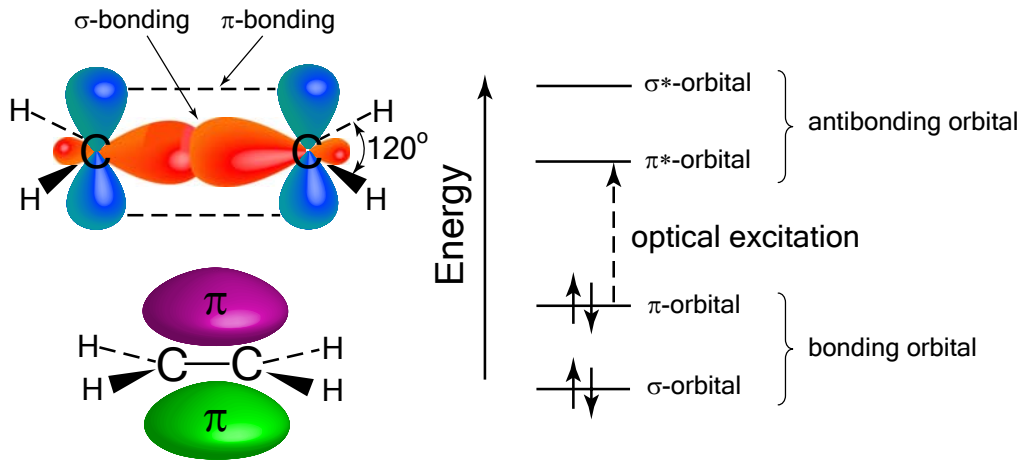

Figure 1.20: A π-conjugated electron system: (*left panel*) σ- and π-bonds in ethene as a simple example of such a system; (*right panel*) electronic excitation between $\pi - \pi^*$ orbitals. Adapted from Ref. [103].

.

Photophysics of Semiconducting Polymer

Semiconducting (conjugated) polymers have a conjugated π-electron system that is formed by the P_z-orbitals of sp^2-hybridized C-atoms in the molecules (Fig. 1.20). The π-bonding is much weaker compared to the σ-bonds forming the backbone of the molecules. Transitions between $\pi - \pi^*$ obitals thus becomes the lowest electronic excitation of a conjugated polymer and usually the energy gap of such a transition is in the range of visible light. The bandgap can be modified by the effective conjugation length, that is the extent of π-delocalization along the backbone. Unlike dye molecules, the emission of which can easily be quenched in their solid-state, semiconducting polymers with highly efficient and stable emission in their solid-state have been improved via, for example, increasing the chemical purity [105] and/or introducing bulky substitution of side groups [106] to separate the polymer chains.

The simplified electronic energy levels of semiconducting polymers are illustrated in Fig. 1.21(a), indicating charge states, singlet excitons and triplet excitons. A singlet state has the total spin of 0, meaning that all electron spins in a molecule are paired; while a triplet state has the total spin of 1, meaning that a molecule has two unpaired electron spins. According to the selection rules of quantum mechanics, the transition from triplet state to singlet state is 'forbidden' through radiatively decay behaviour. Thus the triplet excited states are called metastable states, which usually have lifetimes in the order of millisec-

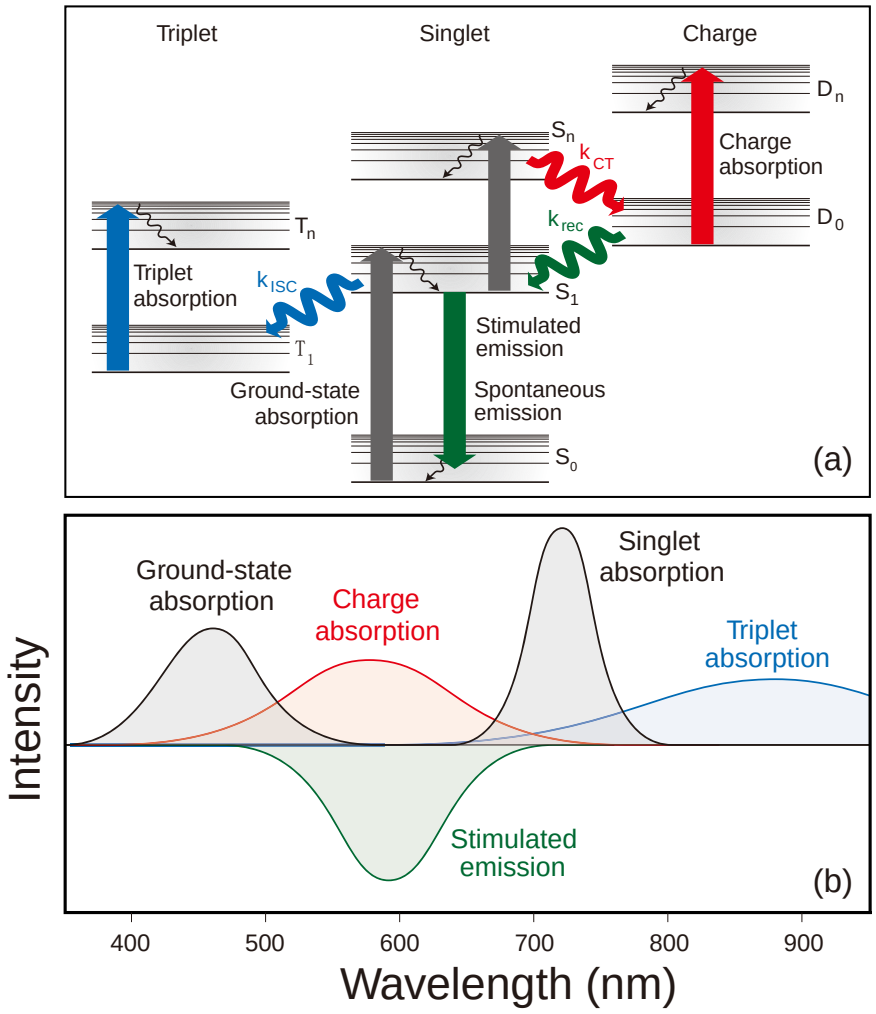

Figure 1.21: Optical properties of organic semiconducting polymers: (a) energy level structure (rate constants: intersystem crossing k_{ISC}, charge generation k_{CT}, charge recombination k_{rec}); and (b) idealized spectra of semiconducting polymers. Adapted from Ref. [104].

.

onds to seconds, while the lifetimes of the singlet excited states are in the order of nanoseconds down to picoseconds through the decay of radiative transition. The triplet states hinder the realization of population inversion thus lasing applications. The optical transitions are illustrated by vertical arrows; while the non-radiative transitions (including vibrational relaxation, intersystem crossing, charge generation/recombination) are illustrated by wavy arrows. For most conjugated polymers, their stimulated emission spectrum overlaps with the spectrum of charge absorption, as indicated in Fig. 1.21(b).

Most importantly, population inversion, a key step to lasing, is easy to achieve

in a conjugated polymer, since the electronic structure can be regarded as a four-level laser system. As illustrated in Fig. 1.21(a), both ground state S_0 and excited state S_1 are split into a series of vibronic states. During the photopumping process, a photon excites an electron from S_0 to S_1 to form a singlet exciton. The excited singlet exciton can then relax to a lower sublevel in S_1 non-radiatively. The optical emission can be amplified via stimulated emission when the conjugated polymer is under the condition of population inversion. Once the feedback is strong enough to overcome the losses including the self-absorption of the material, laser action can occur in the conjugated polymer system.

Tremendous efforts have been put into the development of organic semiconductor lasers making this field in a very promising optoelectronic frontier, details of which can be obtained from literature review [26, 107–114] and references therein.

Poly(*p*-phenylene vinylene) and its Derivatives

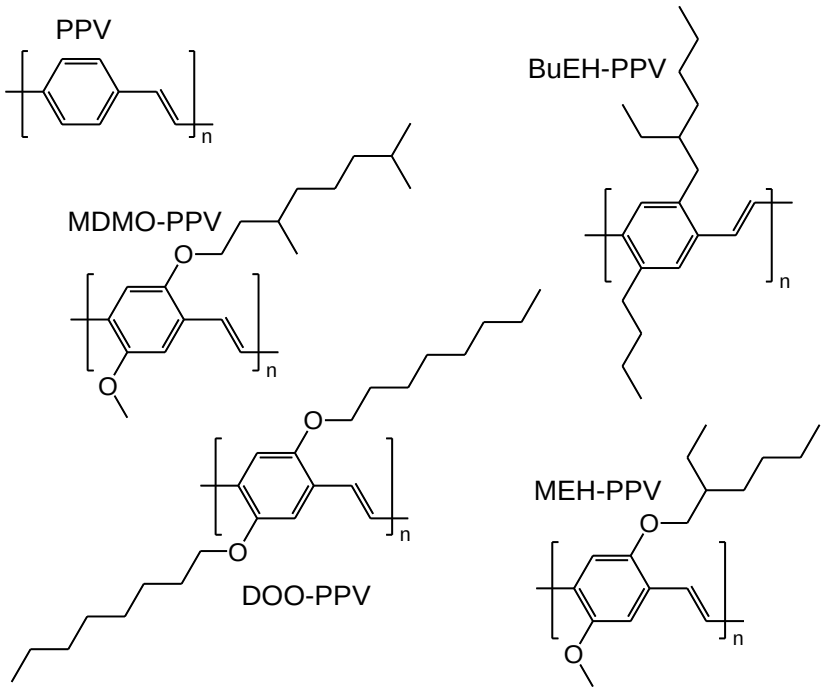

Figure 1.22: Chemical structures of PPV and its derivatives: MDMO-PPV: poly(2-methoxy-5-(3'-7'-dimethyloctyloxy)-1,4-phenylenevinylene); DOO-PPV: poly(2,5-dioctyloxy-1,4-phenylene vinylene); BuEH-PPV: poly(2,butyl-5-(2'-ethylhexyl)-1,4-phenylene vinylene); MEH-PPV: poly(2-methoxy-5-(2'-ethylhexyloxy)-1,4-phenylene vinylene).

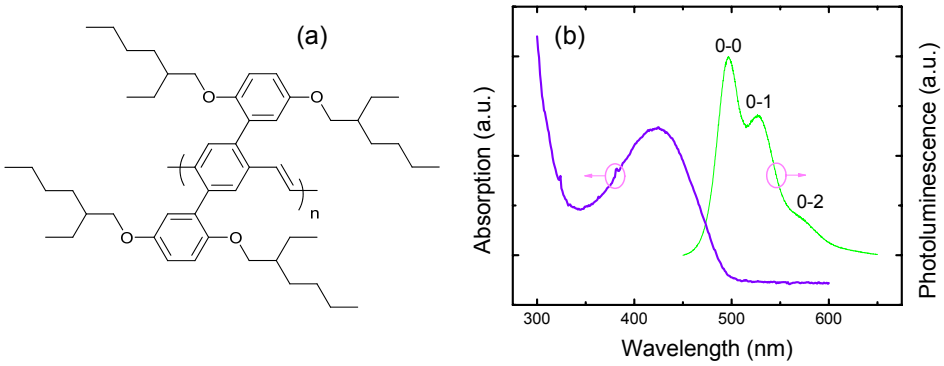

Figure 1.23: (a) Chemical structure of the green organic conjugated polymer: BBEHP-PPV, and (b) absorption and photoluminescence spectra of a BBEHP-PPV thin film on a glass substrate, spin-coated from toluene solution (10 mg/mL). The PL spectrum shows two peaks at around 492 nm (0-0 transition) and 527 nm (0-1 transition), and a shoulder peak at around 575 nm (0-2 transition).

Among many types of conjugated polymers that have been studied as laser materials, the poly(phenylene vinylene) (PPV) family, several chemical structures of which can be seen in Fig. 1.22, have demonstrated particularly promising properties. These include high gain, low threshold, large emission cross section (about 4×10^{-16} cm^2 [115]) as well as great tunability of emission wavelength.

Gain in PPV was first reported by M. Yan *et al.* [115], however, the small value lead the authors to reach the conclusion that '*PPV film lasers are not viable*'. Given that they were aware of the fact that a PPV derivative (MEH-PPV) had already demonstrated lasing [116] though in solution rather than in a solid-state film, their experiment suggested a dominant photo-induced absorption leading to a reduction of net gain. Such a view did not last long, since R. Friend's group soon demonstrated the first solid-state conjugated polymer laser using a 100-nm thick PPV thin film in a F-P cavity structure [117], possibly due to refinements in the synthesis of PPV [112]. Nevertheless, credit should go to M. Yan and coauthors for pointing out that substitution of side groups to the PPV backbone may improve the gain performance [115]. A series of PPV derivatives having different substitution of side groups indeed have demonstrated as promising lasing materials [118].

In this work, poly[2,5-bis(2,5-bis(2-ethylhexyloxy)phenyl)-*p*-phenylene vinylene] (BBEHP-PPV) was used as the organic gain material, the chemical structure and absorption/PL spectra of which are shown in Fig. 1.23. BBEHP-PPV was first synthesized in Swager's group [119] and applied to the application of

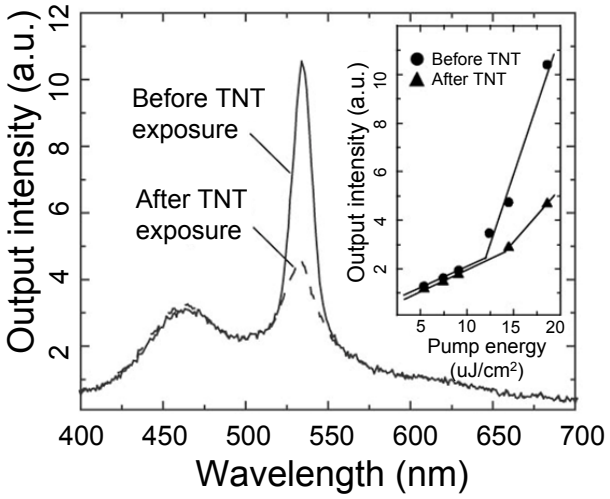

Figure 1.24: Spectral response of ASE emission in BBEHP-PPV laser ring-mode structure before and after exposure to explosive 2,4,6-trinitrotoluene (TNT) molecules vapour pressure. Inset: ASE peak intensity versus pump energy density. Adapted from Ref. [119].

sensing trace vapours of explosive 2,4,6-trinitrotoluene (TNT) molecules (Fig. 1.24). More optical properties of BBEHP-PPV can be referred to Chapter 4.

One drawback that may affect the practical application of conjugated polymers as laser materials is photo-oxidation. Such behaviour may create defects (e.g. C=O species) [120], acting as quenching sites to stop the emission and thus preventing laser action. In our case, it is noteworthy to point out that the molecular structure of BBEHP-PPV effectively encapsulates the polymer backbone via the attached parallel-oriented hydrocarbon side chains. This generates a protective sheath hence limiting self-quenching and potentially enhancing the resistance to photo-bleaching [119].

It is also useful to further incorporate organic gain materials into a host matrix that can prevent them from degrading by isolation from oxygen and water molecules. One of our tactics in order to encapsulate the gain polymer is using a highly UV transparent polymer, 1,4-cyclohexanedimethanol divinyl ether (CHDV) [Fig. 1.25(a)] as a polymer matrix to form composite materials. This is UV-cured to form any shape like a free-standing membrane or rod-structure [Fig. 1.25(b)], thus avoiding the exposure to water and oxygen. The CHDV matrix can be used either as a UV transparent patterned substrate (see Chapter 2), or as host to incorporate gain material (see Chapter 4), and both can be mechanically flexible. In both cases, a UV initiator (the 'photo-acid generator' or PAG) for cationic polymerization, para-octyloxy-functionalized diphenyliodonium hexafluoroantimonate (*Gelest, Inc.*), is added to trigger the photo-crosslinkable behavior via the vinyl ether moieties [121]. This crosslinking process is achieved when the vinyl ether moieties polymerize, and a carbon-based backbone with associated vinyl ether groups is produced [121, 122].

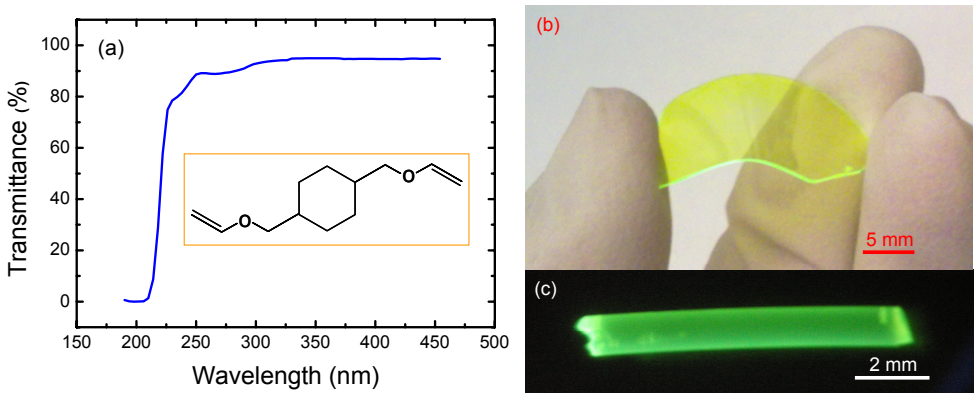

Figure 1.25: (a) Transmission spectrum of the UV transparent polymer matrix for a 20-μm thick film (photoacid generator: 0.5 wt.%). Inset: chemical structure of CHDV monomer, and BBEHP-PPV/CHDV composite cured in the shape of (b) membrane and (c) rod-structure.

The sources of the key materials used in this work are as follows:

- CdSe/ZnS core-shell QDs were purchased from *Evident Technologies, Inc.* and *Sigma-Aldrich Co.*
- BBEHP-PPV were synthesized in Prof. Peter Skabara's research group in the *Department of Pure and Applied Chemistry, University of Strathclyde.*

1.5 Thesis Overview

Bearing in mind the basic foundations of lasers as well as the background knowledge of solution-processable gain materials, the following chapters are categorized into two Parts, which are dedicated to demonstrating laser action in gain media based on either colloidal quantum dots (Part II: Chapters 2 and 3) or semiconducting polymers (Part III: Chapters 4 and 5). Alternatively, the main chapters can be seen as demonstrations of laser action in the form of either a distributed feedback grating structure (Chapters 2 and 4) or a random laser system (Chapters 3 and 5). In the broadest sense, the motivation behind this is to investigate novel laser devices, harnessing the advantages of solution-processable gain materials. For example, they can find niche applications in the rapid development of flexible photonic area, which is one of our further moves in terms of using these new laser devices. Brief concluding remarks with a few perspectives on this rapidly growing field of novel laser devices using solution-processed gain media are summarized in Chapter 6 to complete this thesis.

Part II

Colloidal Quantum Dot (CQD) Lasers

Chapter 2

Flexible DFB CQD Laser

In this chapter, by fabricating a submicron-scale grating structure on a bendable polymer substrate, we demonstrate a flexible distributed-feedback colloidal quantum dot laser. This laser uses cadmium selenide/zinc sulphide (CdSe/ZnS) core-shell nanostructures. It operates in transverse electric polarized multiple-modes, and has a typical threshold pump fluence of $\sim$4 mJ/cm^2.

2.1 Introduction

Flexible-optoelectronics has seen much attention in recent years and examples of resulting applications in which the associated robustness, light weight and ease of fabrication are key factors include flexible displays, sensors, solar cells and electronic paper [123–125]. Lasers form another very important category of device which would benefit from embodiment in mechanically flexible format, in particular if they can be manufactured conveniently by solution-based processing techniques. Colloidal quantum dots (CQDs), such as cadmium selenide/zinc sulphide (CdSe/ZnS) core-shell nanostructures, are attractive solution-based gain materials. They are promising for laser devices due to their spectral size-tunability and temperature stability [96, 126, 127]. The background information of CQDs as laser device building blocks can be seen in Subsection 1.4.1 in Chapter 1.

To date, most CQD laser demonstrations have been based on whispering-gallery-mode structures [128–130] or rigid distributed-feedback (DFB) substrates [131, 132]. Solution-processed mechanically-flexible laser devices are, by contrast, typically fabricated by an all-organic material approach [124, 133, 134], although there is a recent report on a vertical cavity surface emitting laser structure incorporating indium gallium phosphide (InGaP) CQDs [135]. Here we report the fabrication and characterization of a flexible DFB CdSe/ZnS CQD laser based on a UV transparent polymerizable matrix patterned by a submicron grating structure.

2.2 Sample Preparation and Photo-pumping Setup

2.2.1 Sample Fabrication

The basic physics of a DFB laser has been described in Subsection 1.3.1, Chapter 1. For the DFB laser structure fabrication [Fig. 2.1(a)], a simple approach based on a standard commercially available blank digital versatile disk (DVD) was investigated. The blank DVD was immersed in methanol in an ultrasonic bath for about 10 seconds to remove the upper protecting layer. The 'bare' DVD was then used as a replication mask to pattern a submicron-scale grating structure into the UV transparent polymerizable soft-material, 1,4-cyclohexanedimethanol divinyl ether (CHDV). The CHDV (with 0.2 wt.% photoacid generator) monomer solution was drop-coated onto the prepared DVD and exposed under an ultraviolet

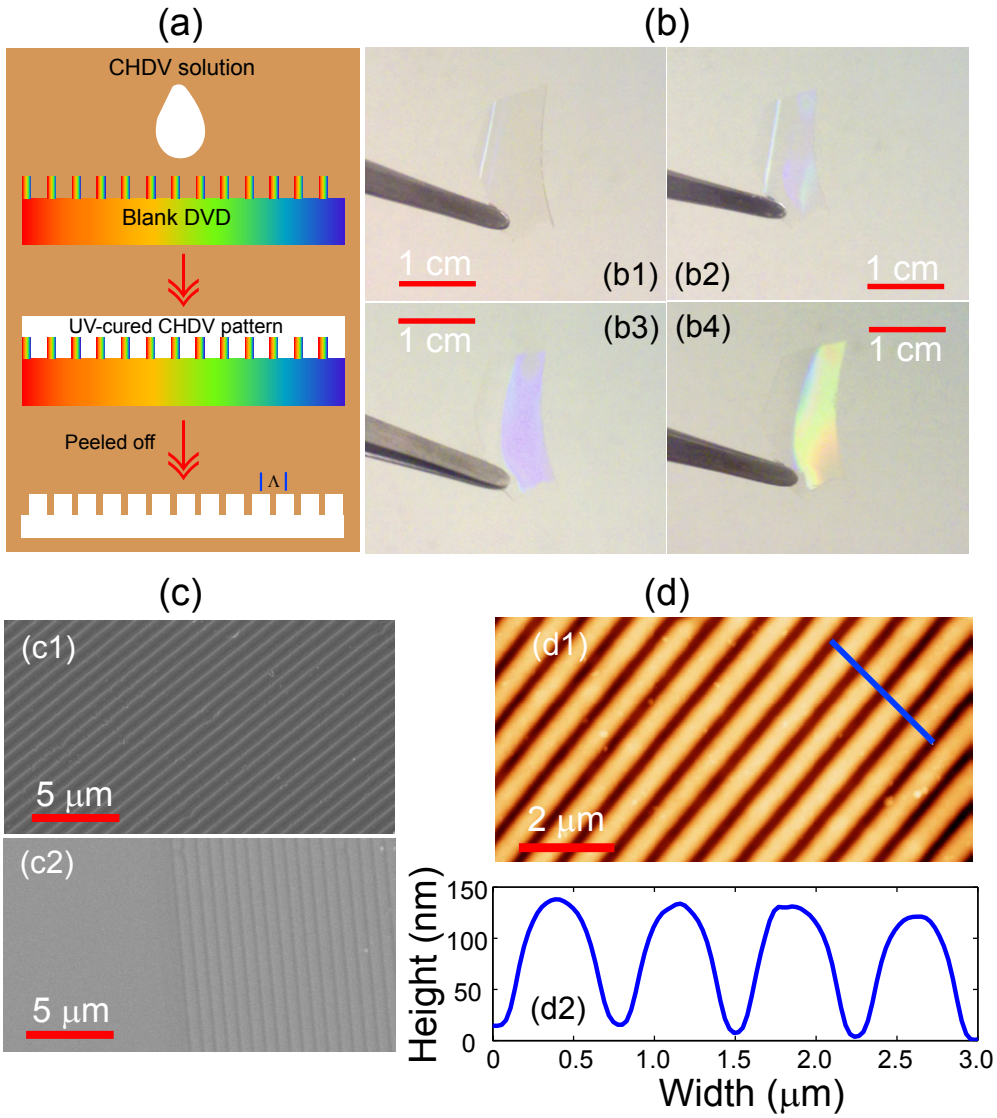

Figure 2.1: Fabrication of flexible DFB substrate: (a) diagram of the fabrication process; (b) colourful photographs (taken from different angles) of the as-prepared CHDV substrate showing light diffraction caused by grating structure; (c) SEM images of (c1) blank DVD as the mask and (c2) grating structure; (d) AFM image (d1) of the replicated grating and (d2) profile of modulation depth corresponding to the line marked in (d1).

(UV) lamp (power density: 200 mW/cm^2) with a wavelength centered at 370 nm for 10 min [134]. The resulting solidified CHDV film (thickness: 50-300 μm) was then peeled off to form a flexible free-standing substrate [Fig. 2.2(a)] with the replicated submicron grating on its surface. The area of this patterned flexible substrate is several cm^2, the exact size depending on the DVD master and on the amount of CHDV material used.

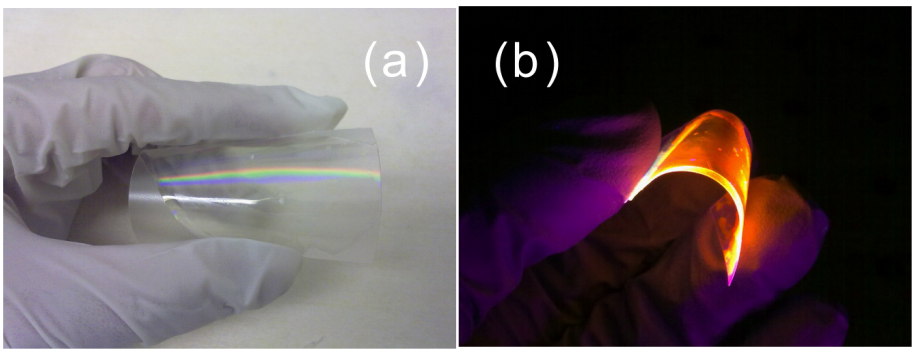

Figure 2.2: Photographs of bending the flexible DVD-grating-patterned CHDV substrate: (a) without and (b) with CQDs coated on the surface (illuminated by a UV lamp).

Fig. 2.1(b) shows photographs of such a free-standing transparent grating-patterned substrate taken from different angles to show the colourful diffraction effect generated by the periodic submicron structure on its surface. The submicron grating structure replicates the commercial track standard of DVD production, with a periodicity of 740 nm, confirmed by measurement made using scanning electron microscope (SEM) and atomic force microscopy (AFM). The SEM images shown in Fig. 2.1(c) indicate that the grating structures for bare DVD and as-prepared CHDV substrate are complementary. The surface profile analyzed from the AFM image shown in Fig. 2.1(d) indicates that the modulation depth of the grating structure is about 130 nm [Fig. 2.1(d2)]. Once this flexible grating substrate was peeled off, solution-based CdSe/ZnS core-shell CQDs (Evidot from *Evident Technologies, Inc.* or Lumidot^{TM} from *Sigma-Aldrich, Inc.*) were drop-coated onto it to form the gain layer [Fig. 2.2(b)]. This deposition method was chosen in order to obtain a CQD density high enough for stimulated emission [96]. However, it also leads to CQD layer thicknesses and inhomogeneity that result in a structure capable of sustaining a high number of modes. Therefore we can expect such CQD lasers to oscillate simultaneously on several modes around the gain maximum. This has however some benefits, as will be shown below, because stimulated emission between 610 nm and 640 nm can be obtained with the same grating structure by simply choosing the CQD mean size.

2.2.2 Photo-Pumping Setup

A frequency-tripled Q-switched Nd:YAG laser [127] (wavelength 355 nm, pulse width 5 ns and repetition rate 10 Hz) was applied to photo-pump the CQD laser sample (Fig. 2.3). The pump energies can be tuned from 6 nJ to 3 mJ per pulse.

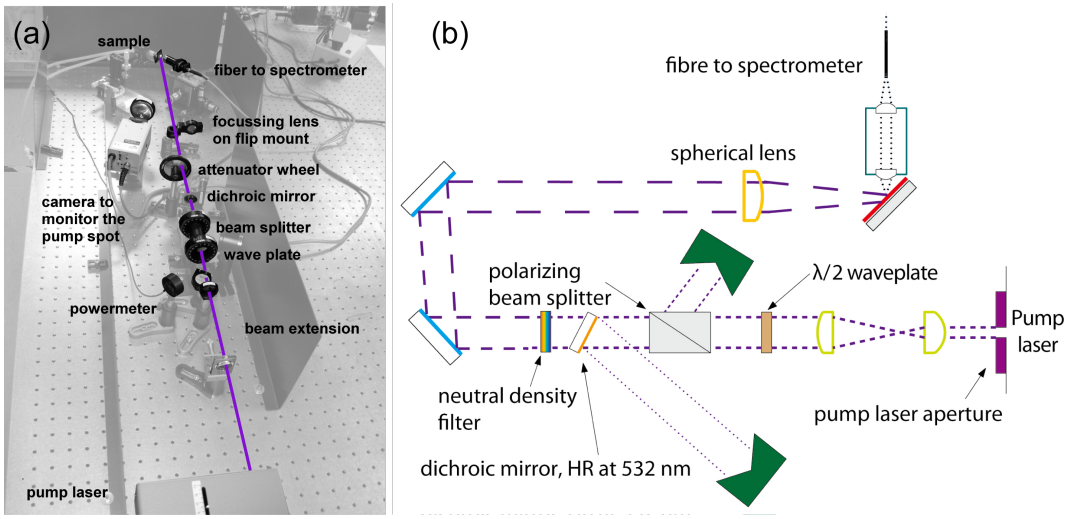

Figure 2.3: Photo-pumping setup for the DFB CQD lasers: (a) photograph (Courtesy of J. Herrnsdorf) and (b) schematic diagram.

532 nm light leaking from the laser aperture is filtered by a dichroic mirror. A $\lambda/2$-waveplate, a polarizer and an attenuator wheel together are used to control the pump energy. A spherical lens (focus length: 15 cm) was used to focus the pump beam at about 45^o to the sample surface, resulting in an excitation spot size of about 1.5 mm^2 [see the pump spot profile in the inset of Fig. 2.4(a)]. For spectral measurement, a fibre-coupled spectrometer (Avantes) having two channels with respective spectral resolutions of 2.4 nm and 0.13 nm was aligned to collect emission from the laser.

2.3 Measurement of Laser Action and Performance

2.3.1 Signature of DFB Lasing

When pumping at low fluence, only the 0th, 1st, 2nd and 3rd diffracted orders from the pump laser are observed [see spots from right to left respectively in a screen 10-cm away from the sample shown in Fig. 2.4(a)]. Above a certain fluence, however, a single-lobe fan-shape red beam appears [Fig. 2.4(b)] in the same direction as the 0th diffraction order of the pump, indicating the transition in the emission to lasing [133]. The angular-dependent polarization measurement, shown in Fig. 2.4(c), demonstrates that the emission of this DFB CQD laser is diffracted out of the grating plane at $\sim 50^o$ angle with respect to the normal

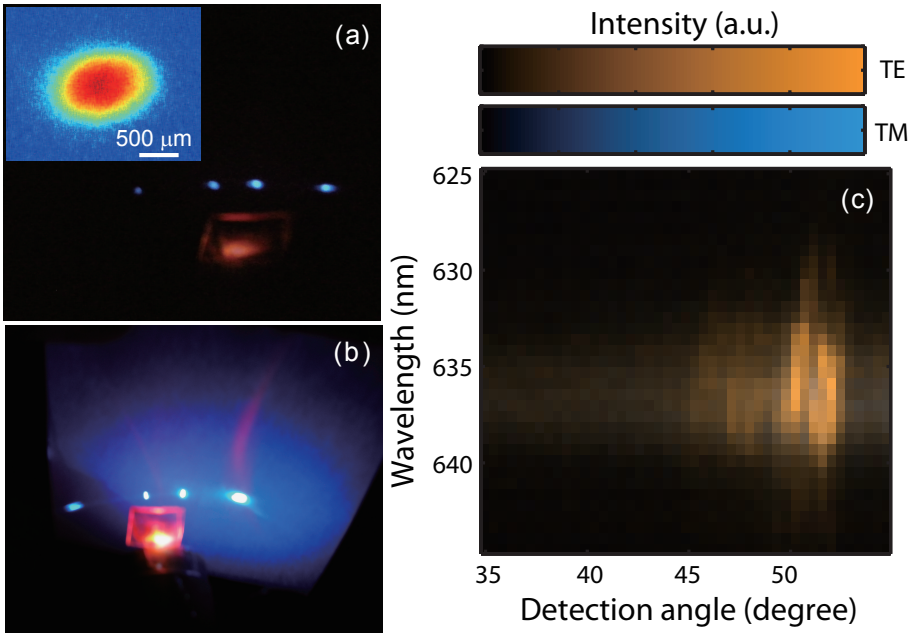

Figure 2.4: Photo-pumping demonstration of CQDs coated on the patterned CHDV substrate (1.5 × 1.5 cm^2): (a) under and (b) above the lasing threshold. Inset of (a): pump spot profile. (c) Angular-dependent measurement of DFB CQD laser emission. The corresponding '0' degree (not shown here) represents the normal to the sample surface plane.

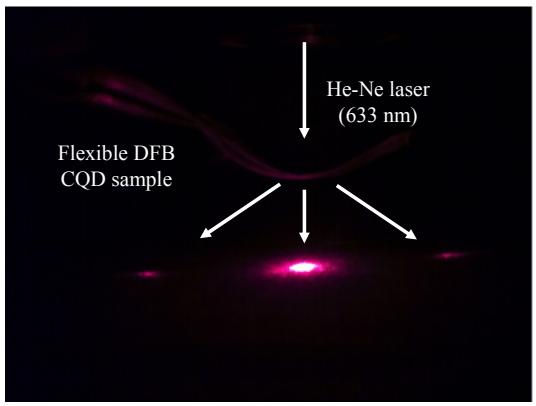

Figure 2.5: Photograph of transmitted diffraction spots using a He-Ne laser (633 nm). The 1st order diffracted angle is around 50° that is in agreement with what the grating equation predicted.

of the grating. This agrees with what Fig. 2.5 demonstrates. The emission is also mainly TE-polarized due to the grating effect, as confirmed by our further measurement (see the following). As a reference, it is noted that when using a plain substrate for the gain demonstration of CQDs, no diffracted beam emission can be observed.

Based on parameters including the central lasing peak wavelength (λ_{em} = 620 nm), the period of the grating (Λ = 740 nm), the refractive indices of the CQD layer (estimated n_{CQD} = 1.7) [131] and of CHDV (n_{CHDV} = 1.472, Sigma-Aldrich's data sheet), and taking into account the grating equation ($m\lambda_{em}$ = (1+sinθ_m)$n_e\Lambda$, where θ_m is the angle of mth diffracted order with respect to the normal and n_e is the effective refractive index of the mode guided in the gain layer embedded in the grating structure for such a DFB CQD laser) [134], the laser emission is attributed to a 4th order DFB grating effect. We identify the laser beam, which is emitted at a 50°-angle to the normal of the sample surface, with the +1 diffracted order as can be expected from the grating equation. The fact that the emitted laser beam is single-lobed means that the modes are symmetric, which can be seen as an indication that the grating effect is dominated by the gain and by inhomogeneities breaking the symmetry of the active layer [136, 137]. The second diffracted order is also visible [between the +1 and +2 pump beams in Fig. 2.4(a), i.e. around to the normal direction] but is less intense. For the laser characterization we aligned the fibre to the +1 order.

2.3.2 Emission Wavelength

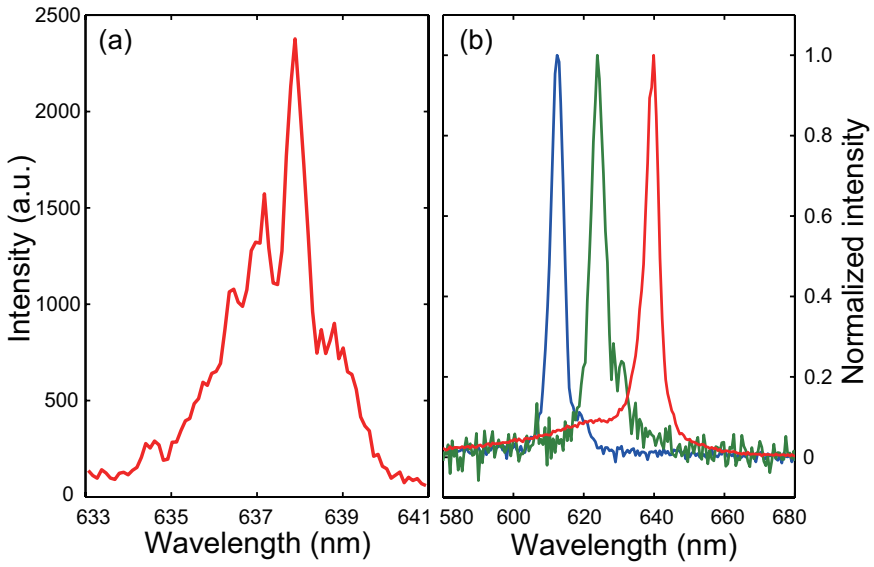

Figure 2.6: Typical DFB CQD laser normalized spectra: (a) 0.13-nm resolution spectrum showing multimode operation and (b) tunable lasing peaks using different sizes of CdSe/ZnS CQDs (2.4-nm resolution).

The flexible CQD laser emission is highly multimode. A typical spectrum above threshold, such as is shown in Fig. 2.6(a), has narrow features (< 0.3 nm)

on top of a broader 5-nm pedestal. Because such CQD lasers operate multimode around the gain peak, it is possible to obtain emission at different wavelengths by choosing CQDs of different sizes while keeping the flexible substrate characteristics constant. This is demonstrated in Fig. 2.6(b) with emission centered at 612, 623 and 638 nm for flexible grating substrates coated with different sizes (mean dot diameters of approximately 4.0, 5.2 and 5.8 nm) of CQDs, respectively. It should be also possible to achieve single-mode lasing in such laser device by improving the quality of the CQD layers (with more homogeneous dot density) and narrowing down the pump spot size (to have a rather uniform active region).

2.3.3 Bending Effect

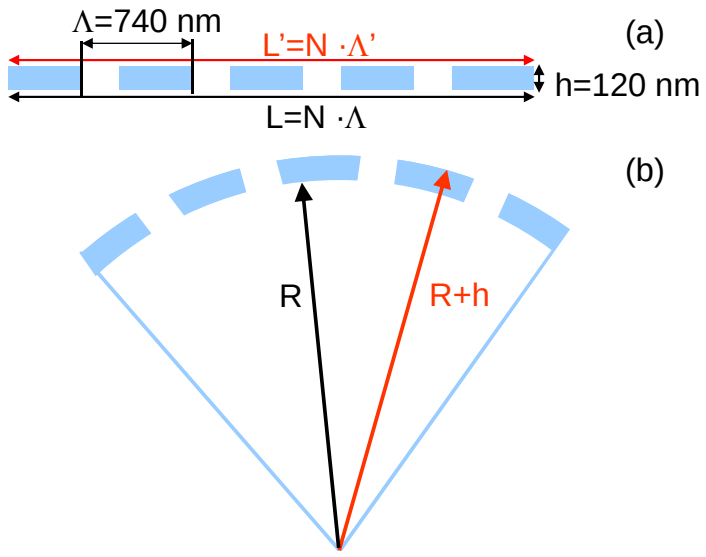

Figure 2.7: (a) Flat and (b) curved grating.

We have also studied the case when the substrate is bended (Fig. 2.7) through analyzing the transformation of the grating structure. The period of the grating base and top is the same for a flat grating, $\Lambda = \Lambda'$. When it is curved, the period of grating top will become larger than the base. From Fig. 2.7, we have:

$$\frac{L'}{R+h} = \frac{L}{R} \Rightarrow \frac{N\Lambda'}{R+h} = \frac{N\Lambda}{R} \Rightarrow \Lambda' = \frac{R+h}{R}\Lambda = (1+\frac{h}{R})\Lambda \tag{2.1}$$

We bended our CQD sample to wrap around glass vials with different cross-section profiles with R in the range of 0.5 and 2 cm (and thus the corresponding bending curvature is in the range of 2 and 0.5 cm^{-1}). Considering the DFB laser grating equation: $m\lambda_{em} = 2n_e\Lambda$, given that $h = 120$ nm, the central lasing peak

would shift by only $(h/R)\lambda_{em} < 0.02$ nm and that is far below our spectrometer's highest resolution. It is therefore no surprise that we did not notice any wavelength shift when bending the CQD laser sample. In other words, we do not have bending-induced tunability in terms of lasing emission wavelength for our CQD DFB laser. This can actually be beneficial for practical applications, since its lasing peak will not be significantly changed when it is bent.

2.3.4 Threshold Behaviour

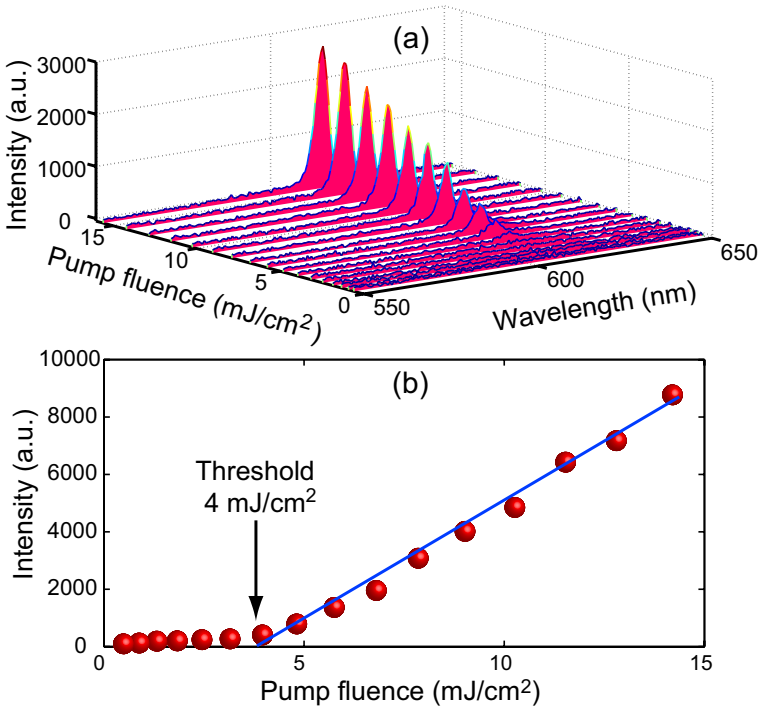

Figure 2.8: DFB CQD laser emission behaviour: (a) spectral evolution as the pump fluence increases and (b) its threshold behaviour.

In the following, by way of example, we present detailed characterization of one flexible DFB CQD laser sample emitting at ~612 nm. To study the threshold behaviour, the evolution of the emission spectrum was recorded at room temperature for increasing pump fluence. The result is shown in Fig. 2.8(a). The integrated peak (610-615 nm) intensity as a function of pump fluence is also plotted [Fig. 2.8(b)] and shows a lasing threshold of about 4 mJ/cm^2. The control sample made with the same CQDs deposited on a smooth substrate also showed stimulated emission albeit with a threshold more than five times higher. It is also worth pointing out that in our study on CQD random lasers [127] (see Chapter 3), the central lasing peak is 606 nm but here for the DFB CQD laser is

612 nm, even though we used exact the same size (4.0 nm) of dots. These along with previous measurements demonstrate that the grating has an effect on the CQD gain and spatial emission properties consistent with a 4th order feedback grating.

2.3.5 Lifetime Performance

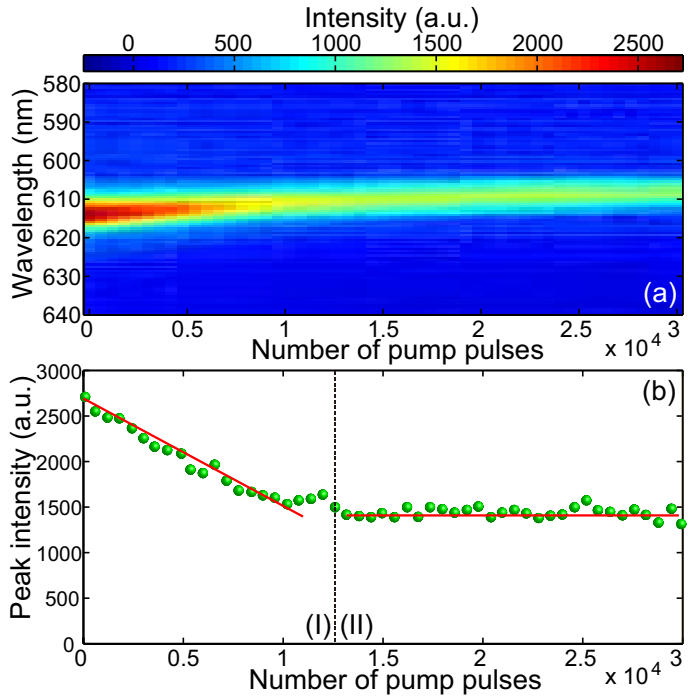

Figure 2.9: Lifetime test for the DFB CQD laser (pump fluence: 6 mJ/cm^2): (a) spectral evolution, and (b) peak intensity, as a function of the number of pump pulses.

The lifetime performance, when operating above lasing threshold at room temperature and in ambient atmosphere was then tested. Figure 2.9(a) shows the evolution of the laser emission spectrum when pumped continuously for 30,000 pulses (10 Hz) at a pump fluence of 6 mJ/cm^2. The peak intensity evolution is plotted in Fig. 2.9(b). The lasing signal initially decreases which may be due to the heating effect melting and evaporating any organic ligand attached to the dots (for instance, the Lumidot^{TM} CQD surface is stabilized with hexadecylamine ligand coating) and the remnant of toluene solvent in the gain layer, thus causing a decrease in the CQD density. Once the remaining solvent is evaporated [after about 12,500 pump pulses, region-I in Fig. 2.9(b)], the lasing signal stabilizes at 50% of its starting value, surviving for more than 17,500 pump pulses [region-II

in Fig. 2.9(b)]. One can also see that the laser emission peak has shifted from 612 to 610 nm, accompanying the decrease in the lasing signal. This effect is attributed to the change of the effective refractive index of the laser structure caused by the change of the dot density.

2.3.6 Polarization Sensitivity

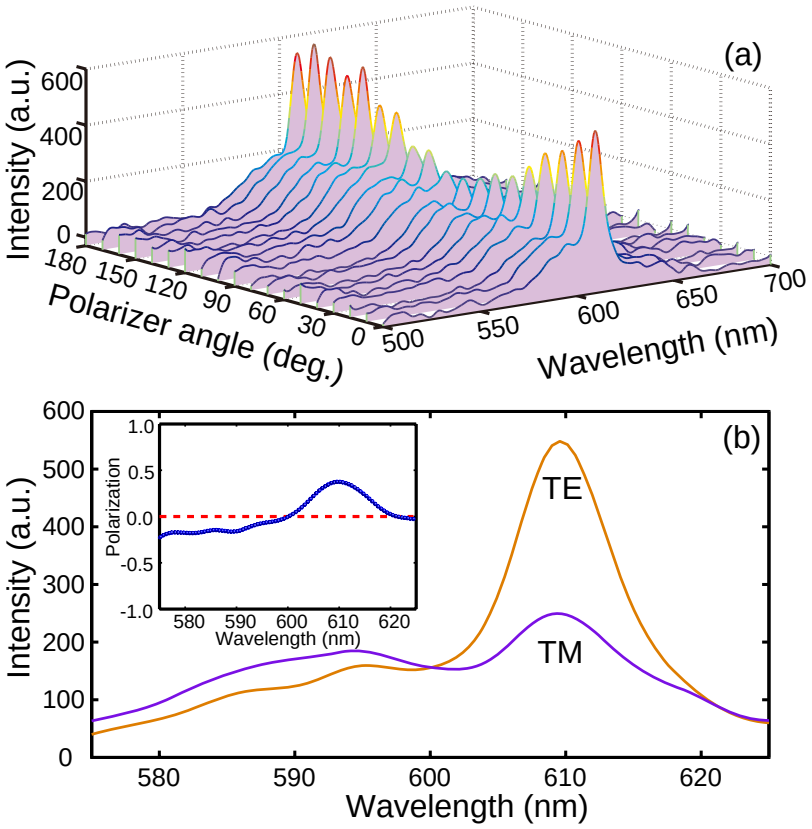

Figure 2.10: Polarization measurement on the CQD lasing behavior (pump fluence: 14 mJ/cm^2; spectral resolution: 2.4 nm): (a) spectral evolution as the polarizer rotation angle changes; (b) TE (0^o) and TM (90^o) spectra with (inset) the polarization intensity ratio of $(I_{\mathrm{TE}} - I_{\mathrm{TM}})/(I_{\mathrm{TE}} + I_{\mathrm{TM}})$.

The polarization of the laser emission was also examined [Fig. 2.10(a)]. The result reveals that the broad PL background is unpolarized, while the DFB CQD laser favours a linearly polarized transverse electric (TE) emission [Fig. 2.10(b)]. The unpolarized PL emission is in agreement with a previous polarization study on circular-shape CQDs (Ref.[138]) and the favoring of TE polarized lasing emission is mainly due to the DFB laser structure itself rather than anything related to the specific gain material [133]. This, together with the angular-dependent

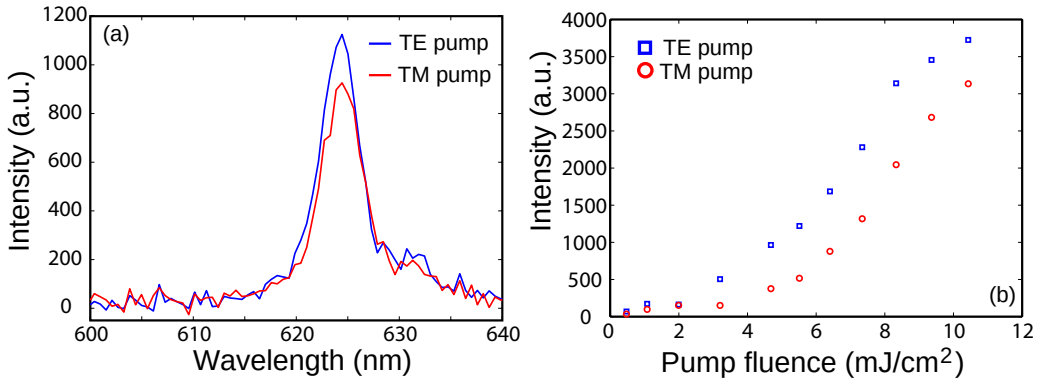

Figure 2.11: Pump-polarization-dependent emission of DFB CQD laser: TE/TM pump (a) spectra and (b) threshold curves.

polarization measurement we showed in the previous discussion confirms that the TE-polarization is indeed brought about by the grating effect.

The influence of the polarization of the pump laser was also studied. Figure 2.11 shows the difference in the spectrum and the threshold for a given DFB CQD laser sample (lasing peak at 624 nm) when pumped by either TE or TM polarized laser beam. Here 'TE pump' means that the electric field component of the pump beam is parallel to the DFB grating, while 'TM pump' means that the electric field component is perpendicular to that direction. The multimode laser emission appears smoothed out in Fig. 2.11 because of the low instrument resolution chosen for this particular measurement. Under constant fluence, the peak intensity of the TE pump spectrum is higher than that of the TM pump. The threshold for the TE pump case is also significantly lower than for the TM pump at 3 mJ/cm^2 and 5 mJ/cm^2 respectively. This suggests that for a 1D grating laser structure, the polarization of the pump laser can have an impact on the lasing threshold, which should be taken into account when design and put into practice a new laser device.

2.4 Summary

In summary, to harness the advantage of solution-processable CdSe/ZnS CQDs with their high gain optical properties as well as low-cost and flexible nature of polymerisable polymer matrix patterned by commercially available DVD sub-micron grating structure, we demonstrated the realization of a flexible DFB CdSe/ZnS CQD laser based on UV transparent polymer matrix CHDV. The

fabrication procedure is straightforward, and the lasing emission can be changed in a 610-640 nm spectral window simply by using different sizes of CQDs. Owing to the low-cost and ease of fabrication, such type of flexible CQD laser is thus expected to be useful in areas like reconfigurable displays and/or photonic sensor devices.

Chapter 3

CQD Random Laser

In this chapter, we report random laser action in a system where optical amplification is provided by colloidal quantum dots (CQDs). This system is obtained by depositing from solution CdSe/ZnS core-shell CQDs into rough micron-scale grooves fabricated on the surface of a glass substrate. The combination of CQD random packing and of disordered structures in the glass groove enables gain and multiple scattering. Upon optical excitation, random laser action is triggered in the system above a 25-mJ/cm^2 threshold. Single-shot spectra were recorded to study the emission spectral characteristics. The results show the stability of the laser mode positions and the dominance of the modes close to the material gain maximum.

3.1 Introduction

Random lasers have been experiencing tremendous developments in recent years. Their concept is based upon light generation and stimulated emission within a multiple-scattering medium with optical gain [41], the basic physics of which has been discussed briefly in Subsection 1.3.2, Chapter 1. Consequently, there is no conventional optical resonator in the laser system, which makes for flexible and, in the long run, potentially low-cost device fabrication. These coherent light sources resemble conventional lasers in many ways, such as spectrally narrow emission, threshold behaviour, relaxation oscillations and photon statistics [61, 139]. However they have unique characteristics that are rich for fundamental studies and which could one day open up interesting applications in areas including new generation display devices, environmental lighting, sensors, optical coding of objects, random number generators and medical diagnostics [41, 140].

To date, phenomena of random laser action have been demonstrated in non-ordered systems formed by various materials such as rhodamine 640 with TiO_2 particles [38], ZnO powder [39], polymer composites [141], rhodamine 6G doped in PMMA film incorporated with Ag nanoparticles [142], and dye-doped POSS solutions [143]. In this work, we report what is to our knowledge a novel random laser material system based on colloidal quantum dots (CQDs).

Optical gain has been demonstrated in CQDs as described elsewhere in this thesis (Chapter 1) Owing to their size-dependent emission wavelength over a broad range (i.e. colour tunability) as well as insensitive radiative transition under various temperatures (i.e. temperature stability), they offer great potential for fabricating new types of laser devices [96, 128–131, 144]. Because random laser action relies on the combined effects of multiple scattering and optical amplification, CQDs certainly appear to be an attractive material system for such applications. They can play the role of gain elements while scattering is inherently obtained by the disorder in their spatial positioning and size (although size disorder could be negligible compared to spatial disorder when using monodisperse CQDs). On the processing side, CQDs, like organic chromophores, can be deposited from solution on a wide variety of substrates and can also be blended with other materials and particles, an interesting feature for random laser experiments. Furthermore, they are inorganic in nature and are therefore quite robust, making them advantageous compared to organic gain materials. However, to the best of our knowledge, there is only one report on random lasing in colloidal CdS/CdSe/CdS quantum wells under cryogenic conditions [145], and no dedicated study on random lasers using CQDs at room-temperature has yet been

made.

The novel random laser system that we report here consists of micron-scale grooves with rough internal surfaces directly written on a glass substrate onto which CQDs are deposited from solution. The groove roughness serves two purposes: on one hand it helps trap CQDs and increases their density in order to enable stimulated emission and on the other hand it enhances light-scattering. Preparation of the system using red-emitting core-shell CdSe/ZnS CQDs and the optical pumping set-up are described in Section 3.2. Random laser action at room-temperature in this system is demonstrated in Section 3.3 and studied in detail in Section 3.4.

3.2 Experimental Part

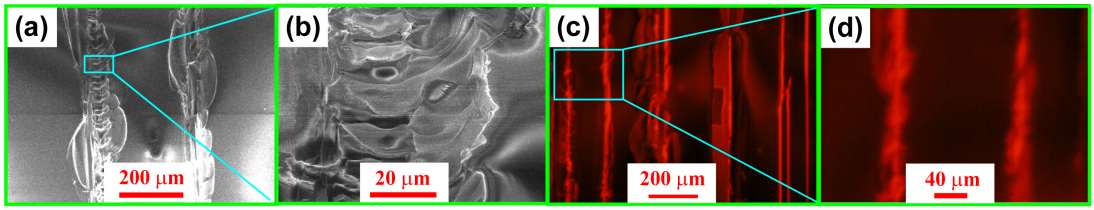

Figure 3.1: (a-b) Scanning electron microscope (SEM) images (with various magnifications) of the micron-scale groove written into the glass substrate, showing roughness that is helpful for enhancing light multiple scattering and (c-d) optical micrographs of CdSe/ZnS core-shell quantum dots deposited in the glass groove under illumination of a handheld UV torch (wavelength: 365-400 nm).

3.2.1 Sample Preparation

The sample was prepared as follows. Micron-scale grooves (width: 40-120 μm and height: 30-60 μm) were written into a 500-μm-thick glass substrate by manually pressing and translating a diamond tip on the surface, as shown in Figs. 3.1(a) and 3.1(b). Several parallel trenches were fabricated in this way. Red-emitting core-shell CdSe/ZnS CQDs (*Evident Technology, Inc.*) having a 5-nm mean diameter were then deposited from toluene solution, at a concentration of 5 mg/ml, onto the substrate by spin-coating at a low speed (300 rpm for 120 s) to allow more CQDs to be trapped. The inside surfaces of the micron-scale trenches are quite rough [Figs. 3.1(a) and 3.1(b)]. The configuration was used here to trap the CQDs inside the groove during the formation of the film [146] and thus

to increase the CQD density above levels enabling light amplification [96, 131]. Figures 3.1(c) and 3.1(d) show micrograph pictures under UV-light illumination of the final sample, i.e. after CQDs deposition. This clearly illustrates the fact that CQDs are mainly concentrated into the grooves [Fig. 3.1(c)], which serve as an assembly template. Finally, the trench roughness is also intended to provide multiple scattering, an essential process to trigger random laser oscillation. To a certain extent the sample can be considered as a series of large-area (about 80 μm $\times$ 40 μm) scattering optical waveguides made of a CQD layer deposited inside rough glass trenches.

3.2.2 Pumping Configuration

The set-up for the measurements is shown in Fig. 3.2. The photograph of the setup can be seen in Fig. 2.3(a). For the random laser experiments, the CQDs sample was photo-pumped by a frequency-tripled Q-switched Nd:YAG laser system yielding 5-ns pump pulses at an excitation wavelength of 355 nm and a repetition rate of 10 Hz. A cylindrical lens (focal length: 40 mm) was aligned to shape the pump beam as a stripe with a full width at half maximum (FWHM) of 0.05 $\times$ 3.0 mm^2. The pump beam was incident on the sample vertically to the substrate plane and the pump fluence could be adjusted through a combination of a half-waveplate-polarizing beam splitter and a neutral density filter. The laser pump stripe was parallel to the glass grooves (inset of Fig. 3.2) and, given its size, only one groove was excited at a time. Both edge and normal emission from the sample could be collected and recorded with 50-μm-core optical fibres connected to a multi-channel grating-CCD spectrometer. The spectrometer had two useable detection channels with respective spectral resolutions of 2.4 nm and 0.13 nm. More detailed description of the photo-pumping setup can be seen in Subsection 2.2.2.

3.3 Signature of CQD Laser Action

3.3.1 Threshold Behaviour

Figure 3.3(a) illustrates the spectral evolution with the pump fluence (spectrometer resolution: 2.4 nm). The integrated peak intensity (602-608 nm) of the edge emission is plotted in Fig. 3.3(b) as a function of the pump fluence. It shows the typical transition of a laser transfer function with a threshold at 25 mJ/cm^2. It is seen that above threshold a peak, centred at 606 nm, appears in the emission

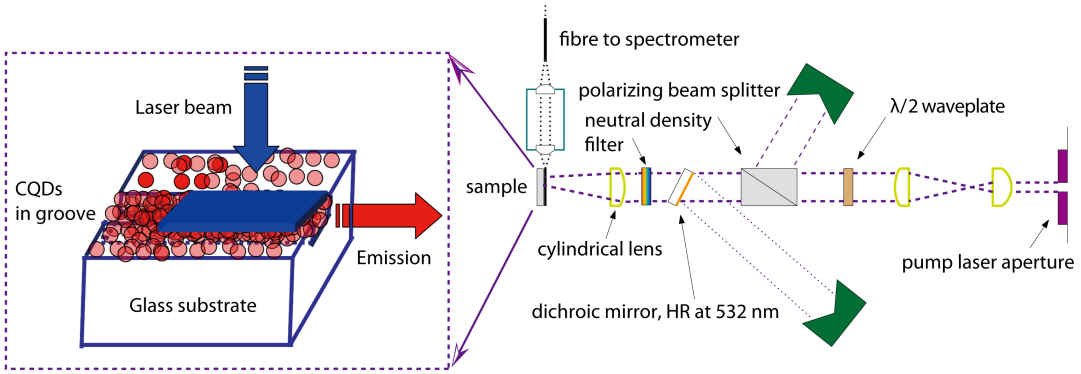

Figure 3.2: Schematic diagram of laser pump set-up and (inset) relationship of pump stripe and the groove containing CQDs.

spectrum and increases with the pump fluence. Its intensity follows a soft threshold curve rather than a sharp threshold which is due to a significant amount of spontaneous emission coupled into the laser mode [133]. This is a well-known and understood effect and is common in micron-sized lasers. It has been studied in more detail for example in the case of ring resonators [147] and distributed feedback lasers [133]. The FWHM of the emission peak drops from 30 nm below threshold to 4 nm above 29 mJ/cm^2.

In Fig. 3.3(b), it is also worth noting that the integrated intensity increases nonlinearly when the increasing pump fluence is below 5 mJ/cm^2. We attribute this effect to the saturation of the 1S excitonic absorption and to biexcitonic Auger recombination [99]. These two effects are indistinguishable on the basis of our measurements because they result in very similar PL curves, leading to a slowly increased PL evolution above 5 mJ/cm^2 before reaching a soft laser threshold at 25 mJ/cm^2.

Normalised edge and vertical emission spectra taken at a 29-mJ/cm^2 pump fluence are superposed in Fig. 3.3(c). Because the pump is above threshold the edge emission spectrum is quite narrow, about 4-nm FWHM as stated previously, but the vertical emission spectrum resembles that of typical CQDs photoluminescence (PL) with a FWHM of about 30 nm. This is an indication that the edge emission is dominated by stimulated emission and that there is indeed net optical gain, but PL dominates the normal emission. We attribute this difference to the fact that both the groove and pump geometry enable stimulated emission in the preferred direction along the groove. Consequently, we only study the edge emission in the following.

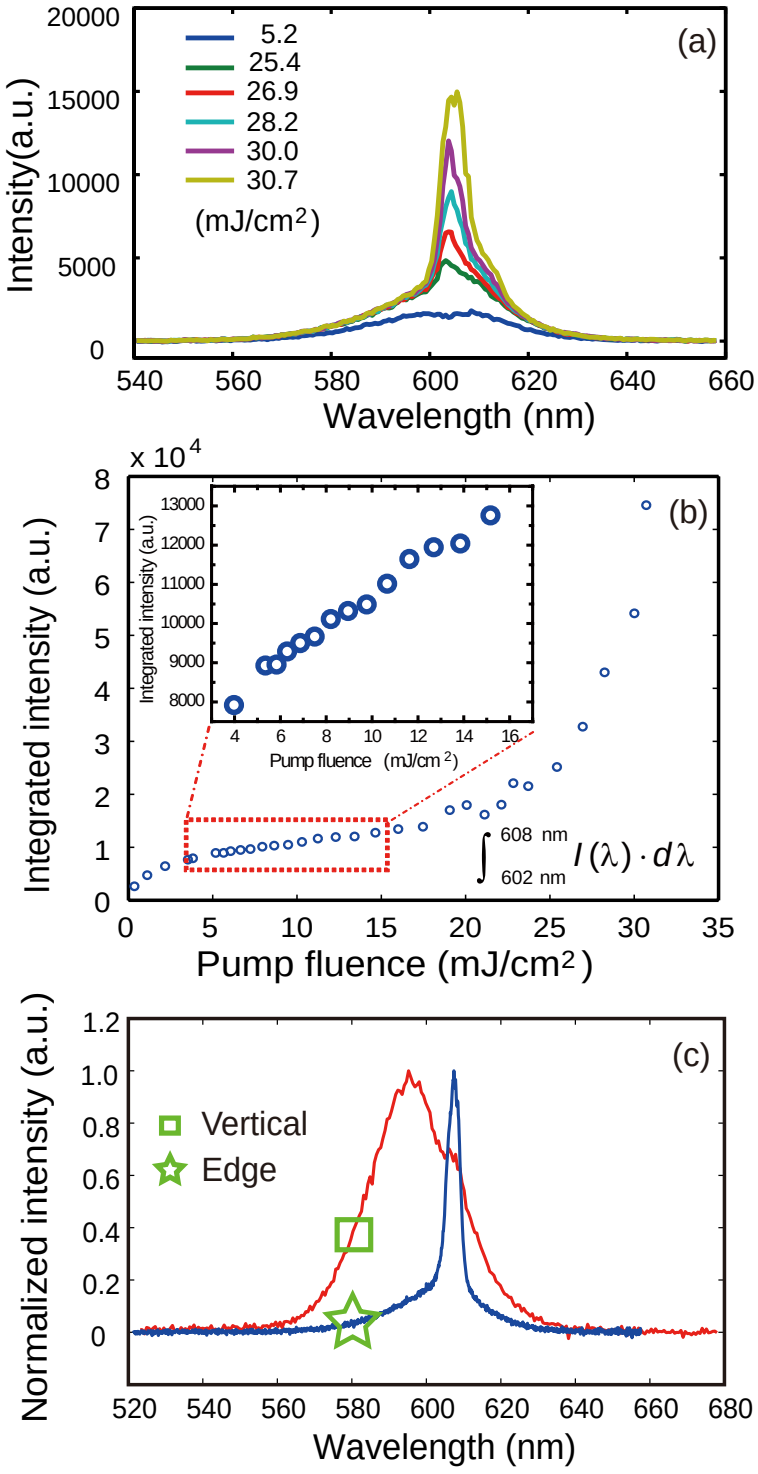

Figure 3.3: (a) Spectral evolution with increased pump fluence, (b) integrated peak (602-608 nm) intensity as a function of the pump fluence showing (inset) sublinear PL evolution above 5 mJ/cm^2 and a soft laser threshold at 25 mJ/cm^2, and (c) emission spectra recorded from vertical and edge directions of the sample under the pump fluence of 29 mJ/cm^2.

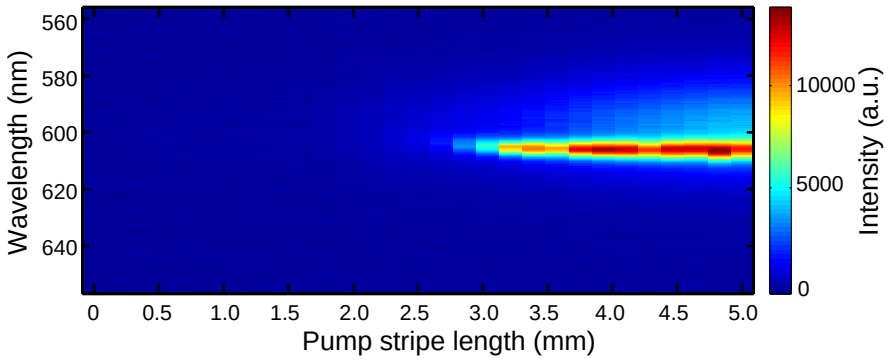

Figure 3.4: Spectral evolution with increased pump stripe length (pump stripe with tunable length in the range of 0 to 5.0 mm and here the pump fluence is 41 mJ/cm^2).

3.3.2 Spectral Evolution vs. Pump Stripe Length

A model of random lasers based on light diffusion under inclusion of optical gain demonstrates that for a given excitation fluence, there exists a critical volume of gain material above which there is stimulated emission and below which there is none [41, 79]. To verify that this effect happens in our sample, the pump stripe length, and hence the excitation volume, was varied while the edge-emission spectra were recorded. This was carried out with a fixed pump fluence of 41 mJ/cm^2 and the results are shown in Fig. 3.4. One can see that the intensity increases dramatically when the pump stripe length reaches about 3.0 mm, corresponding to the amplification length of our CQDs random system at the given pumping level [79].

3.4 Random Lasing Spectrum and its Power Fourier Transform

When the emission spectrum above threshold is detected on the high-resolution channel (0.13 nm) of the spectrometer, it is observed that the 4-nm broad stimulated emission peak actually consists of a multitude of very narrow line-width peaks. Examples of such spectra are shown in Figs. 3.5(a) and 3.6(b) recorded for a pump fluence of 53 mJ/cm^2. These peaks are spectrally narrow with some of them below the spectrometer resolution and their intensities are far above the noise level. This is a typical signature of random laser action when the excited region size somewhat restricts the total number of amplified modes. If we ascribe

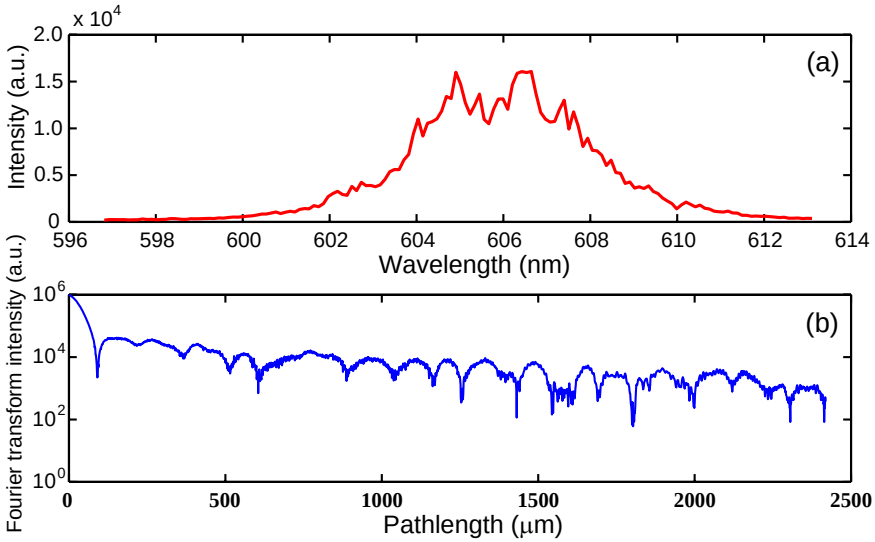

Figure 3.5: (a) Random lasing emission spectra (pump fluence: 53 mJ/cm^2) with (b) its corresponding power Fourier transform, which shows periodicity, suggesting the formation of the cavities in the system.

the random laser modes to these peaks, we can say that there is strong mode competition as evidenced by the fluctuating intensities of the peaks from shot-to-shot. However, for a fixed position of the pump stripe, some of these modes, centred around the stimulated emission maximum, are seen to always dominate as shown by detecting the spectrum over several emitted pulses [Inset of Fig. 3.6(c)].

In a random laser, it is not surprising to see strong intensity fluctuations caused by mode competition under a nanosecond photo-pumping regime [60]. For a random system, the number of modes (N) can be estimated by $N = 2\pi A/\lambda^2$, where A is the excited area and λ is emission wavelength [148, 149]. In our case, $A \sim 0.15$ mm^2 and taking 606 nm as the central wavelength, then $N \sim 2.6 \times 10^6$. Thus mode competition is expected to be strong and only the few modes with the longest lifetime will be amplified efficiently, the other modes suffering as a consequence of a gain reduction [61, 148]. In this situation, single-shot measurements can yield a different spectrum each time a pump pulse excites the gain medium. A previous study showed that semiconductor laser action along scattering paths starting at a spontaneous emission seed will bring phase or frequency fluctuations into the laser emission. As a result, the oscillation amplitudes and gain [150] of the individual laser modes may change. Such an explanation is also applicable for random laser action [148, 151]. To study this effect and also the dominance of some of the modes in our CQDs random laser

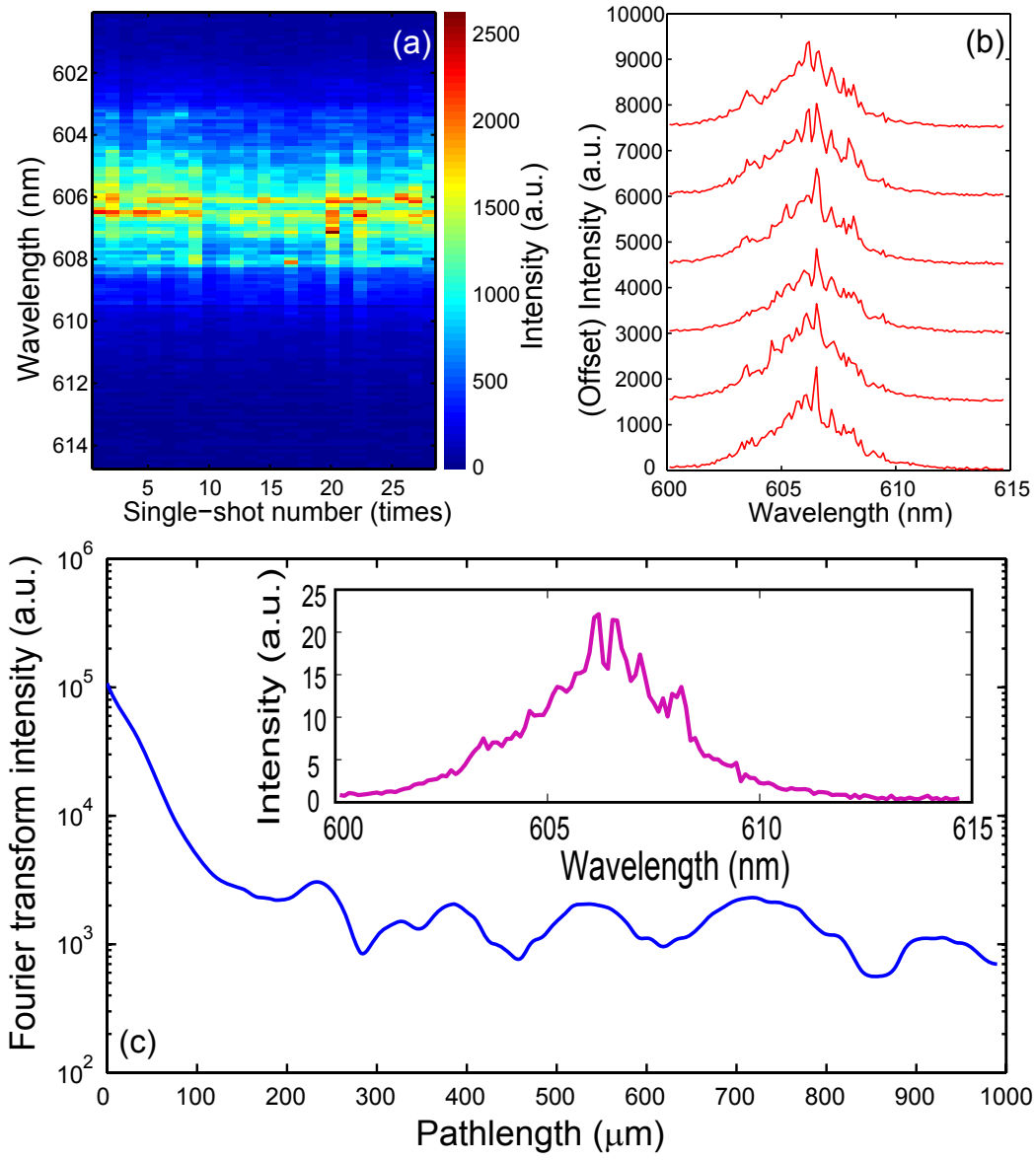

Figure 3.6: (a) Random lasing emission spectra in the single pulse photo-pumping configuration (53 mJ/cm^2) with (b) its corresponding first 5 spectra. (c) The average power Fourier transform (PFT) spectrum for all the 25 single-shot spectra with (inset) added-up (normalized) spectrum.

system, we recorded single-shot spectra for a given pump stripe position on the sample. The random laser single pulse spectrum evolution when pumping at 53 mJ/cm^2 is shown in Fig. 3.6(a) with typical spectral plots in Fig. 3.6(b). Shot-to-shot fluctuations are seen but the mode positions are actually quite stable although the intensities for each one are not. We added up all the (normalized) 25 single-shot spectra, showing the several dominant peaks [inset of Fig. 3.6(c)].

Such peaks correspond to the emitted photons in these specific modes that survive the longest time in the gain region.

Because of the refractive index inhomogeneity in the random gain medium, a simplified model using a random ring-like cavity structure has been applied successfully to explain the mechanism behind phenomena of the random laser action [63]. In any random cavity formed by long-range fluctuations of the refractive index, total internal reflections can take place from the boundaries of the region. Localized modes with close frequencies and quality factors may be generated and it has been studied that the power Fourier transformation (PFT) of the random lasing spectrum can be a very useful method to extract the random cavity diameter in the random gain medium [152]. Corresponding (averaging) PFT of the different spectra are shown in Figs. 3.5(b) and 3.6(c), respectively. For the single-shot results, we took the individual PFT spectrum before averaging the spectra and then averaged the PFT spectra [Fig. 3.6(c)]. In the equivalent cavity representation frame of random lasers with coherent feedback, the periodicity can be attributed to the formation of cavity-like structures in the disordered system [63] In our case the average spatial periodicity length, Δd, extracted from the PFT spectra is about 150 μm. We can then deduce the average equivalent cavity diameter $D = 176$ μm by using the relationship [63] of $\Delta d = n \cdot D/2$, where $n = 1.7$ is the effective refractive index of the gain medium [131] at the lasing wavelength.

3.5 Summary

In summary, we have demonstrated random laser action in a CQD-based system. The system was made by depositing CdSe/ZnS core-shell CQDs into microscale grooves which were fabricated on the surface of a glass substrate. Owing to the random packing of the CQDs and disordered sub-micron structures in the glass groove, multiple optical scattering was obtained and, upon optical excitation, random lasing action occurred. Single-shot spectra were recorded to study the dynamics of the emitted laser modes and the results show the stability of the mode positions and the dominance of modes close to the gain maximum. This is to our knowledge the first experimental demonstration of random laser action at room-temperature based on CdSe/ZnS core-shell CQDs as the amplifying elements and it opens the way to further work on random lasers using this material system.

Part III

Semiconducting Polymer Lasers

Chapter 4

Organic Composite DFB Laser

In this chapter, a free-standing organic composite membrane DFB laser template-patterned by a commercially-available blank digital versatile disk (DVD) is demonstrated. This laser operates at room-temperature and ambient atmosphere. It is based on a specifically designed composite incorporating an organic semiconductor polymer system (BBEHP-PPV) as the gain element. This flexible organic membrane laser oscillates around 521 nm above a 1.1 mJ/cm^2 threshold. Optical gain characteristics of the composite material are also studied. The approach represents a step towards viable low-cost, even 'disposable' organic solid-state lasers.

4.1 Introduction

Since the realization of organic light-emitting diodes (OLEDs) [153, 154], great effort has been put into the investigation of light amplification in organic materials for laser applications [26, 108–111, 113]; see also Chapter 1. Attractive features of organic compounds for the fabrication of lasers and other active photonic devices include the potential for low-cost, high-throughput processing and the possibility to obtain 'plastic-like', mechanically flexible structures that have desired amplifying characteristics [124, 155, 156]. Such structures could be employed in conformal photonic devices and integrated circuits for a range of potential applications [124, 155–162] in fields as varied as flexible displays, lighting, sensors and bio-sensing/monitoring. If their fabrication can be made cost-effective enough and their lifetime under typical operating conditions extended, they could also form the backbone for a range of 'disposable' visible laser sources [163].

In this study, we report a simple and potentially cost-effective-way to produce all-organic flexible composite membrane lasers that operate under photo-pumping in air and at room-temperature. They are made of a specifically designed surface-patterned composite incorporating a recently introduced semiconducting polymer as the gain element.

Conjugated semiconducting polymers have been identified as a promising class of materials for laser applications owing to their high-emission efficiency, large cross sections for stimulated emission and wide spectral coverage [26]. Among these π-conjugated polymers, poly(p-phenylene vinylene) (PPV) and its derivatives, including BuEH-PPV, BCHA-PPV, MEH-PPV, M3O-PPV, TOP-PPV and DOO-PPV, have demonstrated high-gain and low laser oscillation threshold [26, 117, 118, 164, 165], see Chapter 1. Recently, the synthesis of poly[2,5-bis(2',5'-bis(2"-ethylhexyloxy)phenyl)-p-phenylene vinylene (BBEHP-PPV) has been reported for laser chemo-sensing applications [119]. This green-emitting material, introduced in Chapter 1, has potential for a range of applications due in part to its low stimulated emission threshold and improved photo-stability compared to other organic materials.

A further, complementary, way to improve the stability of organic-based amplifying devices, and in turn make them relevant for real-world applications, is to incorporate the active elements into a transparent host matrix [166–170]. In such a configuration, the polymer matrix effectively protects the gain medium from degradation by isolating it from the ambient environment [122, 168–170]. The resulting material benefits from the combination of its constituents and can be tailored to obtain desired optical and mechanical characteristics. Doing so, it

is possible to obtain a photo-polymerized sheet that can emit and amplify light. Other functionalities such as thermal and/or photo-initiated crosslinking can also be added to the composite to further extend its processability.

In this chapter we use this approach to demonstrate laser action in a surface-structured free-standing composite membrane based on BBEHP-PPV. A light-emitting free-standing membrane is obtained by depositing a layer of composite solution on a substrate, photo-curing and subsequent peeling-off of the solidified composite. Because the refractive index of the composite is higher than air, emitted light is effectively confined within the membrane, which acts as a waveguide. By exciting the active element of the composite BBEHP-PPV the generated light can then, in principle, be amplified. In order to trigger laser oscillation a feedback mechanism to re-circulate the amplified light needs to be added. For this membrane geometry, a DFB grating is ideally suited, the physics background of which can be seen Subsection 1.3.1 in Chapter 1, and one demonstration of which in our work has been presented in Chapter 2, where we presented a flexible DFB CQD laser using a passive grating structure.

In this case, however, the active DFB grating structure is inherently integrated to the membrane incorporating the gain material at the fabrication stage. To this end, an exposed standard commercial blank digital versatile disk (DVD) is used as the substrate/template, in effect transferring its sub-micron scale grating structure onto one of the membrane surfaces. Blank DVDs consist of repeating tracks in fact a very long spiral on the disc with a pitch, Λ, of 740 nm. As we will see in Section 4.3, this pitch can correspond to a higher Bragg reflection order for green wavelengths and therefore enables resonant feedback in our composite. Compared with custom-made DFB grating structures, the use of mass-produced blank DVDs has the advantage of simplicity and low-cost [26, 171]. By casting the film on a mass-produced substrate we show the potential for simple low-cost fabrication.

In Section 4.2, the optical characterization of neat BBEHP-PPV and of the composite, including optical gain and loss, is reported. The fabrication and demonstration of the free-standing membrane laser based on this specifically-tailored material are then detailed in Section 4.3.

4.2 Optical Gain and Loss Measurement

BBEHP-PPV was synthesized in the *Department of Pure and Applied Chemistry* according to the literature [119]. For the pure material (BBEHP-PPV), neat films

(S1) of 250-nm thickness were made by spin-coating from 25 mg/ml Chlorobenzene solutions at 2800 rpm for 60 s on quartz substrates for absorption, photoluminescence and ASE characterization. Two obvious vibrational modes can be identified [119] in the PL spectrum at around 496 nm (0-0 transition) and 528 nm (0-1 transition), respectively. The solid-state PL quantum yield (PLQY) of the neat film is 86%.

For the composite, as-synthesized BBEHP-PPV material was incorporated into a UV transparent polymerisable host matrix, 1,4-cyclohexanedimethanol divinyl ether (CHDV) (*Sigma-Aldrich, Inc.*) as introduced previously. In the experiment, to ensure the BBEHP-PPV is properly dissolved, the overall mix was stirred in an ultrasonic bath for 30 minutes. As a control experiment, a set of BBEHP-PPV/CHDV membrane samples (S2, S3 and S4) on plane glass substrates were prepared with concentration of 10, 20 and 40 mg/ml. The optical characterizations of ASE threshold, gain and loss measurements on these samples were conducted in the ASE setup described above. PLQY measurements were made on a 10mg/ml membrane (25 $\pm$ 5 μm thick) using an integrating sphere, following the method of Greenham *et al.* [172], with excitation at 442 nm from a He-Cd laser for excitation. The thicknesses of the membranes were measured using a DekTak 150 Surface Profiler.

Optical characterization, including absorption, PL and ASE measurements (threshold, gain and loss), was conducted on such a plane composite film. The static PL measurement on the BBEHP-PPV/CHDV film was conducted under photo-pumping by a GaN-based cw laser (peak: λ_m=374 nm, power: 15 mW and spot size: $\sim$3 mm in radius). Both absorption and PL features (Fig. 4.1) are slightly blue-shifted (6 nm for absorption and 8 nm for PL on average) compared to the results from the pure BBEHP-PPV neat film, see Chapter 1. This small shift is similar to other cases of doping organic light-emitting materials into a CHDV matrix [121, 122, 168, 169]. The PLQY of the composite material is measured to be 35%, which is lower than in the case of neat BBEHP-PPV. This indicates that some quenching of the radiative transition occurs when BBEHP-PPV is incorporated into CHDV and that some of this effect comes from added non-radiative recombination.

In the ASE measurements, the film or membrane samples were located in a vacuum chamber with a pressure of approximately 10^{-5} mbar. The excitation light was generated by a Nd:YAG laser pumped optical parametric oscillator (OPO) with 4-ns output pulses at a repetition rate of 20 Hz. The pump wavelength was selected to be 425 nm which is close to the absorption maximum of

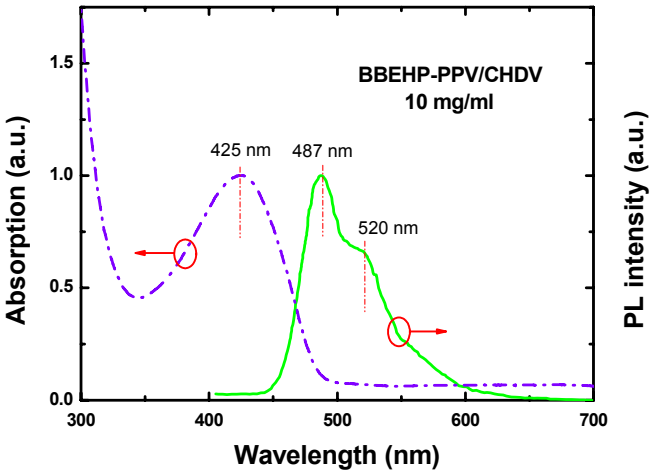

Figure 4.1: Absorption and PL spectrum of BBEHP-PPV/CHDV film on plain glass substrate. The absorption measurement was conducted by Cary 50 UV-Vis spectrophotometer. The PL measurement was conducted under the photo-pumping with a GaN-based cw laser (374 nm).

BBEHP-PPV composite (Fig. 4.1). Calibrated neutral density filters were inserted in the beam path to adjust the pump intensity incident on the samples. A cylindrical lens (focal length: 40 mm) was used to shape the excitation beam into a narrow stripe with a width of approximately 0.046 cm and a length of 0.35 cm. The edge emission from the film was collected and recorded with a fibre-coupled grating spectrograph and a charge coupled device (CCD) detector. This part of the work (gain and loss measurements) was undertaken in collaboration with Prof. I. D. W. Samuel's group at the *University of St Andrews*.

4.2.1 ASE, Gain and Loss

For ASE measurements, the neat film and/or composites were excited by a 4-ns-pulsed pump beam shaped as a stripe and the full-width at half-maximum (FWHM) of the emission spectrum and the relative output power as a function of the pump intensity were both monitored from the edge of the sample (Fig. 4.2).

In theory, when ASE occurs the output intensity from one end of the pump stripe is given by [22]:

$$I(\lambda) = \frac{AI_{\text{pump}}}{g(\lambda)}(e^{g(\lambda)\ell} - 1) \tag{4.1}$$

where $A(\lambda)$ is a constant related to the emission cross section and ℓ is the length of the pump stripe. For gain measurements, the output intensities were recorded

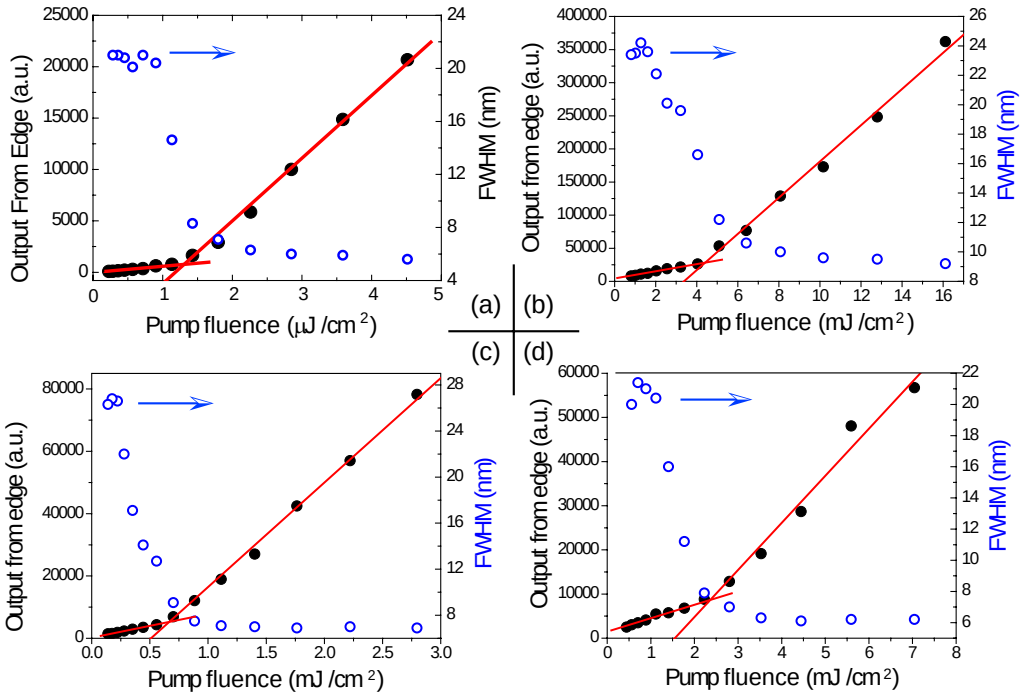

Figure 4.2: Output intensity and full width at half maximum (FWHM) versus the pump energy density for (a) pure BBEHP-PPV thin film (ASE threshold: 1.1 μJ/cm^2), and various BBEHP-PPV/CHDV membrane samples: (b) 10 mg/ml (ASE threshold: 4.6 mJ/cm^2), (c) 20 mg/ml (ASE threshold: 0.70 mJ/cm^2) and (d) 40 mg/ml (ASE threshold: 2.2 mJ/cm^2). Data were taken in collaboration with Prof. Samuel's group.

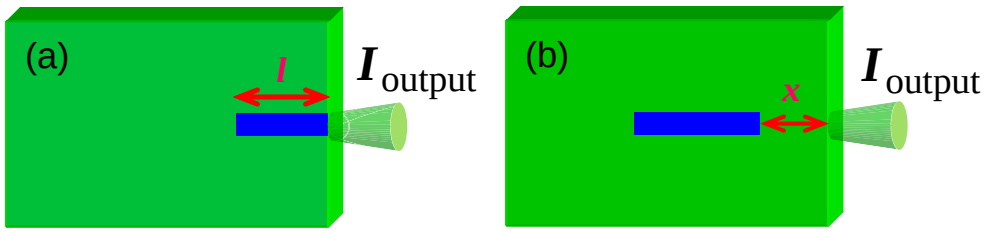

Figure 4.3: Schematic diagram of (a) variable-stripe-length (VSL) technique for optical gain measurement, and (b) shifting-excitation-spot (SES) technique for optical loss measurement.

as a function of excitation length for a range of pump intensities [4.3(a)]. The pump stripe was able to vary in the range of 0.01 cm to 0.25 cm controlled by an adjustable aperture. The results of gain measurements are plotted in the *left panel* of Fig. 4.4, and the fitting parameters of which are listed in Table 4.1.

To measure the waveguide loss coefficient, α, the pumped stripe on the film

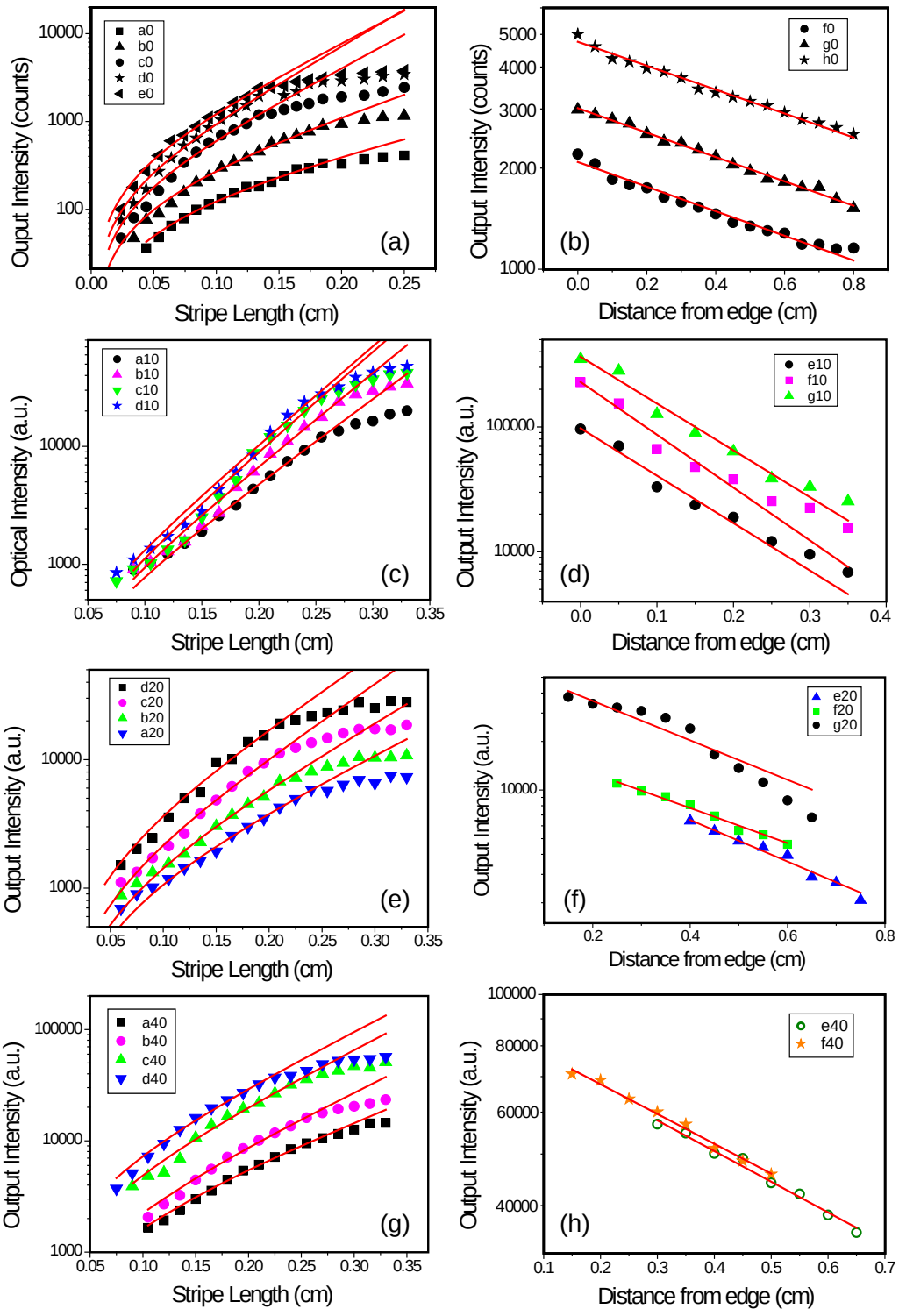

Figure 4.4: Optical gain (*left panel*) and loss (*right panel*) for (a, b) pure BBEHP-PPV thin film, and various BBEHP-PPV/CHDV membrane samples: (c, d) 10 mg/ml, (e, f) 20 mg/ml and (g, h) 40 mg/ml. Data were taken in collaboration with Prof. Samuel's group.

Table 4.1: Parameters for optical gain measurement obtained from fits of Eq. 4.1 to the data in the *left panel* of Fig. 4.4.

		Pump fluence (mJ/cm^2)	AI_{pump} (cm^{-1})	$g(\lambda)$ (cm^{-1})
S1 (pure)	a0	2.33×10^{-3}	809	7.8
	b0	4.56×10^{-3}	1474	11.2
	c0	7.84×10^{-3}	2235	17.4
	d0	12.0×10^{-3}	3114	19.0
	e0	13.5×10^{-3}	3999	18.3
S2 (10 mg/ml)	a10	28	3067	16.4
	b10	30	3312	18.2
	c10	33	3628	19.4
	d10	40	4358	19.2
S3 (20 mg/ml)	a20	1.4	6373	9.4
	b20	1.71	7710	11.2
	c20	2.27	10467	13.0
	d20	3.86	17551	13.0
S4 (40 mg/ml)	a40	4.88	9928	8.58
	b40	6.40	12553	10.5
	c40	9.13	26581	11.2
	d40	15.5	39589	11.0

was moved away up to 0.8 cm from the edge of the sample without changing its length. The pump stripe was fixed in the loss measurements to be 0.47 cm × 0.046 cm. The emission from the edge should then be given by [26]:

$$I = I_{\text{pump}} \mathrm{e}^{-\alpha x} \tag{4.2}$$

where x is the distance between the end of the pump stripe and the sample edge [4.3(b)]. The results of loss measurements are plotted in the *right panel* of Fig. 4.4, fitting parameters of which are listed in Table 4.2.

For the neat film, it is seen [Fig. 4.2(a)] that the FWHM of the edge-emitted PL narrows from 20 to 6 nm when pumping above a pump energy density of 1.1 $\mu J/cm^2$. The net gain coefficient at 535 nm was found to be $g = 19$ cm^{-1} for a pump energy density of 12 $\mu J/cm^2$ [Fig. 4.4(a) and Table 4.1]. At higher pump energy densities the gain coefficient no longer increases because of gain saturation in the neat polymer film. Optical loss measurements suggest a very low loss coefficient of 0.83 cm^{-1} in the neat film [Fig. 4.4(b) and Table 4.2].

ASE measurements on a composite membrane (BBEHP-PPV/CHDV: 10 mg/ml) demonstrate that stimulated emission can be achieved, with a 4

Table 4.2: Parameters for optical loss measurement obtained from fits of Eq. 4.2 to the data in the *right panel* of Fig. 4.4.

		Pump fluence (mJ/cm^2)	I_{pump} (a.u.)	α (cm^{-1})
S1 (pure)	f0	7.20×10^{-3}	2075	0.83
	g0	9.96×10^{-3}	3014	0.83
	h0	15.6×10^{-3}	4755	0.82
S2 (10 mg/ml)	e10	7.7	97536	8.74
	f10	15	229017	9.74
	g10	26	364541	8.63
S3 (20 mg/ml)	e20	2.35	21017	2.50
	f20	2.59	21378	3.00
	g20	6.85	62801	2.82
S4 (40 mg/ml)	e40	12.0	86286	1.33
	f40	14.1	87684	1.30

mJ/cm^2 threshold and $\sim$9-cm^{-1} propagation loss coefficient [Fig. 4.2(b), Fig. 4.4(d) and Table 4.2]. Because the thick membrane supports many transverse optical modes, it is difficult to directly compare results with those of the thin film characterization. However, net gain at saturation is found to be $\sim$19 cm^{-1} at 33 mJ/cm^2 excitation density [Fig. 4.4(c) and Table 4.1] similar to a neat film of BBEHP-PPV [Fig. 4.4(a) and Table 4.1]. Measurements were also done on membranes with higher BBEHP-PPV concentrations (20 and 40 mg/ml). Gains at saturation were found to be lower at 13 cm^{-1} (20 mg/ml) and 11 cm^{-1} (40 mg/ml), respectively.

It is noted that S2 (10 mg/ml) requires too much energy (pump fluence) to be injected to reach the threshold; while S4 (40 mg/ml) shows quench effect since it requires higher pump fluence to obtain similar level of gain coefficient compared to that of S3. S1 is the pure light-emitting polymer, which is not as robust as the composites thus hindering the practical application when requiring good lifetime output performance. Taking into account the results of gain (Table 4.1) and loss (Table 4.2) measurements, S3 (20 mg/ml) is the best candidate among the composites for lasing demonstration as we used in the following. We did not consider output power efficiency in this work; however, if the gain material can sustain higher pump fluence, the output power can be higher.

For photostability characterization, we photo-pumped a 50-μm thick BBEHP-PPV/CHDV (10 mg/ml) membrane sample in ambient atmosphere for about an hour while monitoring the PL peak intensity from the sample edge. The result (Fig. 4.5) shows no obvious degradation for about an hour ($\sim3.5 \times 10^4$ pump

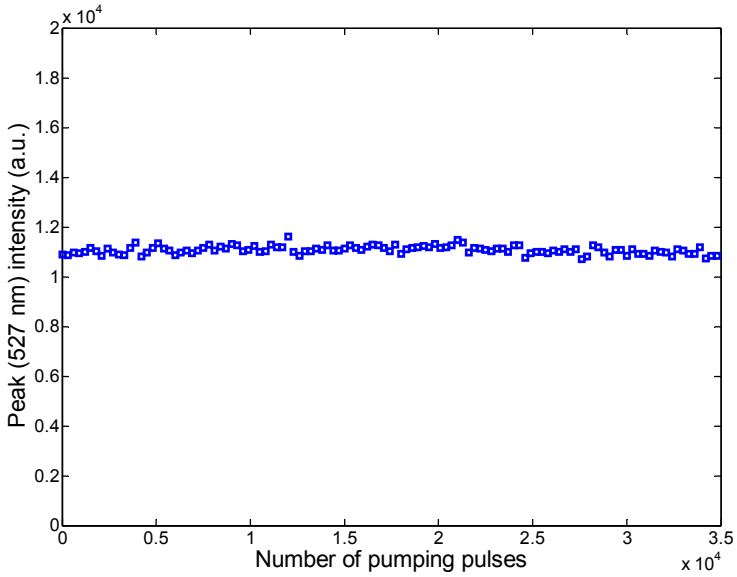

Figure 4.5: Photostability measurement for a BBEHP-PPV/CHDV (10 mg/ml) membrane on a glass substrate. The pump energy density is about 1.0 mJ/cm^2.

pulses) at a pump fluence of about 1.0 mJ/cm^2.

4.3 Membrane Laser: Sample Preparation and Measurement

4.3.1 Membrane Laser Fabrication

By way of example, a layer of this BBEHP-PPV composite (20 mg/ml) was then drop-coated onto a piece of standard blank DVD substrate (∼3 cm × 3 cm). Prior to this over-coating, the DVD substrate was left in an ultrasonic bath of methanol for 30 s in order to remove the protective coating and expose the grating tracks. The composite spread to form a uniform layer due to its low viscosity. The next step was to use a UV lamp (∼370 nm and power density: ∼200 mW/cm^2) to cure (30 s) the BBEHP-PPV/CHDV composite layer [169]. Finally, the cured composite layer (thickness: ∼50 μm) was peeled off from the DVD substrate. The resulting free-standing membrane was mechanically flexible and one of its surfaces was embossed with the negative of the DVD surface tracks. The sample preparation process and morphology can be seen in Fig. 4.6.

A crude but straightforward way to check the uniformity of the replicated grating structure on a surface-patterned membrane is to look at the as-prepared sample from different angles to see whether there exists any effect of diffraction

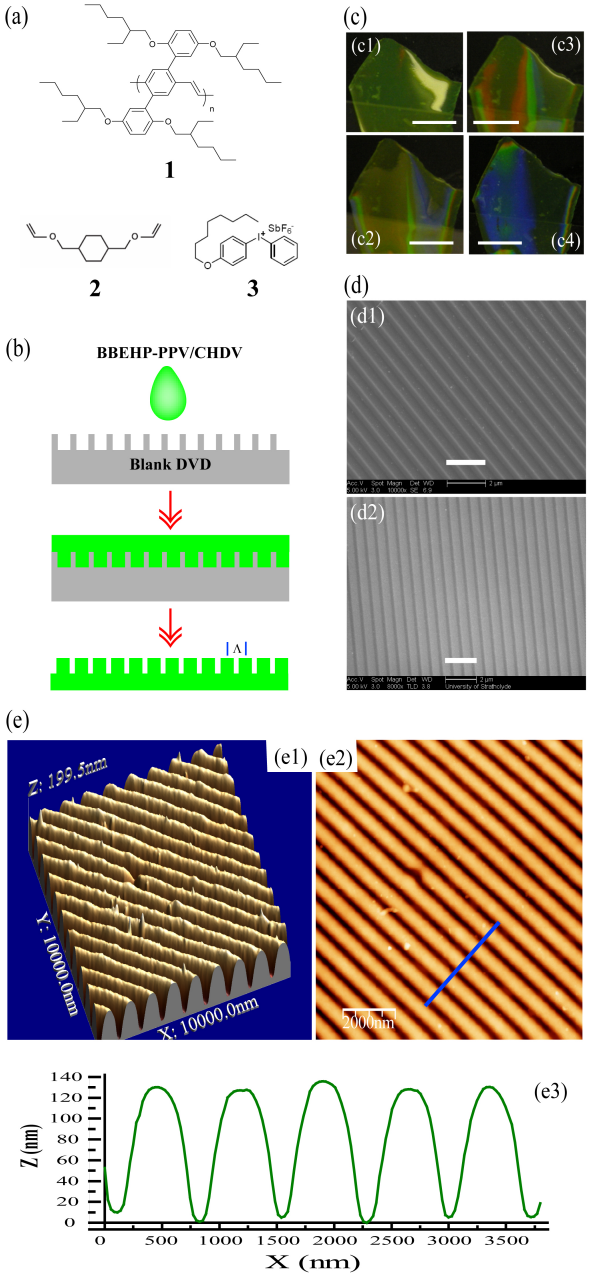

Figure 4.6: Fabrication of flexible DFB organic membrane laser: (a) Chemical structures of the materials used in this work: (1) BBEHP-PPV, (2) CHDV, (3) 'PAG'. (b) Diagram of the fabrication process of the free-standing composite membrane with replication of the grating structure on a blank DVD surface. (c) Optical images of the as-prepared composite membrane sample taken at different angles (c1−c4) demonstrating the light diffraction effect. The scale bar (white line) represents a 1-cm length. (d) SEM images (courtesy of Y. Zhang) of (d1) a blank DVD surface; and (d2) the as-prepared membrane surface. The scale bar (white line) represents a 2-μm length. (e) AFM images (e1: 3-dimensional; e2: 2-dimensional) of the membrane surface structure, with grating profile (e3) marked by the blue line in (e2).

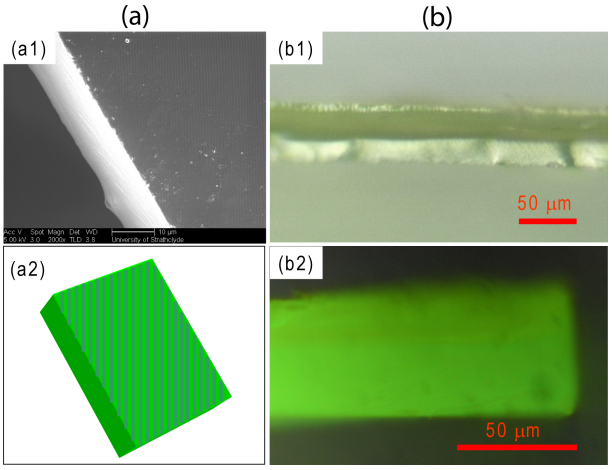

Figure 4.7: (a) SEM image (a1) of a piece of the as-prepared BBEHP-PPV/CHDV membrane showing the edge profile from an oblique angle as shown in the diagram (a2). (b) Cross-section photo images of the membrane, without (b1) or with (b2) exposure to UV light, respectively.

caused by the grating. Here, we simply used a camera to take photographs of the DVD-patterned membrane under white-light illumination. Photographs taken at several different angles are shown in Fig. 4.6(c). Changes in the recorded colours indicate that regular structure on a visible wavelength scale is indeed present on the membrane surface.

In order to examine details at the micron-scale, we used scanning electron microscope (SEM) to study a piece of the membrane and also scanned a sample of blank DVD for comparison. The SEM images in Fig. 4.6(d) clearly show that the two patterns are complementary, confirming the accurate replication of the grating structure from the blank DVD substrate [Fig. 4.6(d1)] to the as-prepared membrane laser [Fig. 4.6(d2)]. Atomic force microscopy (AFM) was also applied to analyze the membrane surface profile [Fig. 4.6(e)], suggesting that the modulation depth of the DFB-textured surface is about 130 nm [Figs. 4.6(e2) and 4.6(e3)], which is suitable to provide sufficient feedback for laser action in a DFB laser structure [173, 174]. The thickness of the polymer membrane was estimated from the optical image of the membrane's cross-section profile to be about 50 μm (Fig. 4.7).

4.3.2 Laser Demonstration

For laser action, photo-pumping of the composite membrane (20 mg/ml) was done in air with a frequency-tripled Q-switched Nd:YAG laser system yielding

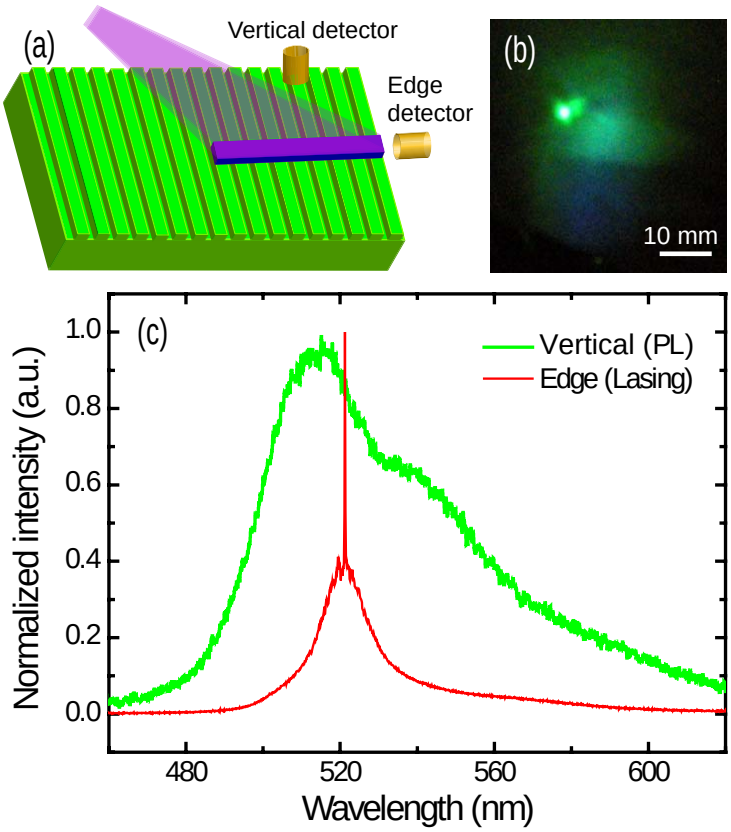

Figure 4.8: (a) Diagram of the photo-pumping setup. (b) Photo image of edge emission lasing spot (green) projected onto a paper screen (∼5 cm away the sample edge). (c) Above-threshold, edge emission (lasing) spectrum and vertical-emission (PL) spectrum.

5-ns pump pulses at a repetition rate of 10 Hz and an excitation wavelength of 355 nm (see Chapter 2). The membrane was pumped at an angle of about 45 degrees. A cylindrical lens was used to shape the pump beam as a stripe resulting in a 0.1×2.9 mm^2 pump area on the membrane surface. Both edge and vertical emission of the sample were collected by a lens-optical fibre combination, which was fed into a spectrometer (Avantes) for analysis. More detailed description of the photo-pumping setup can be seen in Subsection 2.2.2 and Fig. 2.3.

The results show that, when pumping above a certain energy, a laser peak emerges at 521.3 nm in the edge direction while only normal PL is recorded in the vertical direction [Fig. 4.8(a)] at the same time. The edge laser emission was projected onto a paper screen placed about 5 cm away, showing a bright green spot (∼5 mm in size) in Fig. 4.8(b). Above the threshold, the laser peak linewidth reaches the resolution limit of our spectrometer (∼0.2 nm).

One can also see corrugation in the spectrum with a ∼1.9-nm separation (close

to the dominant peak) formed by non-lasing transverse modes. The size and shape of the pump stripe on the membrane limits to a certain extent the number of lateral modes but there are still several transverse modes that can potentially oscillate. Given the thickness ($\sim$50 μm) of the membrane, one would expect the spectral separation between consecutive transverse modes to be around 1.9 nm, which corresponds to the observations.

The evolution of the laser emission behaviour under different pumping energy was investigated [Fig. 4.9(a)]. Results show a laser threshold at around 1.1 mJ/cm^2. It can also be seen in the inset of Fig. 4.9(a) that there is a 1.5-nm blue-shift of the spectral peak (i.e. the gain maximum) between low pumping levels and threshold.

A similar membrane but prepared on a flat substrate, i.e. with no embedded grating on its surface, was pumped under the same conditions. In that case, no laser oscillation signature was observed but only ASE [Fig. 4.9(b)] with a 4.6 mJ/cm^2 threshold. These measurements indicate that the emergence of the laser mode is enabled, or at least facilitated, by the surface grating.

In a DFB grating, the in-line resonant feedback is realized when propagating waves fulfill the Bragg condition [26]:

$$m\lambda_{Bragg} = 2n_{eff}\Lambda \tag{4.3}$$

where n_{eff} is the effective refractive index of the mode in the gain medium, Λ is the period of the grating structure as seen by the propagating mode, and m is the diffraction order.

For our composite membrane, at this wavelength, the refractive indices of BBEHP-PPV and CHDV are approximately $n_{\text{BBEHP-PPV}} \approx 1.7$ [119] and $n_{\text{CHDV}} = 1.472$ (*Sigma-Aldrich, Inc.*), respectively. Given the low concentration of BBEHP-PPV (10 mg/ml in CHDV) in the composite and the rather thick membrane, the effective refractive index can be taken to be close to the matrix index for lower order transverse modes. Because the period of the grating is 740 nm, it is probably the 4-th order diffraction that provides the resonant feedback. For $m = 4$ and a wavelength of 521.3 nm, corresponding to the observed laser emission, one obtains $n_{eff} \sim 1.41$. This is slightly below the composite index and indicates that higher order transverse modes are probably favoured due to a higher modal overlap with the grating.

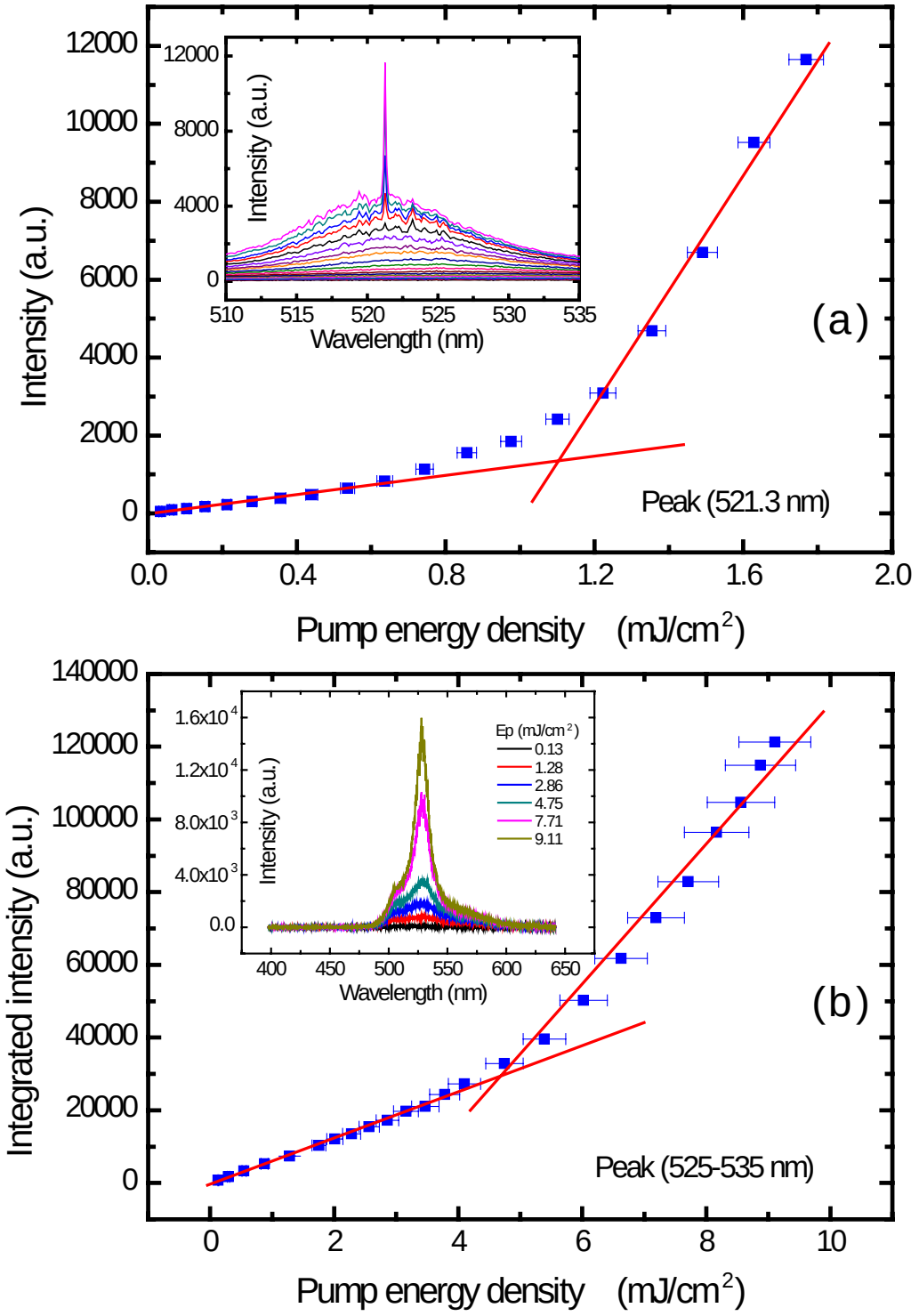

Figure 4.9: (a) Laser threshold curve derived from (inset) the evolution of the sample (membrane with grating pattern) edge emission spectra under various pump energy densities. (b) ASE threshold curve and (inset) typical spectra evolution of the plane membrane (no grating pattern) at various pump energy densities.

4.4 Summary

In summary, we have demonstrated a green-emitting free-standing membrane DFB laser that uses a novel guest-host organic composite with π-conjugated BBEHP-PPV as the chromophore. The composite approach protects the light-emitting elements to a certain extent and benefits from improved processability. The composite membrane itself acts as an amplifying waveguide for the light it generates under optical excitation and the feedback is obtained by a grating embedded onto its surface. This surface-grating is directly formed at the fabrication stage and in this case was obtained by template-patterning the membrane with a commercially-available blank DVD. The resulting membrane laser operates at room-temperature and ambient atmosphere. Such a technique is easy to implement, and promising for the fabrication of low-cost and even 'disposable', green-emitting organic lasers.

Chapter 5

Photonic Glass-based Organic Random Laser

In this chapter, control of the emission wavelength of a random laser (RL) system over a 7-nm waveband is demonstrated. We use a green-emitting π-conjugated polymer infiltrated into a photonic glass formed by nano/micro-size monodisperse silica spheres. The use of a solution-based conjugated polymer enables the complete filling of the voids within the photonic glass without suffering from quenching and the gain can therefore be maximised. The emission wavelength of these structures is set by a combination of the material system spectral gain and of the transport mean free path. The latter is controlled by the mean diameter of the spheres in the nano-scale range. Transport mean free paths of photons in the RL active region are calculated using Mie scattering theory and corroborated with coherent backscattering measurements. Further wavelength modification is also possible by changing the pump spot size and the pump fluence.

5.1 Introduction

We have already pointed out in Chapters 1 and 3 that in recent years there has been a rapidly growing interest in random lasers (RLs). A RL is based on light amplification by stimulated emission via multiple scattering due to randomness in a high-gain disordered medium [41]. The interest in RLs stems not only from their intriguing concept and features but also from their potential for simple and versatile fabrication that may open up new applications. The majority of RL studies to date have focused on proof-of-concept demonstrations and basic physics without too much concern for controllability of the laser characteristics [38, 39, 141–143, 175]. This includes our previous demonstration of CQD RLs [127] in discussed in Chapter 3.

However, in order to develop applications, it is crucial to have at least some control over these characteristics and in particular over the emission wavelength [41]. Among other proposals and demonstrations for RL mode control [65, 176–187], photonic glass systems formed by randomly deposited wavelength-size, monodisperse spheres are promising because they enable the modification of light diffusion properties [188, 189]. In general, photonic crystals are perfectly ordered arranged nanosctructures with their periodicity properties that can modify the propagation of electromagnetic waves when the light is traveling in such periodic optical nanostructures. Such periodicity in photonic crystals is similar to that in semiconductor crystals. The latter can have an impact on the electron motion behaviours. If such periodicity is broken completely, meaning that the optical nanostructures are randomly assembled to form the photonic system platform but the monodisperse individual nanostructures (e.g. micro/nano-spheres) still can have their impact on the modification of photon behaviours, then we called such complex disordered platform a 'photonic glass' system. For example, such assemblies of dielectric spheres exhibit sharp Mie resonances in the strong scattering regime and thus can be applied to the realization of resonance-driven RLs where the emission wavelength is controlled by the size of the spheres [139].

A photonic glass can be created via a modified self-assembly method [188]. The standard self-assembly technique is widely used to grow ordered structures such as opal-based photonic crystals [for example, see the diagram in the *left panel* of Fig. 5.1(a)] from colloidal suspensions of dielectric spheres [190]. The modified technique [188] enables the fabrication of new disordered materials formed by the random packing of nano/micro-size spheres [see the diagram in the *right panel* of Fig. 5.1(a)]. This approach is based on the modification of the charge of the

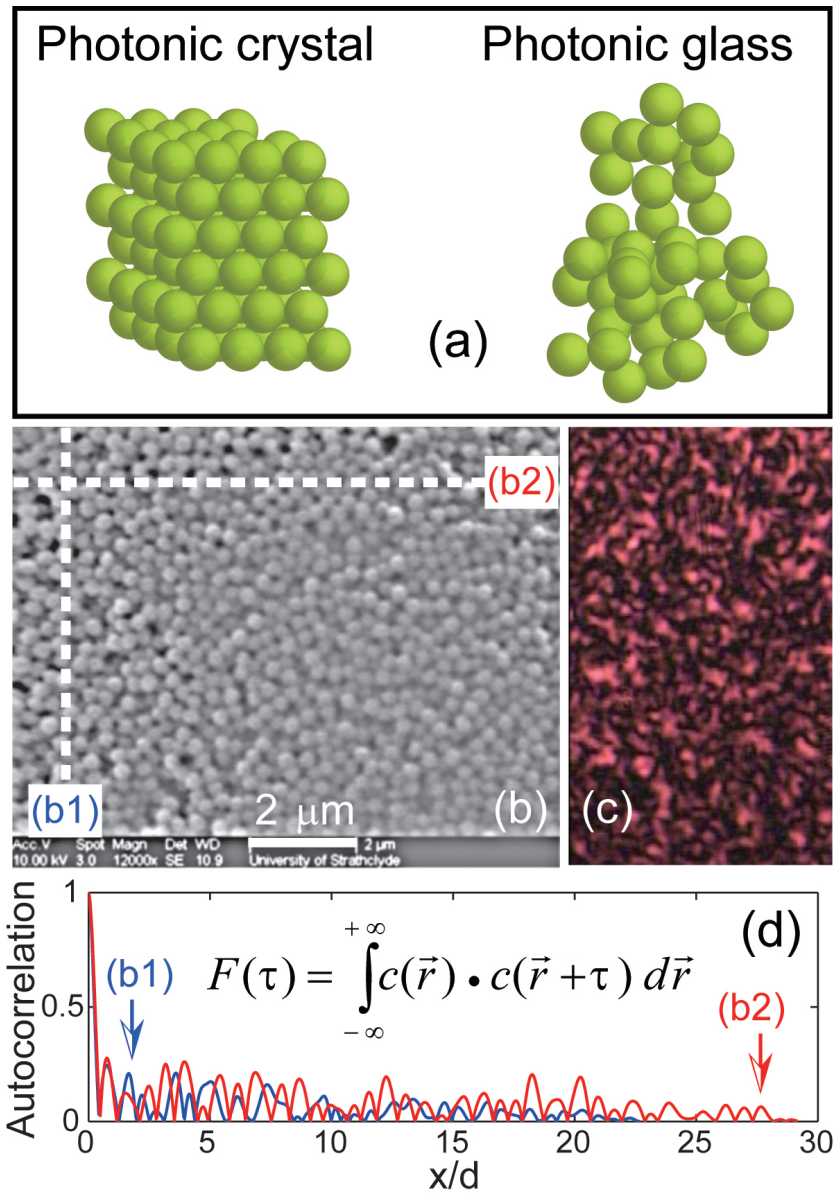

Figure 5.1: (a) Nano/micro-spheres forming a photonic crystal (*left panel*) or photonic glass (*right panel*). (b) Scanning electron microscope (SEM) image (courtesy of Y. Zhang) of SiO_2 spheres with mean diameter of 320 nm forming a photonic glass. (c) light speckle pattern recorded from a back scattering direction of the as-prepared photonic glass sample. (d) Autocorrelation calculation corresponding to two lines marked in the SEM image in (b).

colloidal spheres by the addition of salt or acid into the solution, which then provokes flocculation of the suspended particles. It is noted that a resonance-driven RL action has been demonstrated by using such an approach, with a photonic glass formed by polystyrene nano/micro-spheres and infiltrated with dye molecules [139].

In this work, we demonstrate RL action in an entirely solution-processable silica photonic glass gain medium incorporating a π-conjugated polymer. Conjugated semiconducting polymers have, as we described previously, been identified as an attractive class of materials for laser applications owing to their high-emission efficiency, large cross section for stimulated emission and wide spectral coverage [26].

As opposed to dyes, they do not quench when in a close-packed solid-state format, which means that their density and hence the optical gain can be maximised. It is then expected that the threshold fluence of conjugated polymer-based RLs will be improved (for similar structures) compared to that of dye molecule-based RLs. For example, the RL threshold of $\sim$3 mJ/cm^2 found in our study (see below) compares favourably to the DCM dye-based RL threshold of 5 mJ reported in Ref.[139]. In fact, given that the pump spot size used in Ref. [139] was stated to be 1 mm^2 in diameter, this threshold corresponds to $\sim 6.4 \times 10^2$ mJ/cm^2: the threshold of the conjugated polymer RL reported in this study is therefore two orders of magnitude lower in terms of fluence.

The organic semiconductor material used is the green-emitting π-conjugated polymer poly[2,5-bis(2',5'-bis(2"-ethylhexyloxy)phenyl)-*p*-phenylene vinylene] (BBEHP-PPV). As mentioned previously, this organic semiconductor has been reported as a very promising laser material [119, 134]. The photostability of BBEHP-PPV has been tested in a thin film structure on a planar glass substrate, indicating a 1/e degradation dosage of $\sim$20 J/cm^2 when pumped at a 5-ns/10-Hz laser pulse with wavelength of 355 nm under the fluence of 260 μJ/cm^2 (above gain threshold due to low loss in that case). It is thus not surprising to see no significant degradation of the polymer during our photo-pumping experiment to observe RL action at the threshold in the range of several mJ/cm^2 (with estimated total exposure time under laser pumping for each sample of no more than 5 mins).

The photonic glass used here is made of silica spheres rather than polymer spheres and is consequently more robust and resistant to solvent exposure. This is a critical feature for full solution-processability of the RL structure because toluene was used to dissolve the gain polymer (BBEHP-PPV) thus making it solution processable. Experimentally, it is found that the RL emission spectral peak under photo-pumping can be shifted over 3-nm by varying the transport mean free paths in the photonic glass random systems. The individual Mie resonances are washed-out due to the combined effect of modest refractive index contrast between the silica spheres and BBEHP-PPV and the size dispersity of

the spheres. Further emission wavelength modification (over ∼7 nm) is possible via changing the pump spot area, as well as the pump fluence.

5.2 Fabricating Organic Random Laser based on Photonic Glass

5.2.1 Photonic Glass

We prepared a series of photonic glass samples formed by nano/micro-size silica spheres with mean diameters (d) ranging from 150 nm to 3000 nm (*Bangs Laboratories, Inc.*). These silica spheres are supplied in suspension in an aqueous solution at a concentration of 100 mg/ml. The size dispersity is below 10% for each specified diameter. A 10 percent volume of 0.5 M HCl was added to the solution to provoke the flocculation of the suspended nano/micro-spheres. About 100 μl of the charged solution was then drop-coated onto a clean glass substrate to form a photonic glass sample with specific sphere size. The as-prepared samples were then left in a dry place for two days to allow the water to fully evaporate.

The thickness (L) of the respective photonic glasses was in the range of 200−600 μm as measured under a microscope and the filling fraction (η) is about 50%−60% according to a study presented in the literature [189]. The scanning electron microscope (SEM) image of a 320-nm-diameter SiO_2 sphere assembly is shown in Fig. 5.1(b). The randomness of the as-prepared photonic glass sample was confirmed [188] via measuring the light speckle pattern [Fig. 5.1(c)] and via autocorrelation inspection of the SEM image [Fig. 5.1(d)].

Powder BBEHP-PPV (the synthesis method can be found elsewhere [119]) was dissolved into toluene solution at a concentration of 20 mg/ml, followed by an ultrasonic bath for at least 1 min to allow the polymer to be dissolved completely. BBEHP-PPV/toluene solution was then drop-coated onto the photonic glass samples several times, allowing the gain material to infiltrate into the voids. The photograph of an as-prepared photonic glass sample (with mean diameter of the spheres of 320 nm) can be seen in Fig. 5.2(a). After that, BBEHP-PPV/toluene (20 mg/ml) solution was infiltrated into the random system by repeated drop-coating to form a photonic glass RL sample, as shown in Fig. 5.2(b).

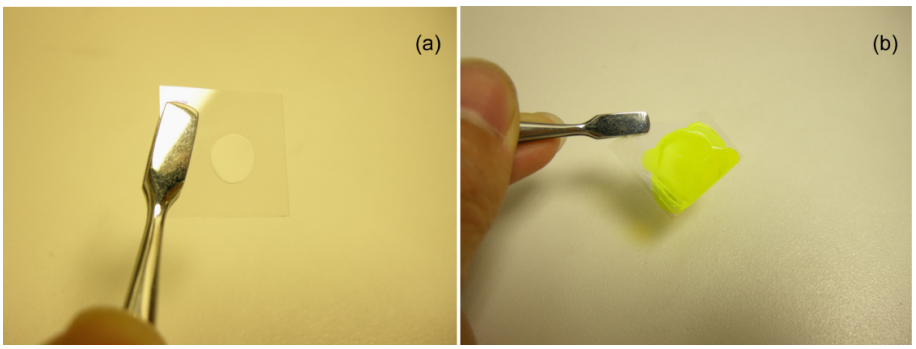

Figure 5.2: Photographs of a photonic glass sample formed by SiO2 spheres with mean diameter of 320 nm: (a) without and (b) with, infiltrated BBEHP-PPV gain material.

5.2.2 Photo-Pumping Setup

The active photonic glass samples were photo-pumped at a 45-degree angle to the surface normal by a frequency-tripled Q-switched Nd:YAG laser system, yielding 5-ns pump pulses at a repetition rate of 10 Hz with an excitation wavelength of 355 nm. The pump spot size could be set in the range of 0.0024 to 0.353 cm^2 by placing an optional spherical lens in the pump light path and was monitored by a CCD camera. Emission normal to the sample was collected by a 50-μm-core optical fiber connected to a multi-channel grating-CCD spectrometer (Avantes: spectral resolution of 0.13 nm). More detailed description of the photo-pumping setup can be seen in Subsection 2.2.2 and Fig. 2.3.

5.3 Modification of Random Lasing Emission Wavelength

5.3.1 Threshold Behaviour

Fig. 5.3 shows the RL characteristics obtained by photo-pumping a system made with 320-nm spheres. The main plot is the integrated intensity − from 536.5 to 540.5 nm − as a function of the pump fluence and presents a threshold, a signature of laser action,[26, 41] at ∼3 mJ/cm^2 (pump spot area: 0.009 cm^2). The relative 'softness' in the threshold turn-on can be explained by spontaneous emission coupled into the large number of laser modes [127, 133]. The inset of Fig. 5.3 shows the normalized photoluminescence (PL) spectrum from a neat film of BBEHP-PPV and a typical RL spectrum from BBEHP-PPV infiltrated into the photonic glass random system (d = 320 nm). The emission spectrum

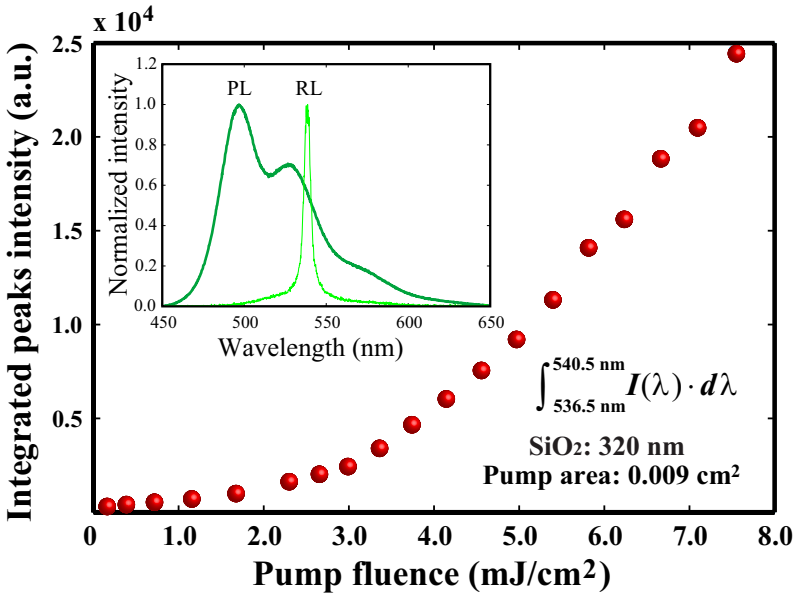

Figure 5.3: Integrated peak (536.5−540.5 nm) intensity as a function of the pump fluence, demonstrating a threshold characteristic behavior. (Inset) Normalized photoluminescence (PL) spectrum from a BBEHP-PPV neat film and random laser (RL) spectrum from BBEHP-PPV infiltrated into a photonic glass (sphere diameter: $d = 320$ nm).

becomes much narrower when pumping above the threshold, which is another signature of laser action [26, 41]. The full width at half maximum (FWHM) of the RL spectrum shown here is slightly broad (∼3.5 nm) though multiple peaks can be observed on top of the spectrum, due to the fact that in a diffusive RL system, many overlapping lasing modes exist and compete [61, 191].

It is also found that for a small active region volume (small pump spot area), the RL spectrum slightly narrows and becomes 'spiky' (i.e. separated narrow peaks appear on top of the broader stimulated emission spectrum) as demonstrated below.

In the rest of the Chapter, for the investigation of the modification of the RL's spectrum, we refer to the central wavelength of the emission spectrum as the peak and study the shift of its position for different parameters.

Random laser systems formed by monodisperse nano/micro-spheres with different diameters were investigated. The influence of the size of the spheres on the laser emission wavelength for various pump fluences and with a large (0.353 cm^2) or small (0.005 cm^2) pump spot areas are summarized in Fig. 5.4. It can be seen that with the same pump spot area and pump fluence, the RL emission peak wavelength blueshifts as the size of the silica spheres increases.

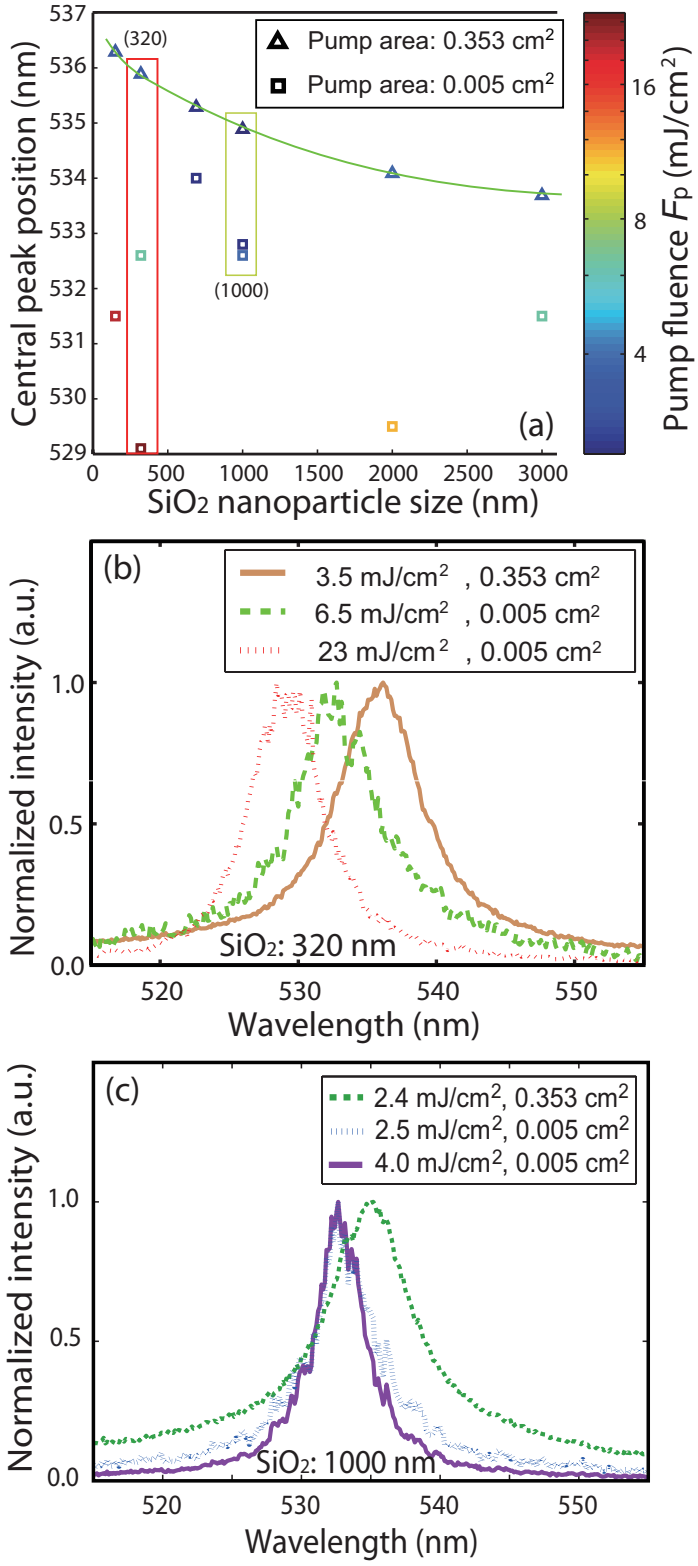

Figure 5.4: (a) Relationship between random laser emission central peak, pump fluence (F_p) and SiO_2 sphere size with typical spectra from the photonic system formed by (b) 320-nm and (c) 1000-nm diameter SiO_2 spheres.

This behaviour is mainly attributed to the difference in transport mean free paths between the photonic glass systems having different sphere sizes. The transport mean free path is a key factor linked to multiple scattering [80, 139, 192] and is determined as the average distance above which the scattering wave is randomized [79], which will be elaborated in the following. Further discussions of transport mean free path can be seen in Subsection 1.3.2, Chapter 1.

5.3.2 Transport Mean Free Path

In order to gain more understanding on how the nano/micro-spheres have an impact on the peak emission wavelength, we applied the Mie scattering theory to map out the wavelength-dependent transport mean free path of our system. In the weak-scattering regime (which is valid in our case because the modest index contrast between scatterers and the gain medium leads to a transport mean free path of light much larger than the wavelength; see below), the wavelength-dependent transport mean free path $\ell_t(\lambda)$ (which should be far less than the sample thickness L for multiple scattering) can be estimated through the following formula [80, 192]:

$$\ell_t(\lambda) = \frac{1}{\rho\sigma_t(\lambda)} \tag{5.1}$$

where $\rho = \eta/(4\pi a^3/3)$ is the density of spheres with filling fraction η ($\eta = 50\%$ was used to do the calculation in the following), and $\sigma_t(\lambda)$ is wavelength-dependent transport scattering cross section. The definitions of scattering cross section (σ_{sc}) and its corresponding asymmetry cross section (σ_{asym}) are given by [193]:

$$\sigma_{sc} = \int d\Omega |f(\theta)|^2 \tag{5.2}$$

$$\sigma_{asym} = \int d\Omega |f(\theta)|^2 cos\theta \tag{5.3}$$

where $|f(\theta)|$ is the scattering amplitude. The transport scattering cross section can then be expressed as [194]:

$$\sigma_t = \int d\Omega |f(\theta)|^2 (1 - cos\theta) = \sigma_{sc} - \sigma_{asym} \tag{5.4}$$

In terms of scattering by a solid dielectric sphere with radius a and refractive index n_{sph}, the scattering cross section is given by [80, 193]:

$$\sigma_{sc} = (2\pi/k^2) \sum_{n=1}^{\infty} (2n+1)(|a_n|^2 + |b_n|^2) \tag{5.5}$$

where $k = 2\pi n_{sur}/\lambda_0$ is the wave vector in the surrounding medium with refractive index n_{sur} and λ_0 is the free space scattering wavelength. Here, a_n and b_n are the scattering coefficients that are given by:

$$a_n = \frac{m\psi_n(mx)\psi_n'(x) - \psi_n(x)\psi_n'(mx)}{m\psi_n(mx)\xi_n'(x) - \xi_n(x)\psi_n'(mx)} \tag{5.6}$$

and

$$b_n = \frac{\psi_n(mx)\psi_n'(x) - m\psi_n(x)\psi_n'(mx)}{\psi_n(mx)\xi_n'(x) - m\xi_n(x)\psi_n'(mx)} \tag{5.7}$$

The parameters of m and x are obtained by the relations $m = n_{sph}/n_{sur}$ and $x = ka$, respectively, while $\lambda_0\psi_n(r) = rj_n(r)$ and $\xi_n(r) = rh_n^{(1)}(r)$, with $j_n(r)$ and $h_n^{(1)}(r)$ the Bessel and Hankel spherical functions of the first type. The asymmetry cross section is then [193]:

$$\sigma_{asym} = (2\pi/k^2)\sum_{n=1}^{\infty}[\frac{2n+1}{n+1}Re(a_n b_n^*) + \frac{n(n+2)}{n+1}Re(a_n a_{n+1}^* + b_n b_{n+1}^*)] \tag{5.8}$$

In our case, we have $n_{sph} = 1.46$ for silica spheres and $n_{sur} = 1.7$ ($\Delta n = |n_{sph} - n_{sur}| = 0.24$) for BBEHP-PPV (Ref.[119]) and the corresponding wavelength-dependent scattering cross section (Fig. 5.5), scattering length (Fig. 5.6), transport mean free paths (Fig. 5.7) were calculated for various sphere sizes for the case with and without ($\Delta n = 0.46$) gain material. From the calculated results, one can see that only transport mean free paths have clear change following the change of the sphere size. The transport mean free paths increase ~5-fold and the Mie resonances are smoothed out going from an index contrast ($\Delta n = 0.46$) [Fig. 5.7(a)] to $\Delta n = 0.24$ [Fig. 5.7(b)] . While, as shown in Fig. 5.7(b), the Mie resonances are still present within the spectral window of the organic semiconductor emission (except for the smallest sphere size $d = 150\ nm$), their reduced strength means that their overall contribution to the transport mean free paths is negligible ($< 5\%$), especially if we take the sphere size dispersity ($< 10\%$ in our case) into account. Thus Mie resonances are expected to have a negligible, or at the very least weak, effect in setting the RL wavelength in the present RL system.

In Fig. 5.7(b), it is seen that ℓ_t increases with the diameter of the spheres. This can be confirmed via coherent backscattering (CBS) measurement (Fig. 5.8; also see Subsection 1.3.2 in Chapter 1 for more discussions) [195, 196], and the experimental values of ℓ_t can be obtained by fitting the CBS cone (Fig. 5.9) using the simplified diffusion CBS model [86, 87]. Table 5.1 presents a comparison of the

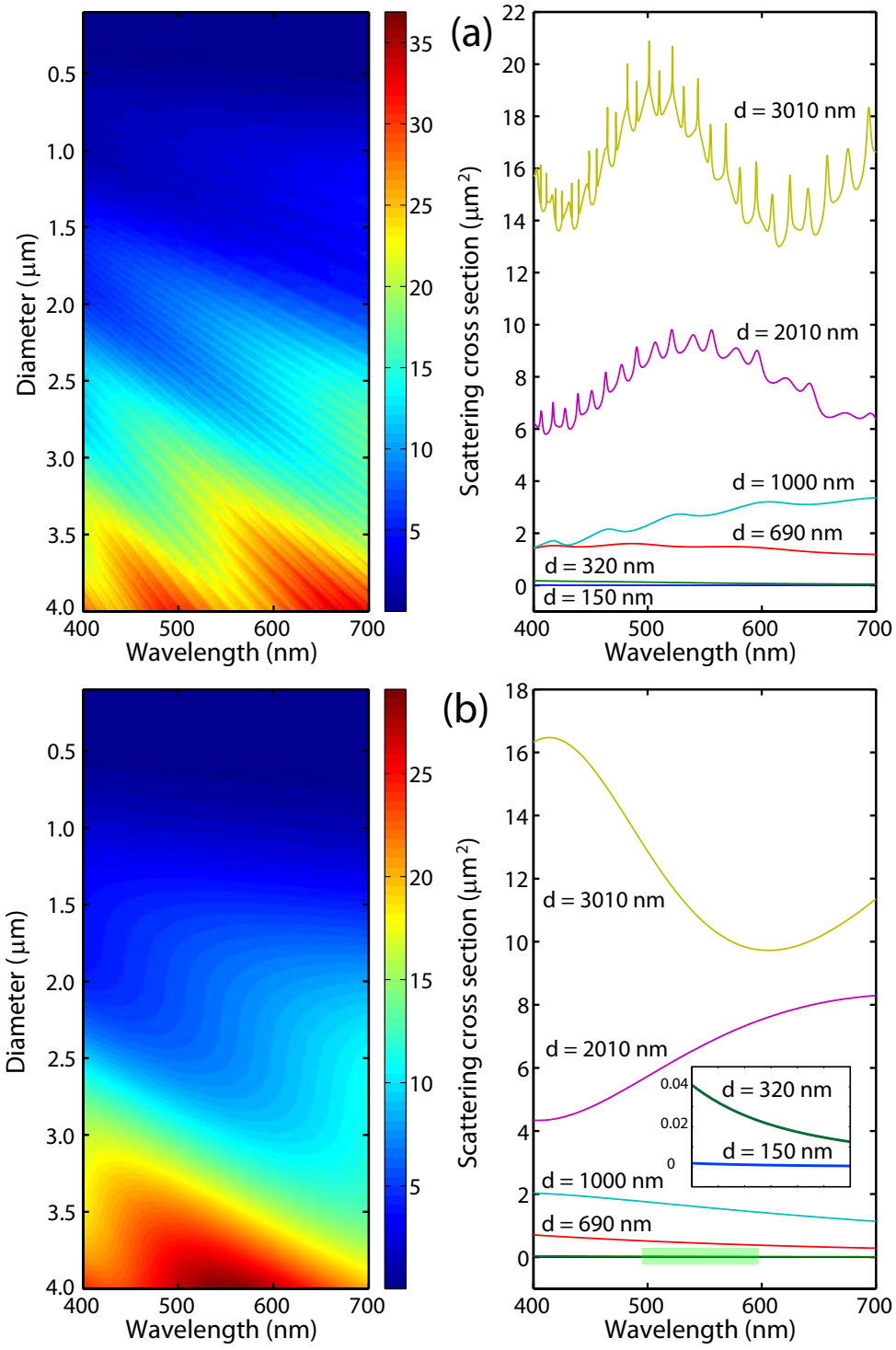

Figure 5.5: (*left panel*) Map of calculated scattering cross section for a random system formed by monodisperse silica spheres ($n_{sph} = 1.46$) surrounded by (a) air and (b) BBEHP-PPV ($n_{sur} = 1.7$). (*right panel*) Plot of scattering cross section versus wavelength for those silica spheres with specific mean diameters used in the experiment.

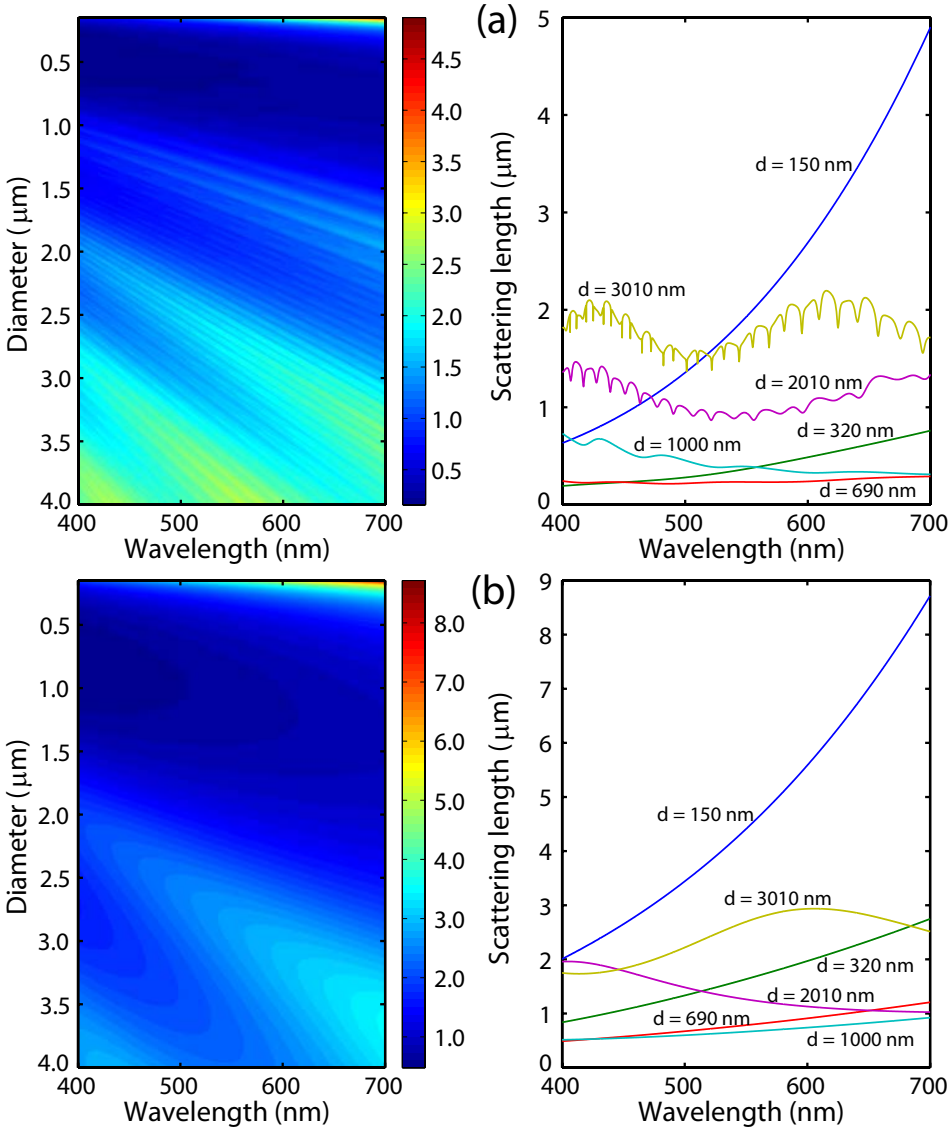

Figure 5.6: (*left panel*) Map of calculated scattering length for a random system formed by monodisperse silica spheres ($n_{sph} = 1.46$) surrounded by (a) air and (b) BBEHP-PPV ($n_{sur} = 1.7$). (*right panel*) Plot of scattering length versus wavelength for those silica spheres with specific mean diameters used in the experiment.

transport mean free path between the calculated and experimental values. The results are consistent, although there is a small discrepancy for bigger spheres. This is mainly due to the simplified assumption for the calculation of ℓ_t simply based on the density of spheres with an estimated filling fraction [80], which will have increasing discrepancy for bigger spheres with about 10% size dispersity. However, it is clear that the transport mean free path is at least an order of

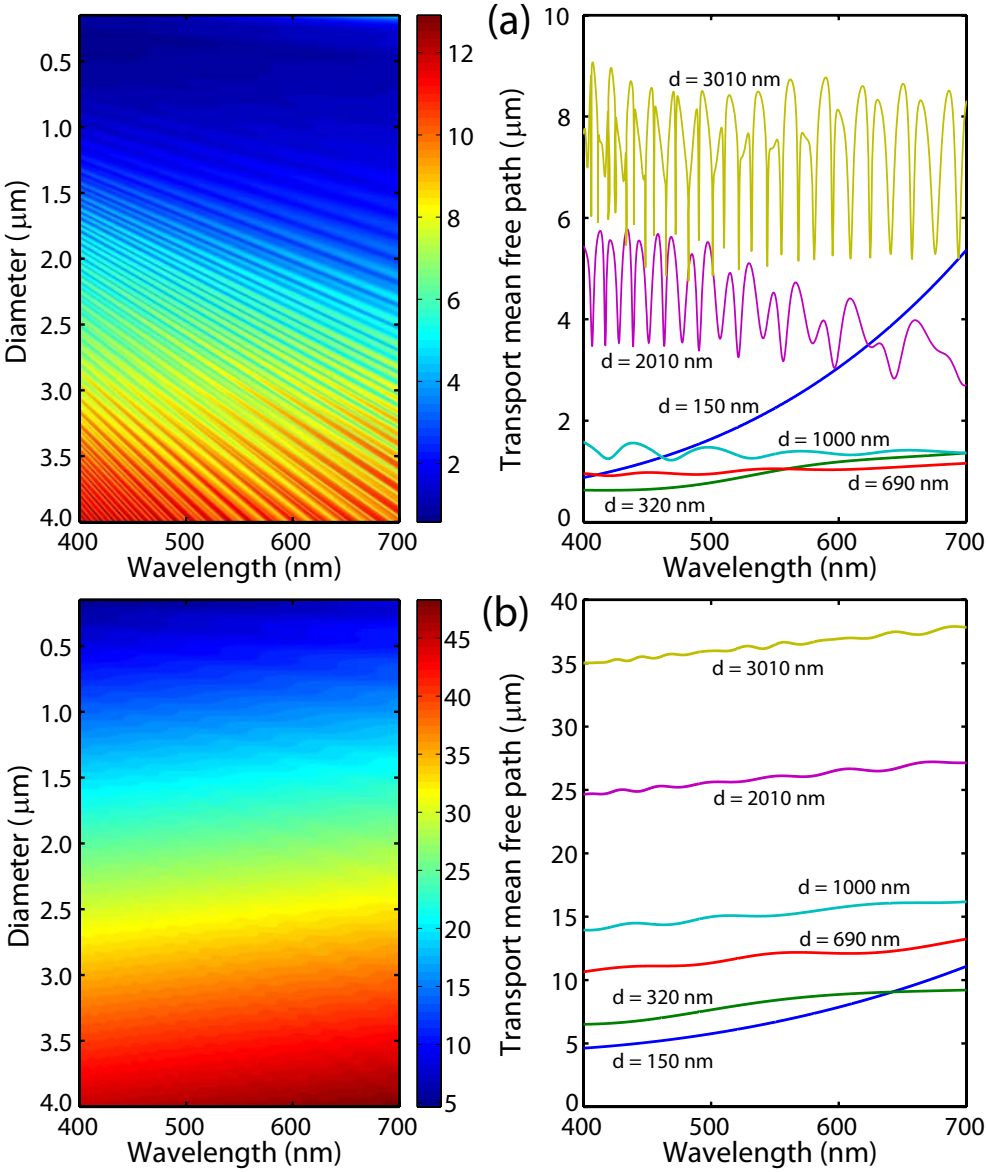

Figure 5.7: (*left panel*) Map of calculated transport mean free path for a random system formed by monodisperse silica spheres ($n_{sph} = 1.46$) surrounded by (a) air and (b) BBEHP-PPV ($n_{sur} = 1.7$). (*right panel*) Plot of transport mean free path versus wavelength for those silica spheres with specific mean diameters used in the experiment.

magnitude larger than the wavelength of interest. According to the Ioffe-Regel criterion ($\lambda \ll \ell_t$) [77]. our photonic glass random laser system operates in the diffusive regime. It is known that in this regime, as can be found by analyzing the rate equations, the random lasing process is dominated by ℓ_t where $\ell_t \ll L$ (the sample thickness) is a prerequisite for multiple light scattering [139].

A longer transport mean free path leads to RL modes which overall interact

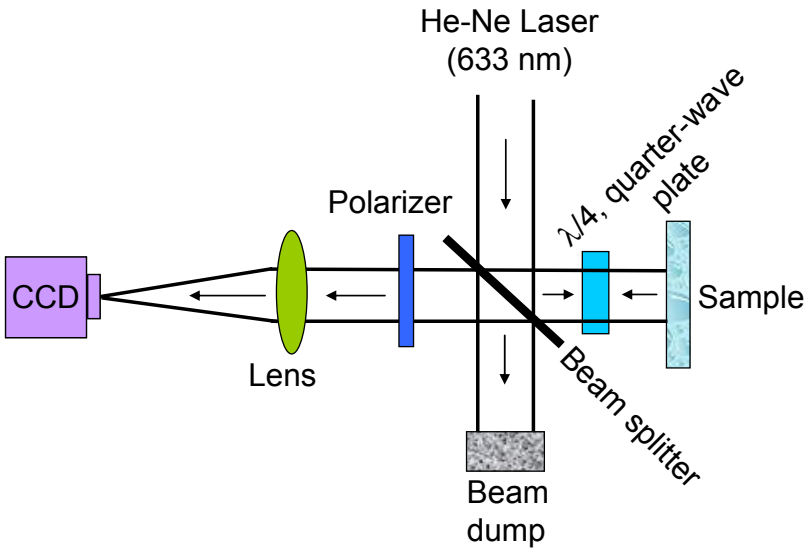

Figure 5.8: Coherent backscattering (CBS) measurement setup.

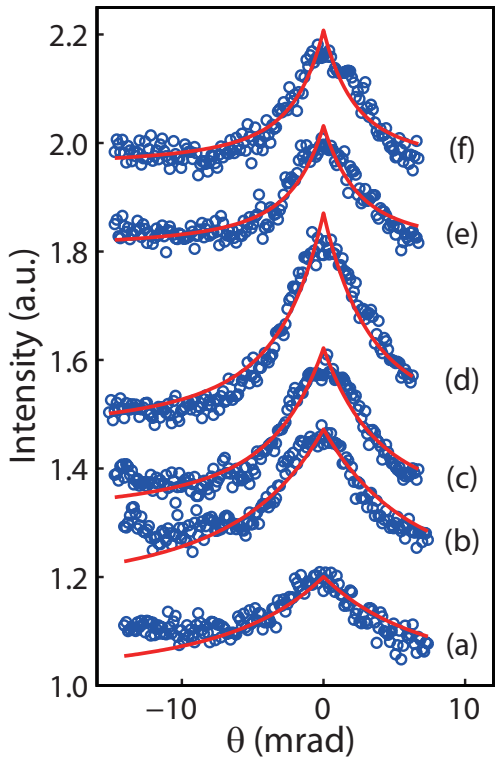

Figure 5.9: Coherent backscattering cone measured (using a He-Ne laser with wavelength of 633 nm) from the as-prepared photonic glass RL samples: $d =$ (a) 150, (b) 320, (c) 690, (d) 1000, (e) 2010, and (f) 3010 nm. The data points are fitted using the CBS model to extract the corresponding ℓ_t. The fitted curves are shifted for clarity. See more discussions on CBS model in Subsection 1.3.2, Chapter 1.

Table 5.1: Transport mean free path ℓ_t ($\lambda = 633$ nm) for the as-prepared photonic glass RL samples.

d (nm)	Calculated ℓ_t (μm)	Experimental ℓ_t (μm)
150	8.8	7.8 (0.5)
320	9.0	8.6 (1.0)
690	12.2	14.0 (1.2)
1000	16.0	16.1 (0.5)
2010	26.5	21.2 (2.1)
3010	37.2	24.0 (1.9)

less with the gain volume, i.e. the photon lifetime in the amplifying region is shorter. Because conjugated polymers are quasi-three level laser systems with non-zero (though small) re-absorption [26], the RL emission wavelength of devices with bigger spheres, hence longer transport mean free paths, is blue-shifted as found experimentally [Fig. 5.4(a)]. While wider wavelength shift is obtained with resonance-driven RL, our diffusive photonic glass RL benefits from the high-gain and relative low threshold conferred by the conjugated polymer. We also note that the 3-nm emission waveband modification is similar to the RL stimulated emission linewidth (3.5-nm FWHM).

5.3.3 Other Factors Modifying Wavelength

Two other factors − the area of the pump spot size and the strength of the pump fluence − can also have an effect on the emission wavelength and can be varied in order to further modify the RL emission wavelength [197–199]. For any of our photonic glass RLs, a smaller pump spot generates a blueshifted emission under the same pump fluence [Figs. 5.4(a) and 5.4(b)]. Furthermore, for the same pump spot area and same diameter of silica spheres, increasing the pump fluence blueshifts the emission central peak position as shown in the rectangular framed data points in Fig. 5.4(a) corresponding to the spectra shown in Figs. 5.4(b) and 5.4(c).

To further demonstrate the effect of the pump area on the RL wavelength, we studied a RL formed by spheres with mean diameter of 320 nm. Spectral evolution as a function of pump fluence was investigated under photo-pumping with two different pump spot areas (Fig. 5.10). It is seen that the overall emission spectrum is narrower (FWHM: $\sim$3 nm) and shows sub-structures or peaks for a small pump spot area (0.0024 cm^2) compared to the result (FWHM: $\sim$5 nm) obtained from a big pump spot area (0.353 cm^2) [see Fig. 5.10(c)]. We then plotted in Fig. 5.11 the laser threshold and the central emission peak position

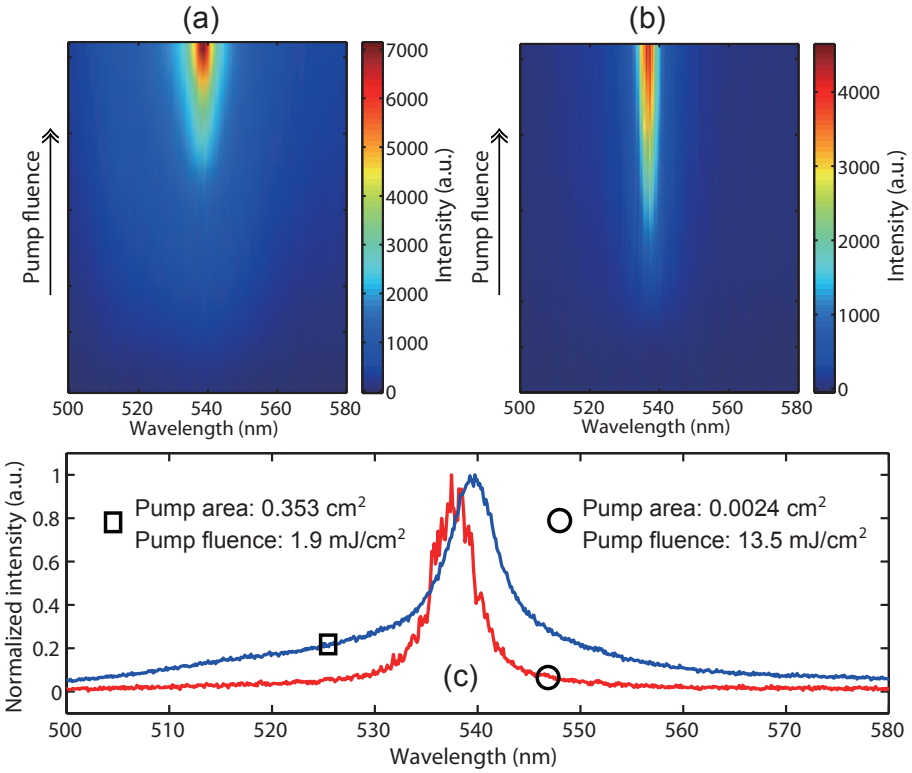

Figure 5.10: Spectral evolution as a function of pump fluence: (a) pump area: 0.353 cm^2 and (b) pump area: 0.0024 cm^2. (c) Normalized emission spectra for the cases of the two different pump spot areas shown in (a) and (b), respectively. The reason for the different pump fluences shown here is that the RL signals reached their own saturation for both cases. All results are for a photonic glass containing 320-nm diameter sphere.

as a function of the pump spot area. The central peak position blueshifts for a smaller pump spot agreeing with the result of Fig. 5.4, while the laser threshold increases (Fig. 5.11). Again, such a spectral blueshift is due to the quasi-three level nature of the organic semiconductor BBEHP-PPV: self-absorption decreases under higher photo-pumping (thus increasing the emitted photon density) or for shorter total interaction length (due to the decrease of gain volume for a smaller pump area). Depletion of the ground state might also play a role by reducing re-absorption. The reason for the change of lasing threshold is that when increasing the pump spot area, emitted photons (in larger gain volume) have a larger chance to trigger stimulated emission events hence generating more gain to compensate for the losses [200]. It is noted that the dependence of threshold fluence (I_{th}) on the pump spot area (A) has been studied in several other cases, showing a similar trend, though its exact mathematical description is still debated [142, 201–203]. In our RL system here, the experimental data of I_{th} against A can be fitted to

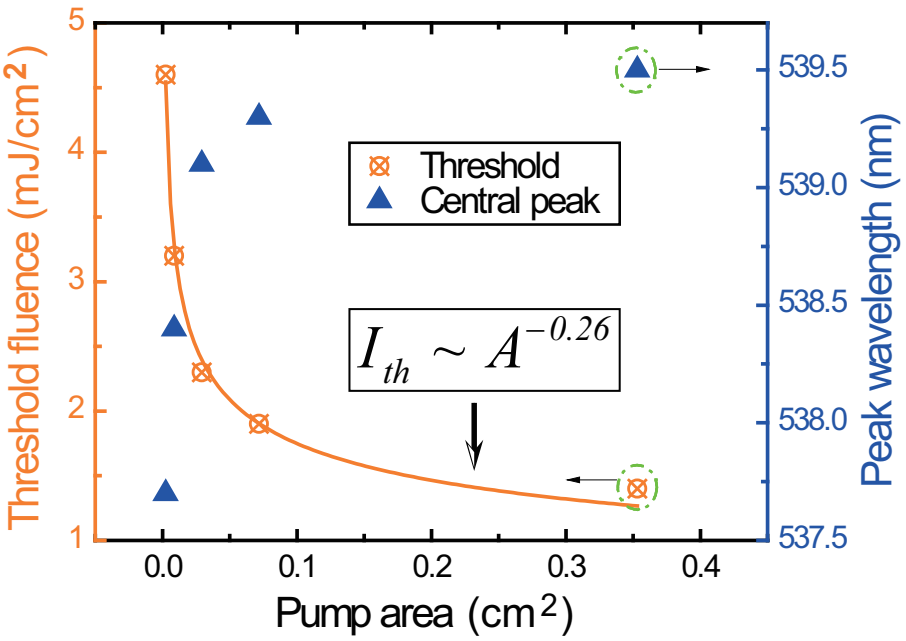

Figure 5.11: Evolution of threshold (I_{th}) and central peak position versus pump spot area (A) for a photonic glass containing 320-nm diameter sphere.

the power law by the formula of $I_{th} \sim A^{-s}$ ($s = 0.26$).

5.4 Summary

In summary, in this chapter we have reported a photonic glass random laser that uses green-emitting π-conjugated polymer, BBEHP-PPV, as a gain medium and can be modified over a 7-nm waveband. The conjugated polymer enables complete filling of the voids within the photonic glass without suffering from quenching and the gain can therefore be maximised. Silica nano/micro-spheres were chosen to form the photonic glass in order to withstand a wide range of solvents and make the RL fabrication entirely solution-processable. The resulting RLs operate in the diffusive regime. The emission wavelength is shifted by changing the size of the spheres in the nano-scale range, thereby altering the transport mean free path, and/or by varying the pump spot size and pump fluence. Therefore, such active solution-processable polymer-based photonic glass systems can be promising candidates for RL applications requiring emission wavelength modification.

Part IV

Summary

Chapter 6

Conclusions and Perspectives

In this chapter, we briefly summarize what we have done. We then discuss a few perspectives including progress and remaining challenges in the area of solution-processed gain lasers.

6.1 Conclusions

We have demonstrated laser action in four types of solution-processed gain media, details of which became major components of this PhD thesis. In order to explain clearly the idea of realizing a laser, the motivation and background information were therefore first introduced in Chapter 1 to build up the foundation of the whole thesis. Starting from the basic concept of how to make a laser, we chose two basic feedback structures (DFB laser and random laser) that are suitable to incorporate solution-processable gain materials such as CdSe/ZnS CQDs and semiconducting polymer BBEHP-PPV. These kinds of laser devices are potentially useful for hybrid integrated laser systems. For the pumping scheme, we adopted an optical pumping setup using a frequency-tripled Q-switched Nd:YAG laser (5-ns pulse, 10-Hz repetition rate and 355-nm excitation wavelength) to photo-pump our laser samples.

Part II is all about CQD-based lasers. In Chapter 2, a flexible DFB CQD laser is presented. We used an exposed standard commercial blank DVD as the mask to fabricate a submicron scale grating structure using a UV transparent polymerisable host matrix (CHDV). Solution-based CdSe/ZnS core-shell CQDs were drop-coated onto it to form the gain layer, the lasing properties of which were examined, including the emission spectra, polarization and lifetime performance. In Chapter 3, in order to explore the lasing behaviour in a scattering gain medium, following the protocol of what key elements required for a random laser, we deposited (CdSe)/ZnS CQDs into rough microscale grooves fabricated on the surface of a glass substrate. Eventually we achieved a CQD random laser and in particular, we applied the FPT method to study the 'possible' naturally occurring resonator inside the scattering gain system.

For embracing great advantages of using organic materials, we also investigated semiconducting polymer lasers, the results of which are presented in Part III. In Chapter 4, we have demonstrated a free-standing membrane DFB laser using a novel guest-host organic composite with π-conjugated BBEHP-PPV as the chromophore. Instead of using a passive grating structure, in this work we doped gain material BBEHP-PPV with CHDV to form an active grating structure. Detailed gain and loss measurement on both the pure BBEHP-PPV thin film and BBEHP-PPV/CHDV membrane samples (with different concentrations) are provided. In Chapter 5, we moved to study how to control the emission wavelength in an organic random laser based on photonic glass structure. BBEHP-PPV was used again as the gain material and monodispersed silica micro/nano spheres were used to form the photonic glass samples. By changing the sphere's size,

we alter the light transport mean free path in the disordered system which, as we explained in Chapter 1, thus influences the lasing properties including the emission wavelength. A simplified Mie scattering model was adopted to calculated the transport mean free paths, which were also corroborated with coherent backscattering measurements, in various photonic glass samples infiltrated the gain (BBEHP-PPV) material. Other than that, we found that further modifying the emission wavelength can be done by varying the pump spot size and pump fluence.

These four types of new laser devices based on solution-processed gain media may have many potential applications including chemosensing. However, at the current stage, they are achieved via optically pumped scheme. The pump source we used is still too bulky and in total the whole system is too expensive when taking into account the price of the Nd:YAG pump laser. It is also noticed that the output of such solution-processed gain lasers is pulsed so far. Both the output beam quality and absolute output power are not good enough to be applied in areas like spectroscopy where currently traditional inorganic solid-state lasers still play an important role. Nevertheless, solution-processed gain lasers offer a range of generic attractive features including the ease of fabrication and can cover a widely tunable emission wavelength compared to their inorganic counterparts. They may also be readily integrated with other mature technology platforms (e.g. silicon or other compound semiconductors) and thus provide potential innovated applications, particularly if the current limitations mentioned above can be overcome.

Practical applications of such laser devices toward market may prefer electrically pumped scheme. Meantime, ultrasmall compact laser devices are key components to integrated optoelectronics. It is therefore that directions toward electrically pumped and possible continue-wave output solution-processed gain lasers and/or toward ultrasmall even nanoscaled lasers are promising topics to explore. In the following, we briefly discuss a few perspectives that are mainly in these topics.

6.2 A Few Perspectives

There is no doubt that there are rapid development in this field of new lasers, particularly using solution-processed gain media. In the following, recent progress and a few perspectives will be discussed, including remaining challenges.

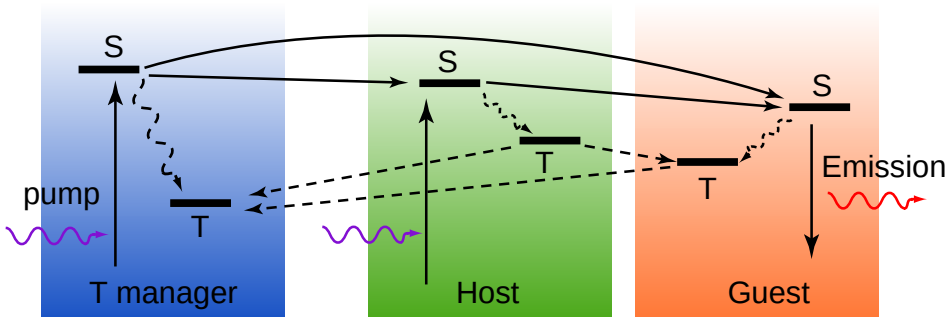

Figure 6.1: "Triplet manager" assisted organic lasing system. Pump photons excite the singlet states of the triplet manager and the host molecules, populating the singlet state of the guest via Förster transfer [204] to generate laser emission. The triplet manager has lower triplet energy and thus the triplet state of the guest can be transferred to the triplet manager via Dexter transfer [205]. The absorption of the triplet manager is shifted from the laser emission, which can minimize self-absorption of the laser emission. Adapted from Refs. [206, 207].

6.2.1 Towards Continuous-Wave Lasing in OSLs

So far, the reported organic semiconductor lasers (OSLs) only operate in pulsed output, typically in the nanosecond range. It is thus highly desirable to try to achieve continuous-wave (CW) lasing output in OSLs, which certainly would have many applications. However, the high triplet population accumulated through intersystem crossing (ISC) in organic gain media is the main obstacle that prevents the CW operation in OSLs. The reason for that is because the direct transition between the triplet state (spin 1 means a molecule with two unpaired electron spins) to the singlet (spin 0 means that all electron spins in a molecule are paired) ground state is forbidden by the rules of quantum mechanics [208].

Several attempts aiming at CW operation in solid-state OSLs have been made by way of mitigating triplet losses. For example, Bornemann *et al.* [209] reported the first realization of a CW solid-state dye laser disc rotated with a frequency of 50-100 Hz in order to avoid the pile-up of triplet excitons in the organic gain medium. Rabe *et al.* [210] and Lehnhardt *et al.* [211] investigated solid-state semiconducting polymer lasers operating at repetition rates up to several MHz and the duration of the laser emission can be extended to about 400 μs pumped using a diode laser with wavelength of 355 nm, which they considered as quasi-CW. More recently, Y. Zhang and Forrest [206] proposed using a three-molecule system including a "triplet manager" to help depopulate the triplet state of the emitter (see Fig. 6.1) and therefore extend the lasing duration which could in principle enable solid-state OSLs to enter the CW lasing regime.

6.2.2 Progress in Electrically Pumped OSLs

At the current stage, no convincing electrically semiconducting polymer laser has been reported yet, which probably remains as one of the key technical issues for practical applications using OSLs.

There has been a bit of history in terms of claims of electrically pumped organic laser diodes. The notorious one is that in 2000, the then-Bell-Labs-researchers, Schön *et al.* [212] claimed that an organic solid state injection laser had been demonstrated using tetracene single crystals. The claimed "breakthrough" of realizing an organic diode was subsequently put under the microscope, including a very detailed theoretical investigation by Baldo *et al* [213], whose study pointed out that the results of the lasing demonstration by Schön *et al.* [212] is unconvincing. It then turned out that the validity of data reported in that paper was concerned in the investigation at Bell Labs, and thus the paper was retracted [214].

Nevertheless, there are several reports showing spectrally narrowing of emission with a cerntain degree of coherent properties from electrically excited organic semiconductors, typically organic dye molecules. In particular, Duarte *et al.* [215–217] argued that the evidence of showing a highly directional (low-divergence emission beam: $\Delta\theta \sim 2.5$ mrad), spatially coherent (high spatial visibility: ~ 0.9), and narrow-linewidth of emission, is leading to the conclusion that the emission of such electrically pumped dye-doped organic semiconductor laser is comparable with the emission from the typical optically pumped pulsed dye laser. Using a similar configuration as Duarte's, Liu *et al.* [218] observed that there exists a threshold with spectral-narrowing of emission, and a spatial visibility of 0.89 above the threshold was recorded via focusing the emission beam onto a pair of slits. A commentary was then appeared in Nature Photonics by Samuel *et al.* [25] raising concerns to doubt the lasing behaviour claimed in Liu *et al.*'s paper [218].

Further analysis [26] suggests that all most organic materials including the currently available conjugated polymers cannot sustain a high current density of above 1 kA/cm^2, that is, the estimated threshold for an organic laser diode. Needless to say that there are additional losses including contacts, injected charges and triplet formation. Therefore, for a typical organic light emitting diode (OLED) structure, the feasibility of achieving electrically pumped lasing is very difficult. Partly because of that, researchers are moving forward to try other innovative architectures like organic light emitting transistors (OLET) [219–222] that can work in a high current density and be able to achieve higher carrier mobility,

which may pave the way toward electrically pumped organic lasers.

It is also noticed that there is another type of organic laser, in which excitons and photons are strongly coupled to form new (coherent) eigenstates, called *polaritons* [223]. Room-temperature optically pumped polariton lasing in an organic microcavity based on a molecular crystal (anthracene) has been demonstrated by Kéna-Cohen and Forrest [224]. Since the threshold of such polariton laser would be lower than that of conventional laser, the feasibility of achieving electrically driven polariton lasing looks promising [225], given that emissive electrically pumped organic exciton-polariton device has been demonstrated [226].

On the other hand, great progress has also been made using laser diodes (i.e. GaN-based) as a pump source to achieve OSLs [227–230], the scheme of which is referred to as indirect electrically driven approach [26]. In this case, the loss due to absorption induced by the injection of charge carriers in the organic gain medium can thus be avoided, which is considered as one of the main challenges in realizing OSLs [231]. Encouraged by that, a further step has been proposed to use a more cheaper and compact LED as the pump source to achieve OSLs [27], experiments of which are currently underway in several research groups, including ours (aming at realizing CMOS-controlled μ-LED pixelated array pumped OSLs, led by Prof. Dawson; see Fig. 6.2) [232]. For instance, a polymer laser pumped by a commercial InGaN LED (in a pulsed mode: 36 ns) has been demonstrated in Samuel's group [233], though the threshold ($\sim$ 144 A) is still too high to have practical applications.

It is therefore that more work needs to be done for making better OSLs. For example, it is desired to explore new organic gain materials to not only lower the lasing threshold but also to be capable of sustain high current density. Meantime, innovative design regarding laser structures should be pursued to optimize and improve lasing performance in order to fabricate robust OSLs for practical applications.

6.2.3 Lasing Spaser or Nanoplasmonic Laser

In recent years, nanophotonics has experienced a period of explosive development in which novel ideas and successful achievements appear in both fundamentals and applications. It is highly desired to concentrate optical energy into regions in the subwavelength scale, potentially for ultra-high density nanophotonic integration [234]. Prediction has been done in theory that stimulated emission of coherent photons can be generated in a gain medium assisted by surface plasmons in a resonating metallic nanostructures, the phenomenon of which is called

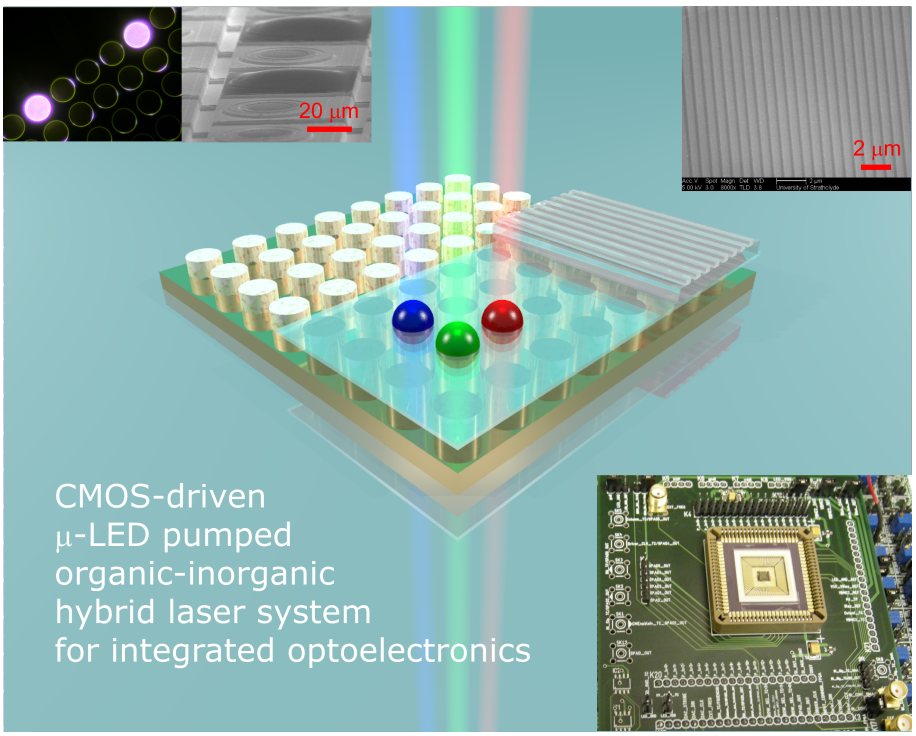

Figure 6.2: μ-LED pumped hybrid laser system. The main component of the image is an art illustration of a 8×8 flip-chip μ-LED pixel array with half area of sapphire being removed and half remained. In an area on the μ-LED chip, dome-shape (Red, Green and Blue) light-emitting organic composites are integrated with the pixels using inkjet printing technique; while in another area, a submicron-scale grating structure is attached with the gain material being either incorporated or spin-coated to form a thin film as active region. Inset in the left upper corner: (left) microscopic photo image of μ-LED pixel array with two pixels being on, and (right) SEM image showing inkjet printed dome-shape organic composite structures sitted on the top of μ-LED pixels. Inset in the right upper corner is a SEM image of a submicron-scale grating structure. Inset in the right lower corner is the electronic circuit board designed and fabricated for CMOS-driven μ-LED chip, in collaboration with Dr. Robert K. Henderson's group at the University of Edinburgh.

a **SPASER**, short for *surface plasmons amplification by stimulated emission of radiation*, introduced by Bergman and Stockman in 2003 [235]. It is pointed out that a spaser, also called a *nanoplasmonic laser*, in theory, should able to overcome the diffraction limit and focus optical energy within the scale much smaller than the wavelength. The reason for that, as Stockman later further explained [236], the optical energy can be concentrated in modes, the so-called *surface plasmons*, which are coherent electron oscillations. Normally, surface plasmons can be excited at the interface between metal and dielectric. For example, Fig. 6.3

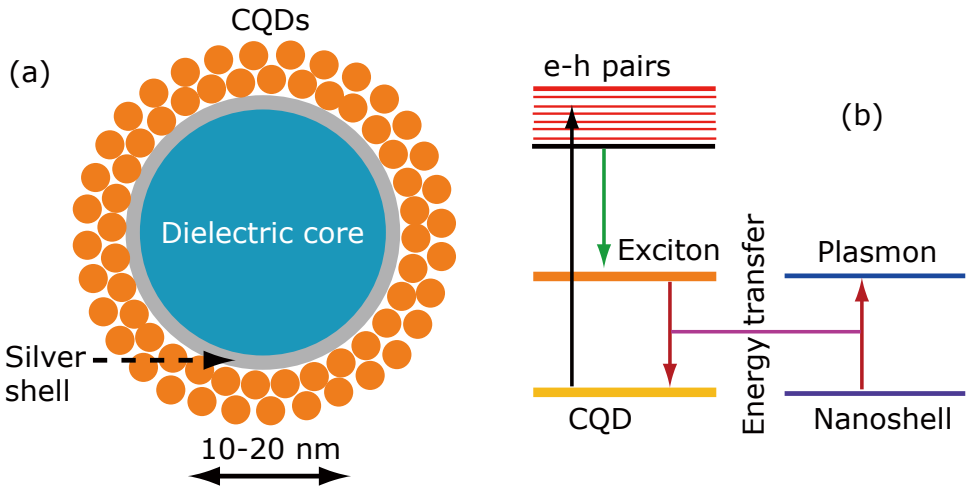

Figure 6.3: The lasing spaser mechanism: (a) a proposed spaser structure using CQDs coated on the surface of a dielectric/silver core-shell nanostructure; and (b) schematic of energy levels and possible transitions in a spaser. The pump energy excites a transition forming electron−hole $(e-h)$ pairs in the higher level (black arrow) and subsequently relax to excitonic levels (green arrow). The exciton recombines and transfer its energy to the plasmon excitation of the silver nanoshell via resonant coupled transitions (red arrows) without emitting a photon. Adapted from Ref. [236].

shows a possible design of spaser using CQDs as a gain material.

Following that, there have been multiple attempts on demonstrating spaser action [237–241]. In particular, Noginov *et al.* [242] reported their experimental demonstration of lasing spaser in a 44-nm diameter nanoparticles formed by a gold core coated with dye-doped silica shell, confirming such prediction. Their results, including others such as a nanowire-based plasmonic laser reported by X. Zhang's group [243], suggest promising applications for nanolasers that can perform far beyond the light diffraction limit, thus realizing ultra-compact lasers in a new generation of nanophotonic systems. Hence this is certainly a promising area that solution-processable gain materials can be involved in.

Bibliography

[1] T. Maiman, "Stimulated optical radiation in ruby," Nature **187**, 493–494 (1960).

[2] A. Javan, W. R. Bennett, and D. R. Herriott, "Population inversion and continuous optical maser oscillation in a gas discharge containing a He-Ne mixture," Phys. Rev. Lett. **6**, 106–110 (1961).

[3] H. Kroemer, "A proposed class of hetero-junction injection lasers," Proc. IEEE **51**, 1782–1783 (1963).

[4] R. Mears, L. Reekie, S. Poole, and D. Payne, "Low-threshold tunable CW and Q-switched fibre laser operating at 1.55 μm," Electron. Lett. **22**, 159–160 (1986).

[5] J. Faist, F. Capasso, D. Sivco, C. Sirtori, A. Hutchinson, and A. Cho, "Quantum cascade laser," Science **264**, 553–556 (1994).

[6] S. Nakamura, M. Senoh, S. Nagahama, N. Iwasa, T. Yamada, T. Matsushita, H. Kiyoku, and Y. Sugimoto, "InGaN multi-quantum-well-structure laser diodes with cleaved mirror cavity facets," Jpn. J. Appl. Phys. **35**, L217–L220 (1996).

[7] A. E. Siegman, *Lasers* (University Science Books, Mill Valley, California, 1986).

[8] O. Svelto, *Principles of Lasers, 5th ed.* (Springer-Verlag, Berlin, 2009).

[9] G. Peters and L. Allen, "Amplified spontaneous emission I. the threshold condition," J. Phys. A **4**, 238–243 (1971).

[10] L. Allen and G. Peters, "Amplified spontaneous emission. II. the connection with laser theory," J. Phys. A **4**, 377–381 (1971).

[11] L. Allen and G. Peters, "Amplified spontaneous emission III. intensity and saturation," J. Phys. A **4**, 564–573 (1971).

[12] G. Peters and L. Allen, "Amplified spontaneous emission. IV. beam divergence and spatial coherence," J. Phys. A **5**, 546–554 (1972).

[13] L. Allen and G. Peters, "Spectral distribution of amplified spontaneous emission," J. Phys. A **5**, 695–704 (1972).

[14] L. Allen and G. I. Peters, "Amplified spontaneous emission and external signal amplification in an inverted medium," Phys. Rev. A **8**, 2031–2047 (1973).

[15] L. Casperson and A. Yariv, "Spectral narrowing in high-gain lasers," IEEE J. Quantum Electron. **QE-8**, 80–85 (1972).

[16] H. Gamo, J. Ostrem, and S. Chuang, "Determination of line-shape parameters of high-gain laser transitions based on line-narrowing measurements," J. Appl. Phys. **44**, 2750–2755 (1973).

[17] L. Casperson, "Threshold characteristics of mirrorless lasers," J. Appl. Phys. **48**, 256–262 (1977).

[18] J. C. Garrison, B. Ritchie, H. Nathel, C. K. Hong, and L. Minner, "Wave-optics description of amplified spontaneous emission," Phys. Rev. A **43**, 4941–4953 (1991).

[19] G. Pert, "Output characteristics of amplified-stimulated-emission lasers," J. Opt. Soc. Am. B **11**, 1425–1435 (1994).

[20] G. J. Linford, E. R. Peressini, W. R. Sooy, and M. L. Spaeth, "Very long lasers," Appl. Opt. **13**, 379–390 (1974).

[21] O. Svelto, S. Taccheo, and C. Svelto, "Analysis of amplified spontaneous emission: some corrections to the Linford formula," Opt. Commun. **149**, 277–282 (1998).

[22] K. Shaklee and R. Leheny, "Direct determination of optical gain in semiconductor crystals," Appl. Phys. Lett. **18**, 475–477 (1971).

[23] F. De Martini and G. R. Jacobovitz, "Anomalous spontaneous-stimulated-decay phase transition and zero-threshold laser action in a microscopic cavity," Phys. Rev. Lett. **60**, 1711–1714 (1988).

[24] T. Ostatnickỳ, J. Valenta, I. Pelant, K. Luterová, R. Elliman, S. Cheylan, and B. Hönerlage, "Photoluminescence from an active planar optical waveguide made of silicon nanocrystals: dominance of leaky substrate modes in dissipative structures," Opt. Mater. **27**, 781–786 (2005).

[25] I. D. W. Samuel, E. B. Namdas, and G. A. Turnbull, "How to recognize lasing," Nature Photon. **3**, 546–549 (2009).

[26] I. D. W. Samuel and G. A. Turnbull, "Organic semiconductor lasers," Chem. Rev. **107**, 1272–1295 (2007).

[27] M. McGehee, M. Díaz-García, F. Hide, R. Gupta, E. Miller, D. Moses, and A. Heeger, "Semiconducting polymer distributed feedback lasers," Appl. Phys. Lett. **72**, 1536–1538 (1998).

[28] G. Turnbull, P. Andrew, W. Barnes, and I. Samuel, "Operating characteristics of a semiconducting polymer laser pumped by a microchip laser," Appl. Phys. Lett. **82**, 313–315 (2003).

[29] K. Yoshino, S. Tatsuhara, Y. Kawagishi, M. Ozaki, A. Zakhidov, and Z. Vardeny, "Amplified spontaneous emission and lasing in conducting polymers and fluorescent dyes in opals as photonic crystals," Appl. Phys. Lett. **74**, 2590–2592 (1999).

[30] A. Jebali, R. Mahrt, N. Moll, D. Erni, C. Bauer, G. Bona, and W. Bächtold, "Lasing in organic circular grating structures," J. Appl. Phys. **96**, 3043–3049 (2004).

[31] H. Kogelnik and C. Shank, "Coupled-wave theory of distributed feedback lasers," J. Appl. Phys. **43**, 2327–2335 (1972).

[32] W. Streifer, D. Scifres, and R. Burnham, "Coupling coefficients for distributed feedback single- and double-heterostructure diode lasers," IEEE J. Quantum Electron. **QE-11**, 867–873 (1975).

[33] A. Yariv, "Coupled-mode theory for guided-wave optics," IEEE J. Quantum Electron. **9**, 919–933 (1973).

[34] W. Streifer, D. Scifres, and R. Burnham, "Tm-mode coupling coefficients in guided-wave distributed feedback lasers," IEEE J. Quantum Electron. **12**, 74–78 (1976).

[35] R. Ambartsumyan, N. Basov, P. Kryukov, and V. Letokhov, "5A10(b)–A laser with a nonresonant feedback," IEEE J. Quantum Electron. **QE-2**, 442–446 (1966).

[36] V. Letokhov, "Stimulated emission of an ensemble of scattering particles with negative absorption," JETP Lett. **5**, 212–215 (1967).

[37] M. Noginov, *Solid-State Random Lasers* (Springer-Verlag, Berlin, 2005).

[38] N. M. Lawandy, R. M. Balachandran, A. S. L. Gomes, and E. Sauvain, "Laser action in strongly scattering media," Nature **368**, 436–438 (1994).

[39] H. Cao, Y. G. Zhao, S. T. Ho, E. W. Seelig, Q. H. Wang, and R. P. H. Chang, "Random laser action in semiconductor powder," Phys. Rev. Lett. **82**, 2278–2281 (1999).

[40] H. Cao, "Random lasers: development, features and applications," Opt. Photon. News **16**, 24–29 (2005).

[41] D. S. Wiersma, "The physics and applications of random lasers," Nature Phys. **4**, 359–367 (2008).

[42] R. Polson and Z. Vardeny, "Random lasing in human tissues," Appl. Phys. Lett. **85**, 1289–1291 (2004).

[43] S. John and G. Pang, "Theory of lasing in a multiple-scattering medium," Phys. Rev. A **54**, 3642–3652 (1996).

[44] R. Balachandran, N. Lawandy, and J. Moon, "Theory of laser action in scattering gain media," Opt. Lett. **22**, 319–321 (1997).

[45] S. V. Frolov, Z. V. Vardeny, K. Yoshino, A. Zakhidov, and R. H. Baughman, "Stimulated emission in high-gain organic media," Phys. Rev. B **59**, R5284–R5287 (1999).

[46] C. M. Soukoulis, X. Jiang, J. Y. Xu, and H. Cao, "Dynamic response and relaxation oscillations in random lasers," Phys. Rev. B **65**, 041103 (2002).

[47] K. L. van der Molen, A. P. Mosk, and A. Lagendijk, "Relaxation oscillations in long-pulsed random lasers," Phys. Rev. A **80**, 055803 (2009).

[48] R. Ambartsumyan, P. Kryukov, V. Letokhov, and Y. Matveev, "Emission statistics of a laser with nonresonant feedback," JETP Lett. **5**, 312–314 (1967).

[49] G. Zacharakis, N. Papadogiannis, G. Filippidis, and T. Papazoglou, "Photon statistics of laserlike emission from polymeric scattering gain media," Opt. Lett. **25**, 923–925 (2000).

[50] H. Cao, Y. Ling, J. Y. Xu, C. Q. Cao, and P. Kumar, "Photon statistics of random lasers with resonant feedback," Phys. Rev. Lett. **86**, 4524–4527 (2001).

[51] M. Patra, "Theory for photon statistics of random lasers," Phys. Rev. A **65**, 043809 (2002).

[52] L. Florescu and S. John, "Photon statistics and coherence in light emission from a random laser," Phys. Rev. Lett. **93**, 013602 (2004).

[53] R. J. Glauber, "Photon correlations," Phys. Rev. Lett. **10**, 84–86 (1963).

[54] X. Jiang and C. M. Soukoulis, "Time dependent theory for random lasers," Phys. Rev. Lett. **85**, 70–73 (2000).

[55] A. L. Burin, M. A. Ratner, H. Cao, and R. P. H. Chang, "Model for a random laser," Phys. Rev. Lett. **87**, 215503 (2001).

[56] V. M. Apalkov, M. E. Raikh, and B. Shapiro, "Random resonators and prelocalized modes in disordered dielectric films," Phys. Rev. Lett. **89**, 016802 (2002).

[57] H. Cao, X. Jiang, Y. Ling, J. Y. Xu, and C. M. Soukoulis, "Mode repulsion and mode coupling in random lasers," Phys. Rev. B **67**, 161101 (2003).

[58] S. Mujumdar, M. Ricci, R. Torre, and D. S. Wiersma, "Amplified extended modes in random lasers," Phys. Rev. Lett. **93**, 053903 (2004).

[59] C. Conti, M. Leonetti, A. Fratalocchi, L. Angelani, and G. Ruocco, "Condensation in disordered lasers: theory, 3D + 1 simulations, and experiments," Phys. Rev. Lett. **101**, 143901 (2008).

[60] J. Fallert, R. Dietz, J. Sartor, D. Schneider, C. Klingshirn, and H. Kalt, "Co-existence of strongly and weakly localized random laser modes," Nature Photon. **3**, 279–282 (2009).

[61] H. E. Türeci, L. Ge, S. Rotter, and A. D. Stone, "Strong interactions in multimode random lasers," Science **320**, 643–646 (2008).

[62] J. Andreasen and H. Cao, "Numerical study of amplified spontaneous emission and lasing in random media," Phys. Rev. A **82**, 063835 (2010).

[63] A. Tulek, R. Polson, and Z. Vardeny, "Naturally occurring resonators in random lasing of π-conjugated polymer films," Nature Phys. **6**, 303–310 (2010).

[64] J. Andreasen, A. Asatryan, L. Botten, M. Byrne, H. Cao, L. Ge, L. Labonté, P. Sebbah, A. Stone, H. Türeci *et al.*, "Modes of random lasers," Adv. Opt. Photon. **3**, 88–127 (2011).

[65] M. Leonetti, C. Conti, and C. Lopez, "The mode-locking transition of random lasers," Nature Photon. **5**, 615–617 (2011).

[66] H. Kalt, "Towards mode-locking," Nature Photon. **5**, 573–574 (2011).

[67] M. Leonetti, C. Conti, and C. Lopez, "A random laser tailored by directional stimulated emission," Arxiv preprint arXiv:1112.3533 (2011).

[68] J. Andreasen, P. Sebbah, and C. Vanneste, "Coherent instabilities in random lasers," Phys. Rev. A **84**, 023826 (2011).

[69] J. Andreasen and H. Cao, "Inherent stochastic linearization of random laser modes," Nonlinearity **25**, 851–868 (2012).

[70] R. Polson and Z. Vardeny, "Spatially mapping random lasing cavities," Opt. Lett. **35**, 2801–2803 (2010).

[71] O. Zaitsev and L. Deych, "Recent developments in the theory of multimode random lasers," J. Opt. **12**, 024001 (2010).

[72] D. Hofstetter and R. Thornton, "Loss measurements on semiconductor lasers by fourier analysis of the emission spectra," Appl. Phys. Lett. **72**, 404–406 (1998).

[73] R. Polson, G. Levina, and Z. Vardeny, "Spectral analysis of polymer microring lasers," Appl. Phys. Lett. **76**, 3858–3860 (2000).

[74] R. Polson, M. Raikh, and Z. Vardeny, "Universality in unintentional laser resonators in π-conjugated polymer films," C. R. Physique **3**, 509–521 (2002).

[75] H. Cao, "Review on latest developments in random lasers with coherent feedback," J. Phys. A **38**, 10497–10535 (2005).

[76] P. W. Anderson, "Absence of diffusion in certain random lattices," Phys. Rev. **109**, 1492–1505 (1958).

[77] S. John, "Electromagnetic absorption in a disordered medium near a photon mobility edge," Phys. Rev. Lett. **53**, 2169–2172 (1984).

[78] P. Anderson, "The question of classical localization: a theory of white paint," Phil. Mag. B **52**, 505–509 (1985).

[79] D. S. Wiersma and A. Lagendijk, "Light diffusion with gain and random lasers," Phys. Rev. E **54**, 4256–4265 (1996).

[80] E. Akkermans and G. Montambaux, *Mesoscopic Physics of Electrons and Photons* (Cambridge University Press, Cambridge, UK, 2007).

[81] S. John, "Localization of light," Phys. Today **44**, 32–40 (1991).

[82] K. L. van der Molen, A. P. Mosk, and A. Lagendijk, "Intrinsic intensity fluctuations in random lasers," Phys. Rev. A **74**, 053808 (2006).

[83] Y. Kuga and A. Ishimaru, "Retroreflectance from a dense distribution of spherical particles," J. Opt. Am. Soc. A **1**, 831–835 (1984).

[84] M. Albada and A. Lagendijk, "Observation of weak localization of light in a random medium," Phys. Rev. Lett. **55**, 2692–2695 (1985).

[85] P.-E. Wolf and G. Maret, "Weak localization and coherent backscattering of photons in disordered media," Phys. Rev. Lett. **55**, 2696–2699 (1985).

[86] E. Akkermans, P. E. Wolf, and R. Maynard, "Coherent backscattering of light by disordered media: analysis of the peak line shape," Phys. Rev. Lett. **56**, 1471–1474 (1986).

[87] D. S. Wiersma, M. P. van Albada, B. A. van Tiggelen, and A. Lagendijk, "Experimental evidence for recurrent multiple scattering events of light in disordered media," Phys. Rev. Lett. **74**, 4193–4196 (1995).

[88] C. Murray, C. Kagan, and M. Bawendi, "Synthesis and characterization of monodisperse nanocrystals and close-packed nanocrystal assemblies," Annu. Rev. Mater. Sci. **30**, 545–610 (2000).

[89] V. Klimov, ed., *Nanocrystal Quantum Dots, 2nd ed.* (CRC Press, Boca Raton, Florida, 2010).

[90] C. Murray, D. Norris, and M. Bawendi, "Synthesis and characterization of nearly monodisperse CdE (E= S, Se, Te) semiconductor nanocrystallites," J. Am. Chem. Soc. **115**, 8706–8715 (1993).

[91] M. Hines and P. Guyot-Sionnest, "Synthesis and characterization of strongly luminescing ZnS-capped CdSe nanocrystals," J. Phys. Chem. **100**, 468–471 (1996).

[92] B. Dabbousi, J. Rodriguez-Viejo, F. Mikulec, J. Heine, H. Mattoussi, R. Ober, K. Jensen, and M. Bawendi, "(CdSe)ZnS core-shell quantum dots: synthesis and characterization of a size series of highly luminescent nanocrystallites," J. Phys. Chem. B **101**, 9463–9475 (1997).

[93] V. Klimov, "Nanocrystal quantum dots: from fundamental photophysics to multicolor lasing," Los Alamos Sci. **28**, 214–220 (2003).

[94] V. Klimov, "Spectral and dynamical properties of multiexcitons in semiconductor nanocrystals," Annu. Rev. Phys. Chem. **58**, 635–673 (2007).

[95] G. Schmid, ed., *Nanoparticles: From Theory to Application* (Wiley-VCH Verlag GmbH, Weinheim, 2004).

[96] V. I. Klimov, A. A. Mikhailovsky, S. Xu, A. Malko, J. A. Hollingsworth, C. A. Leatherdale, H.-J. Eisler, and M. G. Bawendi, "Optical gain and stimulated emission in nanocrystal quantum dots," Science **290**, 314–317 (2000).

[97] S. Ivanov, J. Nanda, A. Piryatinski, M. Achermann, L. Balet, I. Bezel, P. Anikeeva, S. Tretiak, and V. Klimov, "Light amplification using inverted core/shell nanocrystals: towards lasing in the single-exciton regime," J. Phys. Chem. B **108**, 10625–10630 (2004).

[98] V. Klimov, S. Ivanov, J. Nanda, M. Achermann, I. Bezel, J. McGuire, and A. Piryatinski, "Single-exciton optical gain in semiconductor nanocrystals," Nature **447**, 441–446 (2007).

[99] V. Klimov, A. Mikhailovsky, D. McBranch, C. Leatherdale, and M. Bawendi, "Quantization of multiparticle auger rates in semiconductor quantum dots," Science **287**, 1011–1013 (2000).

[100] F. García-Santamaría, Y. Chen, J. Vela, R. Schaller, J. Hollingsworth, and V. Klimov, "Suppressed auger recombination in "giant" nanocrystals boosts optical gain performance," Nano Lett. **9**, 3482–3488 (2009).

[101] R. R. Cooney, S. L. Sewall, D. M. Sagar, and P. Kambhampati, "Gain control in semiconductor quantum dots via state-resolved optical pumping," Phys. Rev. Lett. **102**, 127404 (2009).

[102] D. Steiner, D. Dorfs, U. Banin, F. Della Sala, L. Manna, and O. Millo, "Determination of band offsets in heterostructured colloidal nanorods using scanning tunneling spectroscopy," Nano Lett. **8**, 2954–2958 (2008).

[103] W. Brütting, ed., *Physics of Organic Semiconductors* (Wiley-VCH Verlag GmbH, Weinheim, 2005).

[104] J. Clark and G. Lanzani, "Organic photonics for communications," Nature Photon. **4**, 438–446 (2010).

[105] S. Cho, A. Grimsdale, D. Jones, S. Watkins, and A. Holmes, "Polyfluorenes without monoalkylfluorene defects," J. Am. Chem. Soc. **129**, 11910–11911 (2007).

[106] F. Wu, P. Shih, C. Shu, Y. Tung, and Y. Chi, "Highly efficient light-emitting diodes based on fluorene copolymer consisting of triarylamine units in the main chain and oxadiazole pendent groups," Macromolecules **38**, 9028–9036 (2005).

[107] A. Dodabalapur, E. Chandross, M. Berggren, and R. Slusher, "Organic solid-state lasers: past and future," Science **277**, 1787–1788 (1997).

[108] N. Tessler, "Lasers based on semiconducting organic materials," Adv. Mater. **11**, 363–370 (1999).

[109] V. Kozlov and S. Forrest, "Lasing action in organic semiconductor thin films," Curr. Opin. Solid State Mater. Sci. **4**, 203–208 (1999).

[110] G. Kranzelbinder and G. Leising, "Organic solid-state lasers," Rep. Prog. Phys. **63**, 729–762 (2000).

[111] M. McGehee and A. Heeger, "Semiconducting (conjugated) polymers as materials for solid-state lasers," Adv. Mater. **12**, 1655–1668 (2000).

[112] S. Frolov, M. Shkunov, A. Fujii, K. Yoshino, and Z. Vardeny, "Lasing and stimulated emission in π-conjugated polymers," IEEE J. Quantum Electron. **36**, 2–11 (2000).

[113] U. Scherf, S. Riechel, U. Lemmer, and R. Mahrt, "Conjugated polymers: lasing and stimulated emission," Curr. Opin. Solid State Mater. Sci. **5**, 143–154 (2001).

[114] S. Chénais and S. Forget, "Recent advances in solid-state organic lasers," Polym. Int. **61**, 390–406 (2012).

[115] M. Yan, L. J. Rothberg, F. Papadimitrakopoulos, M. E. Galvin, and T. M. Miller, "Spatially indirect excitons as primary photoexcitations in conjugated polymers," Phys. Rev. Lett. **72**, 1104–1107 (1994).

[116] D. Moses, "High quantum efficiency luminescence from a conducting polymer in solution: a novel polymer laser dye," Appl. Phys. Lett. **60**, 3215–3216 (1992).

[117] N. Tessler, G. Denton, and R. Friend, "Lasing from conjugated-polymer microcavities," Nature **382**, 695–697 (1996).

[118] F. Hide, M. Diaz-Garcia, B. Schwartz, M. Andersson, Q. Pei, and A. Heeger, "Semiconducting polymers: a new class of solid-state laser materials," Science **273**, 1833–1836 (1996).

[119] A. Rose, Z. Zhu, C. F. Madigan, T. M. Swager, and V. Bulović, "Sensitivity gains in chemosensing by lasing action in organic polymers," Nature **434**, 876–879 (2005).

[120] M. Yan, L. J. Rothberg, F. Papadimitrakopoulos, M. E. Galvin, and T. M. Miller, "Defect quenching of conjugated polymer luminescence," Phys. Rev. Lett. **73**, 744–747 (1994).

[121] A. Kuehne, D. Elfström, A. Mackintosh, A. Kanibolotsky, B. Guilhabert, E. Gu, I. Perepichka, P. Skabara, M. Dawson, and R. Pethrick, "Direct laser writing of nanosized oligofluorene truxenes in UV-transparent photoresist microstructures," Adv. Mater. **21**, 781–785 (2009).

[122] A. Kühne, "UV transparent and light emitting photo-polymers for opto-electronic applications," Ph.D. thesis, University of Strathclyde, Glasgow, UK (2008).

[123] W. S. Wong and A. Salleo, eds., *Flexible Electronics: Materials and Applications* (Springer-Verlag, Berlin, 2009).

[124] C. Kallinger, M. Hilmer, A. Haugeneder, M. Perner, W. Spirkl, U. Lemmer, J. Feldmann, U. Scherf, K. Müllen, A. Gombert *et al.*, "A flexible conjugated polymer laser," Adv. Mater. **10**, 920–923 (1998).

[125] J. A. Rogers, T. Someya, and Y. Huang, "Materials and mechanics for stretchable electronics," Science **327**, 1603–1607 (2010).

[126] S. Hoogland, V. Sukhovatkin, I. Howard, S. Cauchi, L. Levina, and E. H. Sargent, "A solution-processed 1.53 μm quantum dot laser with temperature-invariant emission wavelength," Opt. Express **14**, 3273–3281 (2006).

[127] Y. Chen, J. Herrnsdorf, B. Guilhabert, Y. Zhang, I. M. Watson, E. Gu, N. Laurand, and M. D. Dawson, "Colloidal quantum dot random laser," Opt. Express **19**, 2996–3003 (2011).

[128] P. Snee, Y. Chan, D. Nocera, and M. Bawendi, "Whispering-gallery-mode lasing from a semiconductor nanocrystal/microsphere resonator composite," Adv. Mater. **17**, 1131–1136 (2005).

[129] J. Schafer, J. P. Mondia, R. Sharma, Z. H. Lu, A. S. Susha, A. L. Rogach, and L. J. Wang, "Quantum dot microdrop laser," Nano Lett. **8**, 1709–1712 (2008).

[130] T.-J. Yim, T. Zentgraf, B. Min, and X. Zhang, "All-liquid photonic microcavity stabilized by quantum dots," J. Am. Chem. Soc. **132**, 2154–2156 (2010).

[131] H.-J. Eisler, V. C. Sundar, M. G. Bawendi, M. Walsh, H. I. Smith, and V. Klimov, "Color-selective semiconductor nanocrystal laser," Appl. Phys. Lett. **80**, 4614–4616 (2002).

[132] S. Gao, C. Zhang, Y. Liu, H. Su, L. Wei, T. Huang, N. Dellas, S. Shang, S. E. Mohney, J. Wang, and J. Xu, "Lasing from colloidal InP/ZnS quantum dots," Opt. Express **19**, 5528–5535 (2011).

[133] J. Herrnsdorf, B. Guilhabert, Y. Chen, A. Kanibolotsky, A. Mackintosh, R. Pethrick, P. Skabara, E. Gu, N. Laurand, and M. D. Dawson, "Flexible blue-emitting encapsulated organic semiconductor DFB laser," Opt. Express **18**, 25535–25545 (2010).

[134] Y. Chen, J. Herrnsdorf, B. Guilhabert, A. L. Kanibolotsky, A. R. Mackintosh, Y. Wang, R. A. Pethrick, E. Gu, G. A. Turnbull, P. J. Skabara, I. D. Samuel, N. Laurand, and M. D. Dawson, "Laser action in a surface-structured free-standing membrane based on a π-conjugated polymer-composite," Org. Electron. **12**, 62 – 69 (2011).

[135] V. M. Menon, M. Luberto, N. V. Valappil, and S. Chatterjee, "Lasing from ingap quantum dots in aspin-coated flexible microcavity," Opt. Express **16**, 19535–19540 (2008).

[136] N. Carlson, S. Liew, R. Amantea, D. Bour, G. Evans, and E. Vangieson, "Mode discrimination in distributed feedback grating surface emitting lasers containing a buried second-order grating," IEEE J. Quantum Electron. **27**, 1746–1752 (1991).

[137] M. Kasraian and D. Botez, "Single-lobed far-field radiation pattern from surface-emitting complex-coupled distributed-feedback diode lasers," Appl. Phys. Lett. **67**, 2783–2785 (1995).

[138] A. L. Efros, "Luminescence polarization of CdSe microcrystals," Phys. Rev. B **46**, 7448–7458 (1992).

[139] S. Gottardo, R. Sapienza, P. D. García, A. Blanco, D. S. Wiersma, and C. López, "Resonance-driven random lasing," Nature Photon. **2**, 429–432 (2008).

[140] A. Uchida, K. Amano, M. Inoue, K. Hirano, S. Naito, H. Someya, I. Oowada, T. Kurashige, M. Shiki, S. Yoshimori *et al.*, "Fast physical random bit generation with chaotic semiconductor lasers," Nature Photon. **2**, 728–732 (2008).

[141] R. C. Polson, A. Chipouline, and Z. V. Vardeny, "Random lasing in π-conjugated films and infiltrated opals," Adv. Mater. **13**, 760–764 (2001).

[142] X. Meng, K. Fujita, S. Murai, and K. Tanaka, "Coherent random lasers in weakly scattering polymer films containing silver nanoparticles," Phys. Rev. A **79**, 053817 (2009).

[143] A. Costela, I. Garcia-Moreno, L. Cerdan, V. Martin, O. Garcia, and R. Sastre, "Dye-doped POSS solutions: random nanomaterials for laser emission," Adv. Mater. **21**, 4163–4166 (2009).

[144] V. Sundar, H.-J. Eisler, T. Deng, Y. Chan, E. Thomas, and M. Bawendi, "Soft-lithographically embossed, multilayered distributed-feedback nanocrystal lasers," Adv. Mater. **16**, 2137–2141 (2004).

[145] J. Xu and M. Xiao, "Lasing action in colloidal CdS/CdSe/CdS quantum wells," Appl. Phys. Lett. **87**, 173117 (2005).

[146] T. Kraus, L. Malaquin, H. Schmid, W. Riess, N. Spencer, and H. Wolf, "Nanoparticle printing with single-particle resolution," Nature Nanotech. **2**, 570–576 (2007).

[147] Y. Boucher and P. Feron, "Generalized transfer function: a simple model applied to active single-mode microring resonators," Opt. Commun. **282**, 3940–3947 (2009).

[148] S. Mujumdar, V. Türck, R. Torre, and D. Wiersma, "Chaotic behavior of a random laser with static disorder," Phys. Rev. A **76**, 033807 (2007).

[149] J. H. Li and A. Z. Genack, "Correlation in laser speckle," Phys. Rev. E **49**, 4530–4533 (1994).

[150] A. Siegman, "Excess spontaneous emission in non-hermitian optical systems. I. laser amplifiers," Phys. Rev. A **39**, 1253–1263 (1989).

[151] L. Deych, "Effects of spatial nonuniformity on laser dynamics," Phys. Rev. Lett. **95**, 43902 (2005).

[152] R. Polson, M. Raikh, and Z. Vardeny, "Random lasing from weakly scattering media; spectrum universality in DOO–PPV polymer films," Physica E **13**, 1240–1242 (2002).

[153] C. Tang and S. VanSlyke, "Organic electroluminescent diodes," Appl. Phys. Lett. **51**, 913–915 (1987).

[154] J. Burroughes, D. Bradley, A. Brown, R. Marks, K. Mackay, R. Friend, P. Burns, and A. Holmes, "Light-emitting diodes based on conjugated polymers," Nature **347**, 539–541 (1990).

[155] K. Geetha, M. Rajesh, V. Nampoori, C. Vallabhan, and P. Radhakrishnan, "Laser emission from transversely pumped dye-doped free-standing polymer film," J. Opt. A: Pure Appl. Opt. **8**, 189–193 (2006).

[156] F. Scotognella, A. Monguzzi, F. Meinardi, and R. Tubino, "DFB laser action in a flexible fully plastic multilayer," Phys. Chem. Chem. Phys. **12**, 337–340 (2009).

[157] G. Gelinck, H. Huitema, E. Van Veenendaal, E. Cantatore, L. Schrijnemakers, J. Van Der Putten, T. Geuns, M. Beenhakkers, J. Giesbers, B. Huisman *et al.*, "Flexible active-matrix displays and shift registers based on solution-processed organic transistors," Nature Mater. **3**, 106–110 (2004).

[158] T. Someya, Y. Kato, T. Sekitani, S. Iba, Y. Noguchi, Y. Murase, H. Kawaguchi, and T. Sakurai, "Conformable, flexible, large-area networks of pressure and thermal sensors with organic transistor active matrixes," Proc. Natl. Acad. Sci. USA **102**, 12321 (2005).

[159] Y. Noguchi, T. Sekitani, and T. Someya, "Organic-transistor-based flexible pressure sensors using ink-jet-printed electrodes and gate dielectric layers," Appl. Phys. Lett. **89**, 253507–253507 (2006).

[160] C. Bartic and G. Borghs, "Organic thin-film transistors as transducers for (bio) analytical applications," Anal. Bioanal. Chem. **384**, 354–365 (2006).

[161] M. Lu, S. Choi, U. Irfan, and B. Cunningham, "Plastic distributed feedback laser biosensor," Appl. Phys. Lett. **93**, 111113 (2008).

[162] T. Sekitani, T. Yokota, U. Zschieschang, H. Klauk, S. Bauer, K. Takeuchi, M. Takamiya, T. Sakurai, and T. Someya, "Organic nonvolatile memory transistors for flexible sensor arrays," Science **326**, 1516 (2009).

[163] B. Wallikewitz, M. de la Rosa, J. Kremer, D. Hertel, and K. Meerholz, "A lasing organic light-emitting diode," Adv. Mater. **22**, 531–534 (2010).

[164] H. Brouwer, V. Krasnikov, A. Hilberer, J. Wildeman, and G. Hadziioannou, "Novel high efficiency copolymer laser dye in the blue wavelength region," Appl. Phys. Lett. **66**, 3404–3406 (1995).

[165] S. Frolov, M. Ozaki, W. Gellermann, Z. Vardeny, and K. Yoshino, "Mirrorless lasing in conducting polymer poly(2, 5-dioctyloxy-*p*-phenylenevinylene) films," Jpn. J. Appl. Phys. **35**, L1371–L1373 (1996).

[166] K. Yee, T. Tou, and S. Ng, "Hot-press molded poly (methyl methacrylate) matrix for solid-state dye lasers," Appl. Opt. **37**, 6381–6385 (1998).

[167] J. Clark, L. Bazzana, D. Bradley, J. Cabanillas-Gonzalez, G. Lanzani, D. Lidzey, J. Morgado, A. Nocivelli, W. Tsoi, T. Virgili *et al.*, "Blue polymer optical fiber amplifiers based on conjugated fluorene oligomers," J. Nanophoton. **2**, 023504 (2008).

[168] M. Wu, Z. Gong, A. Kuehne, A. Kanibolotsky, Y. Chen, I. Perepichka, A. Mackintosh, E. Gu, P. Skabara, R. Pethrick *et al.*, "Hybrid GaN/organic microstructured light-emitting devices via ink-jet printing," Opt. Express **17**, 16436–16443 (2009).

[169] B. Guilhabert, N. Laurand, J. Herrnsdorf, Y. Chen, A. Mackintosh, A. Kanibolotsky, E. Gu, P. J. Skabara, R. Pethrick, and M. D. Dawson, "Amplified spontaneous emission in free-standing membranes incorporating star-shaped monodisperse π-conjugated truxene oligomers," J. Opt. **12**, 035503 (2010).

[170] A. Costela, I. García-Moreno, C. Gómez, F. Amat-Guerri, M. Liras, and R. Sastre, "Efficient and highly photostable solid-state dye lasers based on modified dipyrromethene.BF_2 complexes incorporated into solid matrices of poly (methyl methacrylate)," Appl. Phys. B **76**, 365–369 (2003).

[171] B. Kaplan, H. Guner, O. Senlik, K. Gurel, M. Bayindir, and A. Dana, "Tuning optical discs for plasmonic applications," Plasmonics **4**, 237–243 (2009).

[172] N. Greenham, I. Samuel, G. Hayes, R. Phillips, Y. Kessener, S. Moratti, A. Holmes, and R. Friend, "Measurement of absolute photoluminescence quantum efficiencies in conjugated polymers," Chem. Phys. Lett. **241**, 89–96 (1995).

[173] J. Lawrence, G. Turnbull, and I. Samuel, "Polymer laser fabricated by a simple micromolding process," Appl. Phys. Lett. **82**, 4023–4025 (2003).

[174] R. Xia, G. Heliotis, P. Stavrinou, and D. Bradley, "Polyfluorene distributed feedback lasers operating in the green-yellow spectral region," Appl. Phys. Lett. **87**, 031104 (2005).

[175] D. Anglos, A. Stassinopoulos, R. N. Das, G. Zacharakis, M. Psyllaki, R. Jakubiak, R. A. Vaia, E. P. Giannelis, and S. H. Anastasiadis, "Random laser action in organic–inorganic nanocomposites," J. Opt. Soc. Am. B **21**, 208–213 (2004).

[176] H. Cao, J. Y. Xu, D. Z. Zhang, S.-H. Chang, S. T. Ho, E. W. Seelig, X. Liu, and R. P. H. Chang, "Spatial confinement of laser light in active random media," Phys. Rev. Lett. **84**, 5584–5587 (2000).

[177] D. S. Wiersma and S. Cavalieri, "Light emission: a temperature-tunable random laser," Nature **414**, 708–709 (2001).

[178] C. Vanneste and P. Sebbah, "Localized modes in random arrays of cylinders," Phys. Rev. E **71**, 026612 (2005).

[179] S. Xiao, Q. Song, F. Wang, L. Liu, J. Liu, and L. Xu, "Switchable random laser from dye-doped polymer dispersed liquid crystal waveguides," IEEE J. Quantum Electron. **43**, 407–410 (2007).

[180] C. J. S. de Matos, L. de S. Menezes, A. M. Brito-Silva, M. A. Martinez Gámez, A. S. L. Gomes, and C. B. de Araújo, "Random fiber laser," Phys. Rev. Lett. **99**, 153903 (2007).

[181] Q. Song, S. Xiao, X. Zhou, L. Liu, L. Xu, Y. Wu, and Z. Wang, "Liquid-crystal-based tunable high-Q directional random laser from a planar random microcavity," Opt. Lett. **32**, 373–375 (2007).

[182] Q. Song, L. Liu, L. Xu, Y. Wu, and Z. Wang, "Electrical tunable random laser emission from a liquid-crystal infiltrated disordered planar microcavity," Opt. Lett. **34**, 298–300 (2009).

[183] H. Ying Yang, S. Fung Yu, and S. Ping Lau, "Wide tunable ultraviolet random lasing action from ZnMgO thin films," J. Crystal Growth **312**, 16–18 (2009).

[184] C.-R. Lee, J.-D. Lin, B.-Y. Huang, T.-S. Mo, and S.-Y. Huang, "All-optically controllable random laser based on a dye-doped liquid crystal added with a photoisomerizable dye," Opt. Express **18**, 25896–25905 (2010).

[185] J.-K. Yang, S. V. Boriskina, H. Noh, M. J. Rooks, G. S. Solomon, L. D. Negro, and H. Cao, "Demonstration of laser action in a pseudorandom medium," Appl. Phys. Lett. **97**, 223101 (2010).

[186] S. K. Turitsyn, S. A. Babin, A. E. El-Taher, P. Harper, D. V. Churkin, S. Kablukov, J. D. Ania-Castañón, V. Karalekas, and E. V. Podivilov, "Random distributed feedback fibre laser," Nature Photon. **4**, 231–235 (2010).

[187] C.-R. Lee, J.-D. Lin, B.-Y. Huang, S.-H. Lin, T.-S. Mo, S.-Y. Huang, C.-T. Kuo, and H.-C. Yeh, "Electrically controllable liquid crystal random lasers below the fréedericksz transition threshold," Opt. Express **19**, 2391–2400 (2011).

[188] P. García, R. Sapienza, A. Blanco, and C. López, "Photonic glass: a novel random material for light," Adv. Mater. **19**, 2597–2602 (2007).

[189] P. D. García, R. Sapienza, and C. López, "Photonic glasses: a step beyond white paint," Adv. Mater. **22**, 12–19 (2010).

[190] J. F. Galisteo-López, M. Ibisate, R. Sapienza, L. S. Froufe-Pérez, A. Blanco, and C. López, "Self-assembled photonic structures," Adv. Mater. **23**, 30–69 (2011).

[191] J. Andreasen and H. Cao, "Spectral behavior of partially pumped weakly scattering random lasers," Opt. Express **19**, 3418–3433 (2011).

[192] X. H. Wu, A. Yamilov, H. Noh, H. Cao, E. W. Seelig, and R. P. H. Chang, "Random lasing in closely packed resonant scatterers," J. Opt. Soc. Am. B **21**, 159–167 (2004).

[193] C. F. Bohren and D. R. Huffman, *Absorption and Scattering of Light by Small Particles* (Wiley-VCH, New York, 1998).

[194] K. Busch, C. M. Soukoulis, and E. N. Economou, "Transport and scattering mean free paths of classical waves," Phys. Rev. B **50**, 93–98 (1994).

[195] G. Labeyrie, F. de Tomasi, J.-C. Bernard, C. A. Müller, C. Miniatura, and R. Kaiser, "Coherent backscattering of light by cold atoms," Phys. Rev. Lett. **83**, 5266–5269 (1999).

[196] M. Gurioli, F. Bogani, L. Cavigli, H. Gibbs, G. Khitrova, and D. S. Wiersma, "Weak localization of light in a disordered microcavity," Phys. Rev. Lett. **94**, 183901 (2005).

[197] S. Yu, C. Yuen, S. Lau, W. Park, and G. Yi, "Random laser action in ZnO nanorod arrays embedded in ZnO epilayers," Appl. Phys. Lett. **84**, 3241 (2004).

[198] A. Vutha, S. Tiwari, and R. Thareja, "Random laser action in ZnO doped polymer," J. Appl. Phys. **99**, 123509 (2006).

[199] A. Stassinopoulos, R. N. Das, S. H. Anastasiadis, E. P. Giannelis, and D. Anglos, "Random lasing action from ZnO–silica nanohybrids," J. Opt. **12**, 024006 (2010).

[200] G. van Soest, M. Tomita, and A. Lagendijk, "Amplifying volume in scattering media," Opt. Lett. **24**, 306–308 (1999).

[201] Y. Ling, H. Cao, A. L. Burin, M. A. Ratner, X. Liu, and R. P. H. Chang, "Investigation of random lasers with resonant feedback," Phys. Rev. A **64**, 063808 (2001).

[202] V. M. Apalkov and M. E. Raikh, "Universal fluctuations of the random lasing threshold in a sample of a finite area," Phys. Rev. B **71**, 054203 (2005).

[203] F. A. Pinheiro and L. C. Sampaio, "Lasing threshold of diffusive random lasers in three dimensions," Phys. Rev. A **73**, 013826 (2006).

[204] V. Kozlov, V. Bulovic, P. Burrows, M. Baldo, V. Khalfin, G. Parthasarathy, S. Forrest, Y. You, and M. Thompson, "Study of lasing action based on förster energy transfer in optically pumped organic semiconductor thin films," J. Appl. Phys. **84**, 4096–4108 (1998).

[205] M. A. Baldo and S. R. Forrest, "Transient analysis of organic electrophosphorescence: I. transient analysis of triplet energy transfer," Phys. Rev. B **62**, 10958–10966 (2000).

[206] Y. Zhang and S. Forrest, "Existence of continuous-wave threshold for organic semiconductor lasers," Phys. Rev. B **84**, 241301 (2011).

[207] M. Wohlgenannt, "Making a laser shine longer," Physics **4**, 104 (2011).

[208] P. Klán and J. Wirz, *Photochemistry of Organic Compounds: from Concepts to Practice* (Wiley-Blackwell, Chichester, U.K., 2009).

[209] R. Bornemann, U. Lemmer, and E. Thiel, "Continuous-wave solid-state dye laser," Opt. Lett. **31**, 1669–1671 (2006).

[210] T. Rabe, K. Gerlach, T. Riedl, H. Johannes, W. Kowalsky, J. Niederhofer, W. Gries, J. Wang, T. Weimann, P. Hinze *et al.*, "Quasi-continuous-wave operation of an organic thin-film distributed feedback laser," Appl. Phys. Lett. **89**, 081115 (2006).

[211] M. Lehnhardt, T. Riedl, U. Scherf, T. Rabe, and W. Kowalsky, "Spectrally separated optical gain and triplet absorption: towards continuous wave lasing in organic thin film lasers," Org. Electron. **12**, 1346–1351 (2011).

[212] J. H. Schön, C. Kloc, A. Dodabalapur, and B. Batlogg, "An organic solid state injection laser," Science **289**, 599–601 (2000).

[213] M. A. Baldo, R. J. Holmes, and S. R. Forrest, "Prospects for electrically pumped organic lasers," Phys. Rev. B **66**, 035321 (2002).

[214] Z. Bao, B. Batlogg, S. Berg, A. Dodabalapur, R. C. Haddon, H. Hwang, C. Kloc, H. Meng, and J. H. Schön, "Retraction," Science **298**, 961 (2002).

[215] F. J. Duarte, L. S. Liao, and K. M. Vaeth, "Coherence characteristics of electrically excited tandem organic light-emitting diodes," Opt. Lett. **30**, 3072–3074 (2005).

[216] F. J. Duarte, "Coherent electrically excited organic semiconductors: visibility of interferograms and emission linewidth," Opt. Lett. **32**, 412–414 (2007).

[217] F. Duarte, "Coherent electrically excited organic semiconductors: coherent or laser emission," Appl. Phys. B **90**, 101–108.

[218] X. Liu, H. Li, C. Song, Y. Liao, and M. Tian, "Microcavity organic laser device under electrical pumping," Opt. Lett. **34**, 503–505 (2009).

[219] M. Muccini, "A bright future for organic field-effect transistors," Nature Mater. **5**, 605–613 (2006).

[220] S. Bisri, T. Takenobu, Y. Yomogida, H. Shimotani, T. Yamao, S. Hotta, and Y. Iwasa, "High mobility and luminescent efficiency in organic single-crystal light-emitting transistors," Adv. Funct. Mater. **19**, 1728–1735 (2009).

[221] M. A. McCarthy, B. Liu, E. P. Donoghue, I. Kravchenko, D. Y. Kim, F. So, and A. G. Rinzler, "Low-voltage, low-power, organic light-emitting transistors for active matrix displays," Science **332**, 570–573 (2011).

[222] C. Santato, F. Cicoira, and R. Martel, "Organic photonics: spotlight on organic transistors," Nature Photon. **5**, 392–393 (2011).

[223] L. Butov, "Solid-state physics: a polariton laser," Nature **447**, 540–541 (2007).

[224] S. Kéna-Cohen and S. Forrest, "Room-temperature polariton lasing in an organic single-crystal microcavity," Nature Photon. **4**, 371–375 (2010).

[225] G. La Rocca, "Organic photonics: polariton lasing," Nature Photon. **4**, 343–345 (2010).

[226] J. R. Tischler, M. S. Bradley, V. Bulović, J. H. Song, and A. Nurmikko, "Strong coupling in a microcavity LED," Phys. Rev. Lett. **95**, 036401 (2005).

[227] T. Riedl, T. Rabe, H. Johannes, W. Kowalsky, J. Wang, T. Weimann, P. Hinze, B. Nehls, T. Farrell, and U. Scherf, "Tunable organic thin-film laser pumped by an inorganic violet diode laser," Appl. Phys. Lett. **88**, 241116 (2006).

[228] C. Karnutsch, V. Haug, C. Gaertner, U. Lemmer, T. Farrell, B. Nehls, U. Scherf, J. Wang, T. Weimann, G. Heliotis, C. Pflumm, J. deMello, and D. Bradley, "Low threshold blue conjugated polymer DFB lasers," in *Conference on CLEO/QELS*, paper CFJ3 (2006).

[229] A. E. Vasdekis, G. Tsiminis, J.-C. Ribierre, L. O. Faolain, T. F. Krauss, G. A. Turnbull, and I. D. W. Samuel, "Diode pumped distributed Bragg reflector lasers based on a dye-to-polymer energy transfer blend," Opt. Express **14**, 9211–9216 (2006).

[230] C. Karnutsch, M. Stroisch, M. Punke, U. Lemmer, J. Wang, and T. Weimann, "Laser diode-pumped organic semiconductor lasers utilizing two-dimensional photonic crystal resonators," IEEE Photon. Technol. Lett. **19**, 741–743 (2007).

[231] V. Kozlov, G. Parthasarathy, P. Burrows, V. Khalfin, J. Wang, S. Chou, and S. Forrest, "Structures for organic diode lasers and optical properties of organic semiconductors under intense optical and electrical excitations," IEEE J. Quantum Electron. **36**, 18–26 (2000).

[232] M. Dawson *et al.*, "Hybrid organic semiconductor / gallium nitride / CMOS smart pixel arrays," (2008–2012). http://hypix.photonics.ac.uk/.

[233] Y. Yang, G. Turnbull, and I. Samuel, "Hybrid optoelectronics: a polymer laser pumped by a nitride light-emitting diode," Appl. Phys. Lett. **92**, 163306 (2008).

[234] P. Prasad, *Nanophotonics* (Wiley-IEEE, New York, 2004).

[235] D. J. Bergman and M. I. Stockman, "Surface plasmon amplification by stimulated emission of radiation: quantum generation of coherent surface plasmons in nanosystems," Phys. Rev. Lett. **90**, 027402 (2003).

[236] M. Stockman, "Spasers explained," Nature Photon. **2**, 327–329 (2008).

[237] D. Bergman and M. Stockman, "Can we make a nanoscopic laser," Laser Phys. **14**, 409–411 (2004).

[238] J. A. Gordon and R. W. Ziolkowski, "The design and simulated performance of a coated nano-particle laser," Opt. Express **15**, 2622–2653 (2007).

[239] A. K. Sarychev and G. Tartakovsky, "Magnetic plasmonic metamaterials in actively pumped host medium and plasmonic nanolaser," Phys. Rev. B **75**, 085436 (2007).

[240] M. Hill, Y. Oei, B. Smalbrugge, Y. Zhu, T. De Vries, P. van Veldhoven, F. van Otten, T. Eijkemans *et al.*, "Lasing in metallic-coated nanocavities," Nature Photon. **1**, 589–594 (2007).

[241] N. Zheludev, S. Prosvirnin, N. Papasimakis, and V. Fedotov, "Lasing spaser," Nature Photon. **2**, 351–354 (2008).

[242] M. Noginov, G. Zhu, A. Belgrave, R. Bakker, V. Shalaev, E. Narimanov, S. Stout, E. Herz, T. Suteewong, and U. Wiesner, "Demonstration of a spaser-based nanolaser," Nature **460**, 1110–1112 (2009).

[243] R. Oulton, V. Sorger, T. Zentgraf, R. Ma, C. Gladden, L. Dai, G. Bartal, and X. Zhang, "Plasmon lasers at deep subwavelength scale," Nature **461**, 629–632 (2009).

Publications

Papers

Drafted/Submitted

[13] **Y. Chen**, J. Herrnsdorf, B. Guilhabert, Y. Zhang, A. Kanibolotsky, P. Skabara, E. Gu, N. Laurand, and M. D. Dawson, "Organic polymer composite random laser operating underwater", In preparation.

Accepted/Published

[12] J. Herrnsdorf, **Y. Chen**, B. Guilhabert, N. Laurand, and M. D. Dawson, "Stripe excitation of high gain media with disorder", *IEEE Journal of Quantum Electronics* (2012), In press.

[11] B. Guilhabert, N. Laurand, J. Herrnsdorf, **Y. Chen**, A. L. Kanibolotsky, C. Orofino, P. J. Skabara, and M. D. Dawson, "Mechanically-flexible organic semiconductor laser array", *IEEE Photonics Journal* 4, 684-690 (2012).

[10] **Y. Chen**, J. Herrnsdorf, B. Guilhabert, Y. Zhang, A. Kanibolotsky, P. Skabara, E. Gu, N. Laurand, and M. D. Dawson, "Modification of emission wavelength in organic random lasers based on photonic glass", *Organic Electronics* 13, 1129-1135 (2012).

[9] **Y. Chen**, J. Herrnsdorf, B. Guilhabert, Y. Zhang, A. Mackintosh, R. Pethrick, E. Gu, N. Laurand, and M. D. Dawson, "Fabrication and optical characterization of a flexible colloidal quantum dot laser", in *Proceedings of IEEE NANO 2011 Conference*, 958-962 (2012).

[8] **Y. Chen**, J. Herrnsdorf, B. Guilhabert, Y. Zhang, A. Kanibolotsky, P. Skabara, E. Gu, N. Laurand, and M. Dawson, "Tunable random laser action in a π-conjugated polymer-based photonic glass gain medium", in *Proceedings of IEEE NANO 2011 Conference*, 559-563 (2012).

[7] **Y. Chen**, B. Guilhabert, J. Herrnsdorf, Y. Zhang, A. R. Mackintosh, R. A. Pethrick, E. Gu, N. Laurand, and M. D. Dawson, "Flexible distributed-feedback colloidal quantum dot laser", *Applied Physics Letters* 99, 241103 (2011), **Cover story for 12 Dec. 2011 issue**.

[6] **Y. Chen**, J. Herrnsdorf, B. Guilhabert, Y. Zhang, I. M. Watson, E. Gu, N. Laurand, and M. D. Dawson, "Colloidal quantum dot random laser", *Optics Express* 19, 2996 (2011).

[5] **Y. Chen**, J. Herrnsdorf, B. Guilhabert, A. L. Kanibolotsky, A. R. Mackintosh, Y. Wang, R. A. Pethrick, E. Gu, G. A. Turnbull, P. J. Skabara, I. D. W. Samuel, N. Laurand, and M. D. Dawson, "Laser action in a surface-structured free-standing membrane based on a π-conjugated polymer-composite", *Organic Electronics* 12, 62 (2011).

[4] J. Herrnsdorf, B. Guilhabert, **Y. Chen**, A. L. Kanibolotsky, A. R. Mackintosh, R. A. Pethrick, P. J. Skabara, E. Gu, N. Laurand, and M. D. Dawson, "Flexible blue-emitting encapsulated organic semiconductor DFB laser", *Optics Express* 18, 25535 (2010).

[3] B. Guilhabert, N. Laurand, J. Herrnsdorf, **Y. Chen**, A. R. Mackintosh, A. L. Kanibolotsky, E. Gu, P. J. Skabara, R. A. Pethrick, and M. D. Dawson, "Amplified spontaneous emission in free-standing membranes incorporating star-shaped monodisperse -conjugated truxene oligomers", *Journal of Optics* 12, 035503 (2010).

[2] Z. Gong, S. Jin, **Y. Chen**, J. McKendry, D. Massoubre, I. M. Watson, E. Gu, and M. D. Dawson, "Size-dependent light output, spectral shift, and self-heating of 400 nm InGaN light-emitting diodes", *Journal of Applied Physics* 107, 013103 (2010).

[1] M. Wu, Z. Gong, A. J. Kuehne, A. L. Kanibolotsky, **Y. Chen**, I. F. Perepichka, A. R. Mackintosh, E. Gu, P. J. Skabara, R. A. Pethrick, and M. D. Dawson, "Hybrid device fabricated by inkjet printing star-shaped oligofluorene truxenes on AlInGaN microstructured light emitting diodes", *Optics Express* 17, 16436 (2009).

Conference presentations

Note: presenters underlined.

[23] B. Guilhabert, N. Laurand, A. Kanibolotsky, J. Herrnsdorf, **Y. Chen**, P. J. Skabara, and M. D. Dawson, "Flexible organic semiconductor laser array" (Oral), *IEEE Photonics 2011* (Arlington, Virginia, USA, October 2011).

[22] P. Tian, E. Xie, Z. Gong, Z. Chen, T. Yu, Y. Sun, S. Qi, **Y. Chen**, Y. Zhang, S. Calvez, E. Gu, G. Zhang, and M. Dawson, "Flexible vertical structure GaN-based light emitting diodes on an AuSn substrate" (Oral), *IEEE Photonics 2011* (Arlington, Virginia, USA, October 2011).

[21] J. Herrnsdorf, B. Guilhabert, J. McKendry, Z. Gong, D. Massoubre, **Y.**

Chen, S. Zhang, A. L. Kanibolotsky, A. R. Mackintosh, P. J. Skabara, A. E. Kelly, E. Gu, N. Laurand, and M. D. Dawson, "Hybrid GaN/organic polymer photonic crystal LED" (Oral), *IEEE Photonics 2011* (Arlington, Virginia, USA, October 2011).

[20] **Y. Chen**, J. Herrnsdorf, B. Guilhabert, Y. Zhang, A. L. Kanibolotsky, P. J. Skabara, E. Gu, N. Laurand, and M. D. Dawson, "Tunable random laser action in a π-conjugated polymer-based photonic glass gain medium" (Poster), *IEEE Nano 2011* (Portland, USA, August 2011).

[19] **Y. Chen**, J. Herrnsdorf, B. Guilhabert, Y. Zhang, A. R. Mackintosh, R. A Pethrick, E. Gu, N. Laurand, and M. D. Dawson, "Fabrication and optical characterization of a flexible colloidal quantum dot laser" (Oral: **Invited talk** presented by Prof. M. D. Dawson), *IEEE Nano 2011* (Portland, USA, August 2011).

[18] E. Xie, Z. Chen, P. Edwards, Z. Gong, Y. Zhang, **Y. Chen**, I. Watson, E. Gu, R. Martin, G. Zhang, and M. D. Dawson, "Strain relaxation in InGaN/GaN micro-pillars evidenced by high resolution cathodoluminescence spectral mapping" (Oral), *The 9th International Conference on Nitride Semiconductors* (Glasgow, UK, July 2011).

[17] Y. Tao, Z. Chen, Z. Gong, E. Xie, **Y. Chen**, Y. Zhang, J. McKendry, D. Massoubre, E. Gu, and G. Zhang, "Size effect on efficiency droop of blue light emitting diode" (Poster), *The 9th International Conference on Nitride Semiconductors* (Glasgow, UK, July 2011).

[16] **Y. Chen**, J. Herrnsdorf, B. Guilhabert, Y. Zhang, E. Gu, N. Laurand, and M. D. Dawson, "Colloidal quantum dot lasers" (Poster), *University Research Day* (University of Strathclyde, Glasgow, UK, June 2011)

[15] B. Guilhabert, N. Laurand, A. R. Mackintosh, **Y. Chen**, J. Herrnsdorf, A. Kanibolotsky, P. J. Skabara, and M. D. Dawson, "Low threshold all-organic composite laser" (Oral), *CLEO/Europe-IQEC 2011* (Munich, Germany, May 2011).

[14] **Y. Chen**, B. Guilhabert, J. Herrnsdorf, Y. Zhang, A. R. Mackintosh, R. A. Pethrick, N. Laurand, and M. D. Dawson, "Flexible distributed feedback colloidal quantum dot laser patterned by a submicron grating structure" (Oral), *CLEO/Europe-IQEC 2011* (Munich, Germany, May 2011).

[13] **Y. Chen**, B. Guilhabert, J. Herrnsdorf, Y. Zhang, A. R. Mackintosh, R. A. Pethrick, N. Laurand and M. D. Dawson, "Flexible DFB colloidal quantum dot laser patterned by submicron grating structure" (Oral), *IoP Quantum Dot Day 2011* (University of Bristol, UK, January 2011).

[12] A. R. Mackintosh, P. J. Skabara, A. Kanibolotsky, R. A. Pethrick, **Y. Chen**, B. Guilhabert, E. Gu, N. Laurand, M. Dawson, J. Herrnsdorf, I. D. Samuel, and G. Turnbull, "Laser action in a surface-structured free-standing membrane based on a π-conjugated polymer-composite" (Poster), *2010 MRS Fall Meeting* (Boston, Massachusetts, USA, November-December 2010).

[11] J. Herrnsdorf, B. Guilhabert, **Y. Chen**, A. Kanibolotsky, A. Mackintosh, R. Pethrick, P. Skabara, E. Gu, N. Laurand, and M. Dawson, "Flexible blue-emitting DFB laser" (Oral), *The 23rd Annual Meeting of the IEEE Photonics Society* (Denver, USA, November 2010).

[10] **Y. Chen**, J. Herrnsdorf, B. Guilhabert, A. Kanibolotsky, Y. Zhang, E. Gu, P. Skabara, N. Laurand, and M. Dawson, "Random laser action in π-conjugated polymer-based photonic glasses system" (Oral), *Photon10 Conference* (Southampton, UK, August 2010).

[9] J. Herrnsdorf, B. Guilhabert, **Y. Chen**, A. Kanibolotsky, A. Mackintosh, R. Pethrick, P. Skabara, E. Gu, N. Laurand, and M, Dawson, "DFB laser action from truxene-core chromophores in an encapsulating polymer matrix on a flexible substrate" (Oral), *Photon10 Conference* (Southampton, UK, August 2010).

[8] **Y. Chen**, J. Herrnsdorf, B. Guilhabert, E. Gu, N. Laurand, and M. D. Dawson, "Random Laser Action in Complex Photonic Systems" (Poster), *University Research Day* (University of Strathclyde, Glasgow, UK, June 2010)

[7] J. Herrnsdorf, **Y. Chen**, N. Laurand, B. Guilhabert, E. Gu, and M. D. Dawson, "Stimulated emission from colloidal quantum dots in a light-emitting polymer film" (Poster), *The 6th International Conference on Quantum Dots* (Nottingham, UK, April 2010).

[6] **Y. Chen**, J. Herrnsdorf, N. Laurand, B. Guilhabert, E. Gu, and M. D. Dawson, "Random lasing action in colloidal quantum dots" (**Nature Publishing Group Prize for Best Student Poster**), *The 6th International Conference on Quantum Dots* (Nottingham, UK, April 2010).

[5] J. Herrnsdorf, **Y. Chen**, N. Laurand, B. Guilhabert, E. Gu, and M. D. Dawson, "Stimulated emission from colloidal quantum dots in a light-emitting polymer film" (Oral), *IOP One-Day Quantum Dot Meeting 2010* (Cambridge University, Cambridge, UK, January 2010).

[4] **Y. Chen**, J. Herrnsdorf, N. Laurand, B. Guilhabert, E. Gu, and M. D. Dawson, "Random lasing action in colloidal quantum dots" (Poster), *IOP One-Day Quantum Dot Meeting 2010* (Cambridge University, Cambridge, UK, January 2010).

[3] J. Herrnsdorf, **Y. Chen**, B. Guilhabert, N. Laurand, E. Gu, A. L. Kanibolotsky, P. J. Skabara, and M. D. Dawson, "Optical gain from light-emitting nanocomposite membranes" (Oral), *SID Organic Electronics UK 2009* (Imperial College, London, September 2009).

[2] **Y. Chen**, J. Herrnsdorf, N. Laurand, B. Guilhabert, A. L. Kanibolotsky, Y. Zhang, E. Gu, G. Turnbull, P. J. Skabara, I. D. W. Samuel, and M. D. Dawson, "Green-emitting organic/inorganic composite as a random lasing medium" (Oral), *SID Organic Electronics UK 2009* (Imperial College, London, UK, September 2009).

[1] J. Herrnsdorf, B. Guilhabert, **Y. Chen**, N. Laurand, E. Gu, I. M. Watson, M. D. Dawson, A. L. Kanibolotsky, P. J. Skabara, A. R. Mackintosh, and R. A. Pethrick, "Free-standing light-emitting organic nanocomposite membranes" (Oral), *The 22nd Annual Meeting of the IEEE Photonics Society* (Belek-Antalya, Turkey, October 2009).